Louisiana State University
LSU Digital Commons

LSU Doctoral Dissertations | Graduate School

2012

Global and local performance of prestressed girder bridges with positive moment continuity detail

Tanvir Hossain
Louisiana State University and Agricultural and Mechanical College, tan_98h@yahoo.com

Follow this and additional works at: https://digitalcommons.lsu.edu/gradschool_dissertations

 Part of the Civil and Environmental Engineering Commons

Recommended Citation
Hossain, Tanvir, "Global and local performance of prestressed girder bridges with positive moment continuity detail" (2012). *LSU Doctoral Dissertations*. 2.
https://digitalcommons.lsu.edu/gradschool_dissertations/2

This Dissertation is brought to you for free and open access by the Graduate School at LSU Digital Commons. It has been accepted for inclusion in LSU Doctoral Dissertations by an authorized graduate school editor of LSU Digital Commons. For more information, please contactgradetd@lsu.edu.

GLOBAL AND LOCAL PERFORMANCE OF PRESTRESSED GIRDER BRIDGES WITH POSITIVE MOMENT CONTINUITY DETAIL

A Dissertation

Submitted to the Graduate Faculty of the
Louisiana State University and
Agricultural and Mechanical College
in partial fulfillment of the
requirements for the degree of
Doctor of Philosophy

in

The Department of Civil and Environmental Engineering

by
Tanvir Hossain
B.S., Bangladesh University of Engineering and Technology, 2004
M.S., Bangladesh University of Engineering and Technology, 2008
May 2012

DEDICATION

To my parents

ACKNOWLEDGEMENTS

I would like to express my sincere gratitude to Dr. Ayman M. Okeil, my advisor, for his excellent guidance, invaluable suggestions and ardent encouragement throughout my Ph.D study at LSU, without which this dissertation would have never come into light. I feel extremely privileged to work under Dr. Okeil whose keen interest and encouragement helped to understand the subject presented in this dissertation.

I would also like to thank my committee members Dr. Steve Cai, Dr. Michele Barbato, Dr. Muhammad Wahab and Dr. Jorge Pulin for evaluating my research work and providing helpful suggestions and comments on my research. Special thanks to the faculty, staff and fellow students at Department of Civil and Environmental Engineering, Louisiana State University who assisted me in my research.

The assistantships offered by Louisiana Transportation Research Center, National Science Foundation and The Department of Civil and Environmental Engineering of LSU are fully acknowledged.

Last but not the least; I would like to thank my family members, friends and colleagues, who have always been beside me through thick and thin.

TABLE OF CONTENTS

LIST OF TABLES

LIST OF FIGURES

ABSTRACT

Global as well as local behavior of prestressed girder bridges made continuous by adding continuity diaphragms with a recently proposed positive moment continuity detail were investigated in this study. The focus of the investigation is on the positive moment caused by temperature gradients, time dependent effects such as creep and shrinkage, and some live load positions, and on the force transfer mechanisms through the diaphragm. The study utilized different approaches including analytical models for temperature evaluations and finite element models for structural assessments. Field data from a bridge using the new detail were used to validate the developed models.

The temperature field of the bridge at different times of the year was estimated using an analytical method. The computed temperature profiles, actual recorded temperatures at the bridge site, and AASHTO specified design gradients are presented and compared. Primary as well as secondary thermal stresses were the calculated and restraint moment caused by temperature gradient was quantified.

A 3-D finite element model capable of predicting the long term behavior of prestressed girder bridges is presented. A temperature independent creep model was adopted and calibrated using early age data. Construction sequence was considered in the analysis. The FE restraint moment predictions were compared to results obtained from other commonly used analytical method. A parametric study was conducted using the analytical method to investigate the creep coefficient values.

Performance of the continuity detail under live load effects was investigated. A live load test was carried out at the bridge site using two loaded trucks. A full bridge 3-D finite element model was also developed and validated with the field data. The validated FE model was also used to investigate the efficiency of the continuity detail.

A more detailed 3-D FE model that zooms in on the joint was also built accounting for critical behavioral aspects of the continuity details under service conditions. Contact between cast-in-place concrete and precast concrete, transfer length of prestressing strands, and actual 180º-hook hairpin bar detail were included in the detailed model. Force transfer mechanism, stress distribution and the effective gross moment of inertia at the end of girder were investigated.

1 INTRODUCTION

This dissertation was constructed following the technical paper format that is approved by the Graduate School at LSU. The objective for this type of format is to encourage graduate degree candidates to publish their research findings. This dissertation consists of eight chapters, all of which, except the introduction and conclusion are based on technical papers that have been accepted, under review or to be submitted to the peer reviewed journals. All the chapters document the research work of the candidate under the supervision of advisors and committee members. Each chapter presents an independent topic; however, some materials may have been repeated for the completeness of the individual chapters. This introductory chapter gives detail of the previous works on the continuous prestressed girder bridges along with the recommendations as well as discussions on the available techniques to analyze the continuous prestressed girder bridges.

1.1 Continuous Girder Bridge Construction

Building bridges using precast concrete elements offers many advantages such as expediting construction, reducing formwork, and improving quality control. Because of these advantages and others, about 80% of newly constructed bridges are built using precast elements. One of the consequences of using precast elements is that adjacent precast elements are not connected by default like the case of monolithic construction. Connecting adjacent precast concrete elements has many advantages including achieving longer span lengths, improving structural redundancy, and eliminating joints and all the problems that they cause. Therefore, engineers have always looked for ways to connect individual precast concrete elements to form structurally continuous bridges. Over the years, several concepts were introduced for jointless bridge construction including (1) integral bridges, where the superstructure is built integrally with the substructure, (2) full superstructure integration, and (3) partial superstructure integration. This dissertation focuses on the second type of jointless bridge construction. In this alternative, adjacent precast concrete girders are made continuous by pouring continuity diaphragms in the gap between them over the supporting piers. As a result of converting simply supported girders into continuous ones, time dependent effects generate secondary effects that must be considered in the design; otherwise adverse effects such as cracking in shear critical locations may occur. Two of the major time dependents effects; namely creep and thermal gradient, are that thoroughly investigated in this study. In this chapter, a review of previous major studies published on the subject of time dependent effects related to the dissertation topic is presented.

1.2 Behavior of Continuous Superstructure

The advantages of continuous precast prestressed girder bridge over simple span bridge are many, which explains the wide spread use in almost all states. Simple span girders made continuous are subjected to different kinds of loading such as live loads, time dependent loading and temperature gradient. Time dependent loadings like creep and shrinkage deformation and temperature gradient introduces secondary moments on the continuous structure depending on the boundary conditions. These secondary moments often exceeds the service moments in the long run. In addition to the service moments, these secondary moments may exceed the cracking

moment of the composite section and the section cracks. Therefore extra precautions need to be accounted for continuous bridge superstructure. This section describes some of the previous works that shed lights on the problems associated with the continuous girder bridges and the recommendations to amend the design procedure are also discussed.

1.2.1 NCHRP Report 322

The National Cooperative Highway Research Program (NCHRP) published its first report on continuous prestressed girder bridges through project 12-29 (Oesterle et al. 1989). This project was intended to resolve the uncertainties associated with the behavior and design provisions of prestressed girder bridges made continuous by extending the composite cast-in-place deck over the gap in between the simply supported precast concrete girders. Therefore, these bridges can be considered as partially continuous. Pretension in a prestressed member usually causes the member to camber upward. If the girder is a simply supported the ends of the member will tend to rotate. However, if the girders were made continuous by pouring a continuity diaphragm in between the adjacent girders and extending positive moment reinforcement at the bottom and negative moment reinforcement at the deck, the end of the girders are restrained from rotating. Consequently, secondary moments develop in the system due to the creep induced camber and similar effects such as thermal gradients. Positive moments also develop when live loads are position on far spans of a continuous bridge. A negative moment is easily resisted by the diaphragm concrete that will be subjected to compression. Positive moments are harder to resist because of the tension that develops at the bottom as depicted in Fig. 1-1.

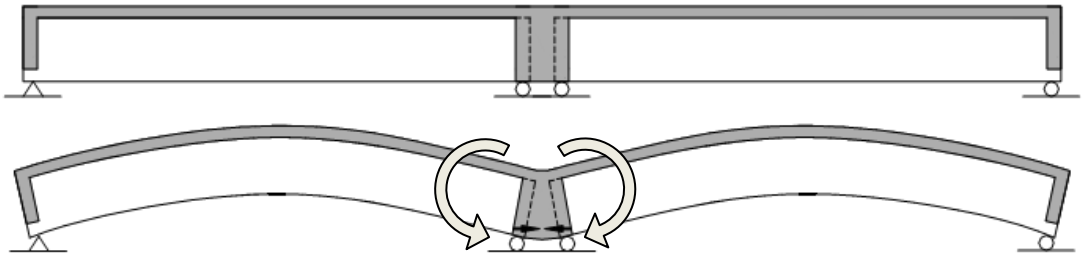

Fig. 1-1 Positive moment development at the diaphragm

Prior to the initiation of NCHRP Project 12-29, continuous bridges were analyzed and designed with the help of PCA established standards (Mattock 1961). This standard includes the influence of precast girders' creep and the differential shrinkage between the deck and girder concrete. A positive moment connection was developed and negative moment reinforcement was suggested over the supporting piers within the decks. The positive moment was calculated as the summation of time dependent effects and live loads. Thermally induced moments were not included. Nevertheless, the bridges designed using PCA standards performed well. However, there were several uncertainties associated with the procedure. One of the limitations was that the PCA procedure assumed the deck and girder concrete has the same creep and shrinkage properties, which in general is not the case. As the mixing and proportion of the concrete for

girder and deck were different they have different properties. Construction sequence also plays a vital role as girder concrete were cast much ahead of time than the deck concrete which results different maturity levels in addition to varying the stress levels. Continuity connections was assumed to be of zero length and fully rigid, whereas, in the actual case it has finite length and rotational stiffness. Full continuity was also assumed in calculating the positive and negative moments. Because of these limitations together with the uncertainties in estimating the positive and negative moments, wide variations existed in the design process. AASHTO specifications were also short in guidance for a design procedure. With the significant advancements in understanding the time dependent creep and shrinkage behavior of concrete and the availability of inexpensive computers, NCHRP Project 12-29's goal was to better understand the time dependent phenomena and to develop a design procedure and specifications for continuity detailing of prestressed concrete girder bridges.

The main objectives of this research projects was to conduct a survey of existing practices of continuity at that time and to analyze the effects of variation in time dependent material behavior and the variation in bridge design parameters on the service moments at the continuity regions and midspan sections. The effects of different design parameters on the inelastic moment redistribution were also analyzed. Developing a computer program that would help simplify the analysis of continuous prestressed concrete girder bridges and recommending new design procedures were also part of the research objectives. Based on the questionnaire, it was confirmed that at that time the practice for design and construction of simple span girders made continuous varied considerably. It was also found that the ultimate creep coefficient 2.35 for concrete as recommended by the ACI was adequate. A parametric study was conducted to study time dependent effects on continuity and was found that continuity for live loads varies from 0 to 100 %. It was also concluded that presence of positive moment reinforcement at the intermediate supports has negligible effects on the reduction of resultant midspan service moments. The construction sequence was found to have profound influence on the effective continuity. A parametric study on the amount of reinforcement in the deck and cross sectional shape of the girders determined a limit of negative moment reinforcement ratio ρ equal to 0.5 ρ_b to ensure ductile behavior and attainment of maximum girder strength. Two computer programs were also developed from this project. A new simplified program named BRIDGERM was developed using the modified PCA method to calculate the time dependent behavior. Another program BRIDGELL was developed to calculate the live load and impact moments.

Several important conclusions were drawn from this study. It was found that the design and construction of simple span girder bridges made continuous was common at that time, however, construction of positive moment connection at supports was difficult, time consuming and costly. AASHTO specifications for continuous bridge at that time was vague, therefore most of the states used the PCA recommended procedure to design continuous bridges. However, it was noted that the PCA procedure has some uncertainties and does not handle some situation that are known to greatly affect the behavior adequately such as the construction timing and sequence. Experimental results of creep and shrinkage properties of steam cured concrete confirmed that ACI-209 (1992) creep and shrinkage prediction procedure gives reasonably accurate predictions. Another important conclusion was that the positive moment reinforcement does not offer any structural benefit. The magnitude of positive restraint moment that develops at the support depends on the amount of reinforcement at the supports. This positive restraint moment at the support resulting from providing the positive reinforcement increases the resultant

midspan moment of the girder. Furthermore, the restraint moment normally causes cracks at the diaphragm, however, the positive moment reinforcement helps keep the crack widths small. The positive moment reinforcement becomes subjected to compression when the continuity moment becomes negative, thus offering no additional structural benefits. It was also concluded that the construction sequence plays an important role in establishing continuity. High level of positive moment continuity can be obtained if the deck and diaphragm cast were delayed. However, if the delay is too much, considerable negative moments will develop over the supports resulting in an increase in the required level of negative moment reinforcement, which may eventually leads to transverse cracking of the decks. The sequence of deck and diaphragm construction affects the development of restraint moment. If the deck is cast before the diaphragm, it will increase the resultant the positive moment at midspan. Conversely, if the diaphragm is cast before the deck, it will slightly decrease the resultant midspan positive moment. Therefore, it was concluded that there was no major economic advantage to sequencing the casting of deck and diaphragm.

Based on the above conclusions several areas were identified from this study which were recommended for further research. One of the potential areas of research was to use special types of preformed joints over the supports and also to use unbonding of the deck reinforcement and unbonding of the deck to girder interface for a certain length on each side of the girder. Hybrid girder with partial post-tensioning capable of taking more dead load moment in continuous bridges was also identified as an area for further research. The use of special moment connections over the piers to increase the continuity was also suggested. Another important recommendations was to include the temperature and moisture gradient in the deck and girder sections and the effects of support settlement on the behavior of and the design moments for continuous bridges. The effect of establishing continuity on the shear design of continuous girders was also suggested as a future research area.

1.2.2 NCHRP Report 519

The authors of NCHRP Report 322 concluded that positive moment continuity detailing is costly and offers no structural benefit as the positive moment connection restrains the girder ends, which leads to the development of positive moments that must be added to the live load moments at midspan. They also concluded that the maximum positive moment at the midspan is virtually the same whether the girder was designed as simply supported or continuous. However, these conclusions were not universally accepted and many engineers argue that there are still some benefits in converting simple span girder bridges into continuous ones with the help of positive moment connections including helping in arresting the cracks that develop at the diaphragm. There was another inconclusive decision amongst the engineers about the length and number of bent strands or bent bars that extend from girder ends into the continuity diaphragm. Reinforcement congestion in the diaphragm area was also a major concern as it may limit the capacity of the connections due to the inadequate bar interactions with the surrounding concrete. To answer all these questions and to come up with a unified design practice for positive moment connection, a new project (NCHRP Project 12-53) was initiated, from which a final report summarizing the project's findings was published as NCHRP Report 519 (Miller et al. 2004).

Similar to Project 12-29, Project 12-53 started by conducting a survey to determine the various continuity connections used in different states. Experimental tests were then conducted to determine the capacities and behavior of connections with positive moment reinforcement. Design provisions were later drafted and recommended for adoption by the AASHTO LRFD

(2008) specifications to make the simple span girders continuous for live load. The report contains some of the important findings about the continuity detailing that are already in service in different states of USA (Hastak et al. 2003). The survey showed that most of the states, designers and fabricators used some kind of detailing in the continuity diaphragm. Almost every one used extra reinforcements in deck for negative moment continuity. Only one respondent from the survey used special kind of mechanical splice in the flange for the negative moment continuity detailing. The overwhelming response from the survey for positive moment continuity detailing conveyed a strong message about its importance. When looking at the types of detailing used by the different states, it was found that almost half used bent bars and other half used bent strands. Some details used mechanical strand connectors. A majority of the details used overlapping bars or strands, and some used transverse reinforcement through the girder web into the diaphragm. Most of the continuity details were used with I-shaped and bulb-T girders. However, the other girder types were not excluded. The report also states that most of the cases the girders were embedded into the diaphragm, and the depth of embedment varies from 2 inches to more than 12 inches. There were no clear preferences in varying the depth of embedment. However, there were cases where, the girders ends were not embedded into the diaphragm; i.e. girder end was flush to the diaphragm's edge. The survey respondents indicated that the detail was used with girder concrete strengths between 4000 and 9000 psi at 28 days, whereas deck concrete strengths were from 3000 to 5000 psi at 28 days. The use of high performance concrete both in deck and girder was also reported. In most cases, the girders were supported on elastomeric bearing pads, with some cases where it was indicated that the girders were directly placed over the bearing surface.

The construction sequence plays a vital role on the performance of the continuity diaphragm. In most of the cases, the diaphragm and the deck were cast at the same time. Some respondents indicated that their state's practice calls for the diaphragm, or part of it, to be cast before the deck was cast. According to the survey, the minimum girder age before the deck and diaphragm were cast varies from 28 days to 90 days. The report also indicates that the common problems associated with all the cases were the congestion of reinforcement in the diaphragm. There were also problems with the fabrication. Nevertheless, the cost of adding the positive moment continuity detail was found to be insignificant as it was estimated not to exceed 200 dollars per girder.

Based on the answers from the survey about the existing continuity details, the NCHRP 519 research team carried out tests on six different types of detailing on Type II AASHTO stub girders as depicted in Fig. 1-2. All the six tested specimens were subjected to cyclic loadings until failure. The applied load was equivalent to the combination of live loads, time dependent loads (creep and shrinkage), and temperature effects. In Specimen 1, the connection was reinforced with the bent strand, where the prestressing strands were extended at the end of the girder, and then bent 90° upward. Each strand was extended for 26"; of which it was extended straight for 8" from the girder end and then bends upward 90° for another 18". In this test setup, the girder was not embedded into the diaphragm. The girders were kept apart 10" from each other, making the width of the diaphragm 10". When subjected to the cyclic loadings, the specimens survived for 16,000 cycles and then failed. The mode of the failure was splitting type; indicating the slipping and pull out of the strand.

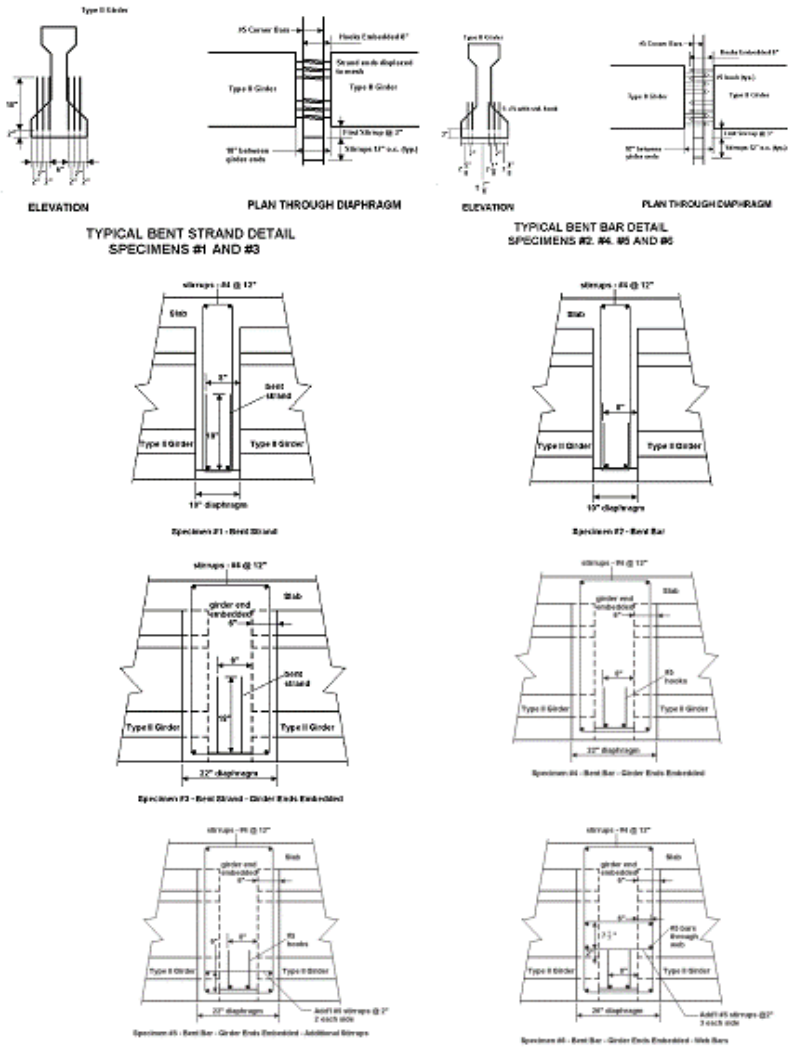

Fig. 1-2 Details of the connections (Miller et al. 2004)

Specimen 2 was similar to Specimen 1 except that bent bars were used for positive moment reinforcement in the connection. The reinforcing bars were extended from the girder end and then bend 90° upward. The bent bars were not symmetrical to make room for concrete. The girder end was not embedded into the diaphragm. When subjected to the cyclic loadings, this specimen was survived for 25,000 cycles before failure. At failure there was a diagonal crack in the faces of the diaphragm, and part of the diaphragm was spalled off. The bras were found fractured due to fatigue. Specimen 3 was identical to Specimen 1 except that the girder ends were embedded into the diaphragm for 6” making the diaphragm width of 22”. The specimen lasted for about 55,000 cycles when subjected to the cyclic loadings before failure. The mode of failure was different than the one observed for Specimen 1. The embedded specimen exhibited cracking and spalling at the face of the diaphragm. Specimen 4 was identical to Specimen 2, except that the girder ends were embedded into the diaphragm by 6”. This specimen lasted only 11600 cycles when subjected to the cyclic loadings. Specimen 5 was identical to the specimen 4 except additional stirrups were placed at the bottom flange close to the outside edge of the diaphragm. The objective of this test was to find whether adding the extra stirrups increases the

capacity of the diaphragm. The specimen survived for 56,400 cycles before failure, and mode of failure was similar to the one observed for Specimen 4. The addition of stirrup did not increase the strength of the connection; however ductility increased, which may be useful in seismic zones. Specimen 6 used the same bent bar configuration of specimen 5, however, additional horizontal bar through the web were used here. This specimen lasted for about 133,000 cycles before failure indicating that this configuration significantly improved the connection. The mode of failure was the fracture of the bar and girders pulling out of the diaphragm.

The finite element (FE) program ANSYS was used to develop a three dimensional FE model for the purpose of evaluating the behavior of positive moment connections. The model was capable of mimicing the nonlinear effects of concrete cracking and crushing as well as yielding of steel bars and strands. The construction sequence plays a vital role in effectively predicting the connection behavior. Relative casting of girder, deck and diaphragm needs to be properly defined. However, it was assumed that the bridge is a continuous superstructure system in the analysis reported in NCHRP Report 519. The cold, or construction, joint at the interface between the girder surface and diaphragm was not modeled in this study. Therefore, the load deflection curve from this finite element study was not able to match with the experimental results. Several improvement of the finite element model were suggested, the construction sequence should be modeled appropriately, cold joint between the girder diaphragm interface which will allow the openings to occur needs to be model.

Based on the research results, the NCHRP Report 519 concluded that positive moment connection with a capacity 20% higher than the cracking moment of the composite section, 1.2 M_{cr} is not efficient. If it is estimated that the positive moment connection is to be subjected to moments exceeding 1.2 M_{cr}, a minimum age of girders should be specified before continuity is established to allow some of the girder creep and shrinkage to take place. Equations developed by Salmons et al (1974) to calculate the number of strands and the length of strands were found adequate and have been adopted in the AASHTO LRFD Bridge Design Specifications. Bent bars were found to have adequate strength if designed such that the embedment of the bar into the girder and the embedment of the hooks into the diaphragm have sufficient length. Girder embedment into the diaphragm reduces the stress in the positive moment area, however due to the cold joint this effect is difficult to quantify. The use of additional stirrups in the diaphragm outside of the girders do not increase the strength of the connection, however it was found that the stirrups increase the ductility of the connection. Placing horizontal bars through the webs of the girders increases the strength and ductility of the connections, however results in significant cracking in the girders which is undesirable. Casting some part of the diaphragm before the deck slab to limit the tensile stress at the bottom is found to be marginally effective. The study also concluded that temperature effects on the system are significant. Daily temperature changes caused end reaction to vary +- 20% per day which is approximately 60% of the positive cracking moment of the section or 2.5 times the positive live load moment. The analytical models treat the joint between the girder and diaphragm as monolithic, however in actual case there is a cold joint in between them. Therefore the analytical model predicts the reduction of continuity only when there the diaphragm cracks. However, the cold joint behaves like a crack in the actual behavior. The report also concludes that the presence of positive moment cracking does not affect the negative moment capacity of the connection with an exception when the positive moment cracking extends into the slab.

1.2.3 Dissertation of Charles D. Newhouse

There are several methods of designing this systems or details used for the continuity connections. To aid the designers in choosing the most appropriate methods, an analytical and experimental study was undertaken at Virginia Tech which was also the research topic for Dr. Charles D. Newhouse's Ph.D. work. Analytical and experimental investigations on different types of continuity connections were carried out and the findings were documented in his dissertation titled, "Design and Behavior of Precast, Prestressed Girders Made Continuous-An Analytical and Experimental Study" (Newhouse 2005).

Analyses were done to compare the difference between the predicted continuity moments resulted from different design methods and assumptions over a wide range of commonly used Precast Concrete Bulb Tee (PCBT) girders with cast in place deck slabs. Results of these analyses were used to develop three different continuity connections using full depth PCBT 45 inch deep girders with 6 ft. wide slab. The first two girders were made continuous with the help of continuity connection at the girder bottom flange by extending the prestressing strands into the diaphragm in one test and using 180 degree bent bars in other test. A third test was performed where only the deck was cast across the top of the girders. The first two girders performed as intended under service, cyclic and ultimate loads. It was observed that the specimen with 180 degree extended bars was stiffer during cyclic loading and thus recommended for use. In the third case, two primary cracks were formed above the ends of the girder during service load testing, after which no significant increase in damage took place. Analytically, it was found that the positive thermal restraint moment may be significant, and the magnitude is almost equal to the positive cracking moment. The experimental study also showed that positive moment develops due to the thermal expansion of deck as well as differential shrinkage between the deck and girder concrete. However, the magnitude of this positive moment is much less than what was predicted analytically.

Four distinct objectives were in this study. First, study three different types of continuity connections, propose an optimal continuity detail, and determine the cracking moment capacity of the proposed connection. Second, investigate the effects of creep shrinkage and temperature on the behavior of the continuity system based on measured shrinkage properties of deck concrete. Third, quantify the effective continuity of each of the connections under different types of loads by monitoring end reactions and member deflections to determine the connection's ability to transfer the moment for each connection. Fourth, develop a structural model that can best predict the behavior of the continuous composite structural system.

The following conclusions were made based on the results presented in the research work. The predicted thermal restraint moment can be significant for most of the girder spacing and span lengths. The thermal restraint moment can be as high as 0.7 to 1.3 times the cracking moment of the sections. Among the currently available design methods, it was concluded that the PCA method is the most conservative in estimating positive restraint moment due to time dependent effects such as creep and shrinkage. It was also found that as the span length decreases the predicted positive restraint moment also generally decreases. At very early age of continuity some method estimates the time dependent restraint moment to be greater than 1.2 times the cracking moment capacity; however, this is true only at early age of continuity. Almost all the methods estimate that if continuity is established after 90 days of girder casting, there will be no positive restraint moment due to time dependent effects.

During the material testing phase it was found that the ACI equation predicting the modulus of rupture $f_r = 7.5(f_c')^{0.5}$ under predicts the modulus of rupture for high strength concrete by an average of 180 psi, where as for lower strength concrete it predicts reasonably well. ACI equations for predicting modulus of elasticity $E = 57000{f_c'}^{0.5}$ predicts modulus of elasticity for high strength girder concrete reasonably well and very well for lower strength deck concrete. The coefficient of thermal expansion for deck and girder concrete appears to be lower than the specified 5.8 $\mu\varepsilon$/°F for typical concrete by the vibrating wire gauge manufacturer. For the girder concrete a value of 4.7 $\mu\varepsilon$/°F and for deck concrete 5.1 $\mu\varepsilon$/°F was recorded. Vibrating wire gauges readings were corrected for the temperature and if the difference between the actual and predicted thermal coefficient is big, it could impart big errors in the readings.

Bed temperatures changes significantly due to the heating or cooling of the steel forms causing the strands to elongate or contract, thus changing the prestressing force prior to casting. In this study a loss of prestress of about 3.6 ksi was recorded prior to the casting of concrete. The actual bed temperature during steam curing may be much higher than the fabricator anticipated temperature. While testing the control cylinder it was noted that an early autogenous shrinkage, where as the girder displays early age expansion due to thermal effects. Locked in mechanical strain due to thermal gradient may be another source of prestress loss in the strands. Measured change in strain during detensioning indicates that the loss of prestress during casting is much less than predicted by other models.

During the static phase it was observed that immediately after casting the deck some positive moment develops at the continuity diaphragm due to the heating of deck concrete which last for about one day. After one day, a negative restraint moment develops and continues to develop rapidly for four days. After four days negative restraint moment develop but at a slower rate. The magnitude of the observed restraint moment is much less than predicted by the conventional analysis. The conventional analysis's ability to predict the restraint moments at the early age is limited. During the static phase, significant compressive strains were measured in the deck reinforcement, indicating shrinkage is taking place at the deck concrete. The reasons between the measured and the predicted restraint moment by different models may be due to the presence of reinforcement in the deck, softening in the continuity diaphragm connection, shrinkage of deck and girder concrete takes place at the same rate, the deck shrinkage at the top of deck is higher than at the bottom of the deck, and the extensibility of the deck concrete reduces the forces on the top of the girder. During the service and cyclic loading phase it was concluded that the initial positive cracking moment capacity at the interface of girder end and diaphragm is lower than the current recommendation in practice. The cold joint form between the diaphragm and girder end may be attributed to this lower positive cracking moment.

Several recommendations were given at the end of this study. It is recommended that the girders should be made continuous with the addition of continuity diaphragm and not with the continuous deck only. This is a result of confirming the continuity diaphragm's ability to transfer moment between adjacent girder ends. The girder end should be detailed to remain flush with the continuity diaphragm, i.e. embedment of the girder end into the diaphragm is not recommended. The continuity diaphragm should be designed for a positive moment due to the factored service load, which should be the maximum of the positive moment due to thermal gradient or due to the creep and shrinkage. It is also suggested that for age of continuity of 60 days, thermal restraint moment dominates.

1.2.4 Stephanie Koch Thesis

After Charles D Newhouse published his dissertation on continuity details on 2005, another research effort was published at Virginia Tech by Stephanie Koch on continuity details. In 2008, she published her thesis "Prestressed PCBT Girders Made Continuous and Composite With a Cast-in-Place Deck and Diaphragm" (Koch 2008), which addressed some of the important questions regarding continuous prestressed girder bridges. The areas of investigation were to find whether Charles D Newhouse proposed detailing works well on other types of girder than that used in the earlier study, the minimum time of storage of the girders before the continuity established so that no adverse positive restraint moment develops at the diaphragms, and also to investigate whether PCA proposed creep coefficient gives the accurate estimation of time dependent restraint moment.

One of the main objectives of Stephanie Koch's thesis was to investigate, whether the PCA method is adequate in estimating the restraint moment that would developed in continuity diaphragms in a continuous prestressed girder bridges. An alternative method known as the Trost-Menn Method or the Separate Section Method (Menn 1986) was used to calculate the restraint moment at the diaphragms due to the time dependent loading of creep and shrinkage. The Separate Section Method is based on the equations of internal equilibriums and compatibility of deformations through the depth of the cross section. The stresses at different locations of the cross sections were estimated using the PCA method and the Separate Section Method and were compared. Two important assumptions were made in the PCA method calculations. First, the differential shrinkage between the deck and girder were ignored; and second, the creep coefficient of girder and deck were assumed equal. Different combinations of parameters were used (Different PCBT Girders, span length, girder spacing and strand pattern) and stresses were compared between the two analytical approaches. In all of the cases it was found that the PCA method overestimates the restraint moment. Therefore it was concluded that the PCA method is well capable of estimating restraint moment of any composite section. The study was further advanced to find out the appropriate creep coefficient for the PCA method which will produce restraint moment that matches the restraint moment well calculated from the Separate Section Method. A parametric study was conducted and creep coefficient of 1.8 was found to give restraint moment from PCA method very similar to that of the Separate Section Method. Another study was carried out to introduce two different creep coefficients for girder and deck concretes to be used in the PCA method.

Several important recommendations resulted from the study. One of which is the importance of finding a more accurate creep coefficient for determining the stresses in composite systems using the PCA method. Using different deck and girder concrete creep coefficient produced inaccurate results. Aging factors has a significant impact on the creep coefficient in the PCA method and consideration of additional aging coefficient was recommended. It is also recommended that the available models for determining long term effects rely on creep and shrinkage parameters that need to be updated based on recent material information. Most of the current models were developed when typical concrete strengths were fairly low and the applicability of these models to high strength concrete is in doubt. Nowadays, concrete constituent components and admixtures that is considerably different than in the past. Therefore new models need to be developed to analyze more modern concrete.

1.3 Time Dependent Deformation Models for Prestressed Concrete

Two types of deformation take place in the concrete. One is change in volumetric strain without the influence of any externally applied stress. This type of deformation is also known as the shrinkage of concrete. Another type is the change in strain subjected to sustained stress. This type of deformation is known as creep. Both the shrinkage and creep are time dependent phenomena and are responsible for some adverse effects (excessive deflection, development of secondary restraint moment, and cracking of concrete) on concrete in general and prestressed girder bridges in particularly. In order to mitigate these adverse effects, the designer needs to know how the structure would behave over time. There are several analytical models which can predict time dependent effects. This section shed lights on some of the available analytical models that can be used to predict the time dependent phenomenon of concrete.

1.3.1 ACI-209

ACI Committee 209 (1992) proposed equations for the determination of creep strain, elastic strain and the total strain at any time. The ultimate creep coefficient and the shrinkage strain are determined using the properties and mix proportion of concrete and then later modified by appropriate time ratio to the creep strain and shrinkage strain at any desired time. The total strain is the summation of creep strain and the elastic strain, and the ultimate creep coefficient is the ratio of creep strain to the elastic strain. The total strain is given as:

$$\varepsilon_t = (\varepsilon_{sh})_t + \frac{\sigma}{E_0}(1 + \nu_t) \tag{1-1}$$

where E_0 is the modulus of elasticity of the concrete at the time of loading, σ is the applied stress and ν_t the creep coefficient is for any time for moist cured concrete for 7 days or steam cured concrete for 1-3 days is given as:

$$\nu_t = \frac{t^{0.60}}{10+t^{0.60}}\nu_u \tag{1-2}$$

where ν_t is the creep coefficient at any time t, and ν_u is the ultimate creep coefficient determined as:

$$\nu_u = 2.35\gamma_c \tag{1-3}$$

where $\gamma_c$is the product of the correction factors for loading age γ_{la}, ambient relative humidity γ_λ, size γ_{vs}, and concrete composition including slump γ_s, fine aggregate percentage γ_ψ, and air content γ_α.

The shrinkage strain after 1-3 days for steam cured concrete is determined as:

$$\varepsilon_{sht} = \frac{t}{55+t}\varepsilon_{shu} \tag{1-4}$$

where ε_{sht} is the shrinkage strain at any time t, and ε_{shu} is the ultimate shrinkage strain given as:

$$\varepsilon_{shu} = 780\gamma_{sh} \times 10^{-6} \tag{1-5}$$

where $\gamma_{sh}$is the product of the correction factors for ambient relative humidity γ_{λ}, size γ_{vs}, and concrete composition including slump γ_{s}, fine aggregate percentage γ_{ψ}, cement content $\gamma_{c}$and air content γ_{a}.

The correction factors for ultimate creep coefficient and shrinkage strain are given as follows:

The loading age correction factor for concrete creep, γ_{la}, is given as follows for steam cured concrete of ages 1-3 days:

$$\gamma_{la} = 1.13 t_{la}^{-0.094} \tag{1-6}$$

where $t_{la}$is the loading age in days.

The correction factor for ambient relative humidity, is given as follows for creep calculations for relative humidity greater than 40%:

$$\gamma_{\lambda} = 1.27 - 0.0067\lambda \tag{1-7}$$

The corresponding correction factor for shrinkage calculations is given as:

$$\gamma_{\lambda} = \begin{cases} 1.40 - 0.010\lambda & \text{for } 40 \leq \lambda \leq 80 \\ 3.00 - 0.030\lambda & \text{for } 80 \leq \lambda \leq 100 \end{cases} \tag{1-8}$$

where λ is the relative humidity in percent.

The size correction factor depends on the volume to surface ratio of the member. For members with volume to surface ratio other than 1.5 the correction factor γ_{VS} for creep is given as:

$$\gamma_{vs} = \frac{2}{3}\left(1 + 1.13 e^{-0.54V/S}\right) \tag{1-9}$$

and the corresponding correction factor for shrinkage calculations is given as:

$$\gamma_{vs} = 1.2 e^{-0.12V/S} \tag{1-10}$$

The correction factor for concrete composition is often hard to quantify because the concrete composition during the design phase is often unknown, and in most cases these factors are not excessive and tend to offset each other, and therefore, are often neglected. The correction factor for concrete slump for creep is given as:

$$\gamma_{s} = 0.82 + 0.067s \tag{1-11}$$

And for shrinkage correction factor for concrete slump is given as:

$$\gamma_{s} = 0.89 + 0.041s \tag{1-12}$$

where s is the slump of the concrete in inches.

The correction factor for fine aggregate percentage in concrete for creep is given as:

$$\gamma_{\psi} = 0.88 + 0.0024\psi \tag{1-13}$$

And for shrinkage, the correction factor for fine aggregate percentage is given as:

$$\gamma_{\psi} = \begin{cases} 0.30 + 0.014\psi & for\ \psi \leq 50\% \\ 0.90 + 0.002\psi & for\ \psi > 50\% \end{cases} \quad (1\text{-}14)$$

where ψ is the ratio of fine aggregate to the total aggregate of the concrete weight expressed in percent.

Correction factor for cement content in the concrete for shrinkage is given as:

$$\gamma_c = 0.75 + 0.00036c \quad (1\text{-}15)$$

where c is the cement content in pounds per cubic yards. The effect of cement content on the creep is very negligible, thus ACI Committee 209 does not recommend including this correction factor for concrete creep.

Finally, the creep correction factor for air content in concrete is given as:

$$\gamma_{\alpha} = 0.46 + 0.09\alpha \geq 1.0 \quad (1\text{-}16)$$

And the corresponding value for shrinkage is given as:

$$\gamma_{\alpha} = 0.95 + 0.008\alpha \quad (1\text{-}17)$$

where α is the air content in concrete in percent.

1.3.2 PCI Bridge Design Manual:

The PCI Bridge Design Manual (PCI-BDM) (Mattock 1961) makes recommendations for the determination of creep coefficient and shrinkage strain for concrete at any time. There are two methods, the first is based on the recommendation of ACI-209 and is applicable to concrete of compressive strength 3-5 ksi. The second method is based on the modifications of ACI-209 by Huo (1997) and is applicable to concrete compressive strength of 4-12 ksi. In the first method when the concrete strength is 3-5 ksi, the creep coefficient at any time, t, is given as:

$$C_{t,t_0} = \frac{(t-t_0)^{0.6}}{10+(t-t_0)^{0.6}} C_u \quad (1\text{-}18)$$

where t_0 is the time of application of prestress and C_u is the ultimate creep coefficient, which is given as

$$C_u = 1.88k_c \quad (1\text{-}19)$$

where k_c is the correction factor for loading age. The shrinkage strain for 1-3 days of steam cured concrete and strength of 3-5 ksi is given as:

$$S_{t,t_0} = \frac{(t-t_0)}{55+(t-t_0)} S_u \quad (1\text{-}20)$$

where

$$S_u = 545k_{sh} \times 10^{-6} \quad (1\text{-}21)$$

where k_{sh} is the correction factor for the average relative humidity k_h and size of the member k_s. The creep coefficient for concrete with compressive strength in the range between 4 and 12 ksi is given as:

$$C_{t,t_0} = \frac{(t-t_0)^{0.6}}{(12-0.5f_c')+(t-t_0)^{0.6}} k_{st} C_u \quad (1\text{-}22)$$

for which

$$k_{st} = (1.18 - 0.045f_c') \quad (1\text{-}23)$$

where f_c' is the 28-day concrete compressive strength in ksi, and k_{st} is the correction factor accounting to the fact that high strength concrete less creep. The shrinkage strain for concrete of compressive strength 4-12 ksi is given as:

$$S_{t,t_0} = \frac{(t-t_0)}{(65-2.5f_c')+(t-t_0)} k_{st} S_u \quad (1\text{-}24)$$

where

$$k_{st} = 1.2 - 0.05f_c' \quad (1\text{-}25)$$

The correction factor for concrete loading age k_{la} for creep is given as:

$$k_{la} = 1.13(t_{la})^{-0.094} \quad (1\text{-}26)$$

where t_{la} is the loading age in days. The correction factor for relative humidity for concrete creep is given as:

$$k_h = 1.586 - 0.0084H, \qquad for\ 40 \le H \le 100 \quad (1\text{-}27)$$

The correction factor for relative humidity for concrete shrinkage is given as:

$$k_h = \begin{cases} 2.000 - 0.0143H & \text{for} \quad 40 \le H \le 80 \\ 4.286 - 0.0429H & \text{for} \quad 80 < H \le 100 \end{cases} \quad (1\text{-}28)$$

Correction factor for size of the member for concrete creep is given as:

$$k_s = \frac{2}{3}\left(1 + 1.13e^{-0.54V/s}\right) \quad (1\text{-}29)$$

and for concrete shrinkage is given as:

$$k_s = 1.2e^{-0.12V/s} \quad (1\text{-}30)$$

1.3.3 AASHTO LRFD

AASHTO LRFD allows designers to use both the CEB-FIP code model and ACI-209 model in the articles 5.4.2.3.2 and 5.4.2.3.3 of the specifications for the concrete creep coefficient and shrinkage strain (AASHTO 2008). The creep coefficient and shrinkage strain

model are taken from Collins and Mitchell (1991), which is a modified version of the ACI 209 model based on the more recent data. Here the creep coefficient is given as:

$$\psi(t,t_i) = 3.5k_c k_f \left(1.58 - \frac{H}{120}\right) t_i^{-0.118} \frac{(t-t_i)^{0.6}}{10.0+(t-t_i)^{0.6}} \qquad (1\text{-}31)$$

where

$$k_f = \frac{1}{0.67+\left(\frac{f_c'}{9}\right)} \qquad (1\text{-}32)$$

and

$$k_c = \left[\frac{\frac{t}{26e^{0.36V/S}+t}}{\frac{t}{45+t}}\right] \frac{1.80+1.77e^{-0.54V/S}}{2.587} \qquad (1\text{-}33)$$

where k_c is a factor that accounts for effect of the member's volume to surface ratio and k_f is the factor for the concrete compressive strength, H represents the relative humidity in percent, and t_i is the concrete maturity at the time the creep causing load is applied in days. For concrete maturity, one day of accelerated steam curing is taken as equivalent to seven days of moist curing. In the above equations, t represents the concrete maturity at which the creep coefficient is desired. The shrinkage strain ε_{sh}, at any time t, is given by the following equation:

$$\varepsilon_{sh} = -k_s k_h \left(\frac{t}{55+t}\right) 0.56 \times 10^{-3} \qquad (1\text{-}34)$$

where k_s is the size factor of the member and is given as:

$$k_s = \left[\frac{\frac{t}{26e^{0.36V/S}+t}}{\frac{t}{45+t}}\right] \left[\frac{1064-94V/S}{923}\right] \qquad (1\text{-}35)$$

and k_h is a factor account for the relative humidity and is given as:

$$k_h = \begin{cases} \frac{140-H}{70} & \text{for } H < 80\% \\ \frac{3(100-H)}{70} & \text{for } H \geq 80\% \end{cases} \qquad (1\text{-}36)$$

1.3.4 CEB-FIP-90

The CEB-FIP (1990) model gives recommendations for the determining the concrete creep coefficient and shrinkage strain. These recommendations are applicable to concrete with compressive strengths ranging from 1,700 psi to 11,600 psi and subjected to compressive stresses less than 40% of the strength at the application of the load causing creep. Relative humidity should be 40 to 100% and the range of temperature 41 to 86°F. First, the notional creep coefficient, ϕ_0 and the notional shrinkage strain, ε_{cs0} are determined from the concrete properties. The concrete creep coefficient, $\phi(t,t_0)$ and shrinkage strain, $\varepsilon_{cs}(t,t_0)$ at any time, t, are then determined using appropriate time step. The total strain is given as:

$$\varepsilon(t) = \varepsilon_{cs}(t,t_0) + \sigma\left[\frac{\phi(t,t_0)}{E_c} + \frac{1}{E_c(t_0)}\right] \qquad (1\text{-}37)$$

where t_0 is the time of application of load, $E_{c(t_0)}$ is the modulus of elasticity of concrete at the time of application of load and E_c is modulus of elasticity of concrete and given as:

$$E_c = 3{,}117{,}500\left(\frac{f_{cm}}{1{,}450}\right)^{1/3} \tag{1-38}$$

where f_{cm} is the mean compressive strength of the concrete in psi, and if not known can be taken as:

$$f_{cm} = f_c' + 1200 \quad psi \tag{1-39}$$

The creep coefficient at any time is given as:

$$\phi(t, t_0) = \phi_0 \beta_c (t - t_0) \tag{1-40}$$

where ϕ_0 is the notional creep coefficient and $\beta_c(t - t_0)$ is the development of creep over time. The notional creep coefficient is given as:

$$\phi_0 = \phi_{RH} \beta(f_{cm}) \beta(t_0) \tag{1-41}$$

where

$$\phi_{RH} = 1 + \frac{1 - {RH}/{100}}{0.46\left({h}/{4}\right)^{1/3}} \tag{1-42}$$

is the correction factor for the relative humidity, where h is 2 times member cross sectional area divided by the perimeter in contact with the environment. The correction factor for the concrete compressive strength is given as:

$$\beta(f_{cm}) = \frac{5.3}{\left({f_{cm}}/{1{,}450}\right)^{0.5}} \tag{1-43}$$

The correction factor for concrete maturity at the application of creep causing load for which one day of steam curing is equivalent to seven days of normal moist curing is given as:

$$\beta(t_0) = \frac{1}{0.1 + t_0^{0.2}} \tag{1-44}$$

Development of creep with time is given as:

$$\beta_c(t - t_0) = \left[\frac{t - t_0}{\beta_H + (t - t_0)}^{0.3}\right] \tag{1-45}$$

where β_H is the correction factor for humidity and is given as:

$$\beta_H = 150[1 + (0.012RH)^{18}]\frac{h}{4} + 250 \leq 1500 \tag{1-46}$$

The shrinkage strain is given as a function of time as:

$$\varepsilon_{cs}(t - t_0) = \varepsilon_{cs0} \beta_s (t - t_s) \tag{1-47}$$

where ε_{cs0} is the notional shrinkage strain and given as:

$$\varepsilon_{cs0} = \varepsilon_s(f_{cm})\beta_{RH} \quad (1\text{-}48)$$

where

$$\beta_{RH} = -1.55\left[1 - \left({}^{RH}/_{100}\right)^3\right] \quad (1\text{-}49)$$

and

$$\varepsilon_s(f_{cm}) = \left[160 + 10\beta_{sc}\left(9 - \frac{f_{cm}}{1450}\right)\right] \times 10^{-6} \quad (1\text{-}50)$$

where β_{sc} is the factor accounting the types of cement used in the concrete, a value of 4 is used for slow hardening cement, 5 for normal or rapid hardening cement, and a value of 8 for rapid hardening high strength cement.

$\beta_s(t - t_s)$ is the development of shrinkage over time and is given as:

$$\beta_s(t - t_s) = \sqrt{\frac{(t - t_s)}{\left[350\left(\frac{h}{4}\right)^2 + (t - t_s)\right]}} \quad (1\text{-}51)$$

1.3.5 NCHRP 496

NCHRP commissioned a research project (Project 18-07) to develop prestress loss models in high strength pretensioned concrete bridge girders. The project resulted in a new prestress loss model, which was published in NCHRP Report 496 (Tadros et al. 2003). In addition to the prestress loss models, expressions for creep and shrinkage are also presented here. These expressions for creep and shrinkage are similar to those presented by ACI-209 with the modifications of components and correction factors based on more recent data. The creep coefficient is defined as the ratio of creep strain at any time after loading t, to the elastic strain at the time of loading, t_i and is given as:

$$\psi(t, t_i) = 1.90\gamma_{cr} \quad (1\text{-}52)$$

where γ_{cr} is the product of five correction factors and is given as:

$$\gamma_{cr} = k_{td}k_{la}k_sk_{hc}k_f \quad (1\text{-}53)$$

The first factor, k_{td}, is a time development correction factor and is given as:

$$k_{td} = \frac{t}{61 - 4f'_{ci} + t} \quad (1\text{-}54)$$

where f'_{ci} is the concrete strength at release in ksi. k_{la} is a correction factor for the loading age for which seven days of moist curing is equivalent to one day of accelerated curing and is given as:

$$k_{la} = t_i^{-0.118} \quad (1\text{-}55)$$

The size correction factor, k_s, is given as:

$$k_s = \frac{1064 - 94^{V}/_{S}}{735} \quad (1\text{-}56)$$

where $^{V}/_{S}$ is the volume to surface ratio in inch. The correction factor for humidity is given as:

$$k_{hc} = 1.56 - 0.008H \quad (1\text{-}57)$$

where H is the relative humidity in percent. Correction factor for concrete strength is given as:

$$k_f = \frac{5}{1 + f'_{ci}} \quad (1\text{-}58)$$

Concrete shrinkage strain is given as:

$$\varepsilon_{sh} = 480 \times 10^{-6} \gamma_{sh} \quad (1\text{-}59)$$

where

$$\gamma_{sh} = k_{td} k_s k_{hs} k_f \quad (1\text{-}60)$$

where k_{td}, k_s and k_f are same as creep and k_{hs} is the correction factor for humidity for shrinkage and is given as:

$$k_{hs} = 2.00 - 0.0143H \quad (1\text{-}61)$$

1.4 Temperature Effects on the Continuous Superstructure

Bridge superstructures, whether simply supported or continuous, will contract or elongate uniformly when subjected to a uniform temperature field. This scenario rarely happens in bridges and more often different parts of the bridge are heated, or cooled, differently. In general, a bridge superstructure will be subjected to a temperature gradient; i.e. the top and bottom of the bridge will be subjected to different temperature levels. In the case of a simply supported bridge, the temperature gradient induces primary stresses as a result of the cross section's maintaining its planar geometry while subjected to different temperature. Additional secondary stresses develop in continuous structures when they become subjected to temperature gradients. The secondary stresses are the result of the indeterminacy imposed by the boundary conditions. This secondary stress when combined with other stresses may have detrimental effects on the structure. Thus temperature gradient effect needs to be accounted for in the design phase of the bridge superstructures, especially continuous ones. A detailed description of the procedure to determine the temperature field from the available atmospheric data and geographical locations is presented in this research. Determination of temperature induced primary stresses and restraint moments and its effect on the structural component are also presented.

1.5 Research Objectives

The main objective of this dissertation is to investigate the global and local behavior of prestressed concrete girder bridges made continuous with positive moment continuity details. More specifically, three major factors were the focus of this research effort. They are:

- The effects of the temperature field on continuous prestressed concrete girder bridges,
- The creep behavior of prestressed concrete girder bridges, and
- The behavior of prestressed concrete girder bridges made continuous with positive moment continuity details under live loads

To achieve the goals of the study, analytical, health monitoring and finite element analysis were employed. Data from a long term health monitoring project will be utilized to evaluate the performance of the NCHRP 519 proposed positive moment continuity detailing, and to validate numerical and analytical models to be used in the evaluation. Furthermore, a live load test is conducted to evaluate the performance of the detailing under service condition. Full, girder line, and joint 3-D finite element models will be developed to investigate the behavior. The full model will be the tool for assessing the live load performance from a global perspective. The girder line model, which will be calibrated using field data, will be used to understand the creep behavior of precast prestressed concrete girders made continuous, its long term deformation, the corresponding restraint moment that develop at the continuity diaphragm as a result of these deformations. A joint model will be used to understanding the force transfer mechanism and to determine the effective composite cross section that would be used in the cracking moment calculation of the section. Finally, an analytical model that can predict the temperature field using meteorological data will be used to determine the temperature gradient, which will also be compared to field measured temperatures. The temperature induced restrained moment will also be estimated based on the observed gradients.

1.6 Overview of the Dissertation

A brief summary of each chapters of this dissertation is described in the following. Chapter 2 describes the health monitoring system of a three span continuous bridge. The objectives of the monitoring, time line, types of sensor used, challenge faced during monitoring as well as preliminary readings from different sensors are presents in this chapter. Chapter 3 describes the results from the health monitoring as well as the evaluated performance of the continuity details. Analytical model to predict the temperature field and temperature induced restraint moment at the continuity diaphragm are presented in Chapter 4. Calibrated finite element creep model that predicts the long term deformation of prestressed girder bridges is presented in Chapter 5.Chapter 6 describes the field live load test as well as the full scale 3-D finite element model. A detailed finite element joint model that shows the load transfer mechanism at the continuity diaphragm as well as effective composite section is presented in Chapter 7. Finally the conclusion and the future recommendations are presented in Chapter 8.

1.7 Reference List

AASHTO (2008). "LRFD Bridge Design Specifications." American Association of State Highway and Transportation Officials, Washington, D.C.

ACI (1992). "Prediction of creep, shrinkage and temperature effects in concrete structures." Manual of Concrete Practice, ACI 209R-92. American Concrete Institute, Farmington Hills, MI.

Collins, T. M., and Mitchell, D. (1991). "Prestressed Concrete Structures." Prentice Hall, Ebglewood Cliffs, NJ.

Comite Euro-Internationale Du Beton (CEB) (1990). "CEB-FIP model code 1990." *Rep. No. Buletin D'Information No. 213/214*, Lausanne, Switzerland.

Hastak, M., Mirmiran, A., Miller, R. A., Shah, R., and Castrodale, R. (2003). "State of Practice for Positive Moment Connections in Prestressed Concrete Girders Made Continuous." *Journal of Bridge Engineering*, 8(5), 267-272.

Huo, X. S. (1997). "Time-dependent analysis and application of high performance concrete in bridges." Ph.D Dissertation, Department of Civil Engineering, University of Nebraska.

Koch, S. (2008). "Prestressed PCBT Girders Made Continuous and Composite with a Cast-in-Place Deck and Diaphragm." M.S. Thesis, Virginia Polytechnique Institute and State University, Virgina, USA.

Mattock, A. H. Precast-Prestressed Concrete Bridges, 5. Creep and Shrinkage Studies. 1961.

Menn, C. (1986). "Prestressed Concrete Bridges." Springer-Berlag,Wein., Viena, Austria.

Miller, R. A., Castrodale, R., Mirmiran, A., and Hastak, M. (2004). "Connection of Simple-Span Precast Concrete Girders for Continuity." *Rep. No. NCHRP Report 519*, Transportation Research Board, Washington, D.C.

Newhouse, C. D. (2005). "Design and Behavior of Precast, Prestressed Girders Made Continuous- An Analytical and Experimental Study." Ph.D. Dissertation, Virginia Polytechnique Institute and State University, Virginia, USA.

Oesterle, R. G., Glikin, J. D., and Larson, S. C. (1989). "Design of Precast Prestressed Bridge Girders Made Continuous." *Rep. No. NCHRP Report No. 322*, Transportation Research Board, Washington, D.C.

Salmons, J. R., and May, G. W. (1974). "Strand Reinforcing for End Connection of Pretensioned I-Beam Bridges." *Rep. No. Interim Report 73-5B*, Missouri Cooperative Highway Research Program, Missouri State Highway Department.

Tadros, M. K., Al-Omaishi, N., Seguirant, S. J., and Gallt, J. G. (2003). "Prestressed losses in pretensioned high-strength concrete bridge girders." *Rep. No. NCHRP Report 496*, Transportation Research Board, Washington, D.C.

2 A LONG TERM MONITORING SYSTEM FOR PERFORMANCE EVALUATION OF POSITIVE MOMENT CONTINUITY DETAIL IN PRESTRESSED GIRDER BRIDGES

2.1 Introduction

Longer, more efficient and optimum designs have always been the goal and priority of bridge engineers. Use of new materials, developing new structural systems, and improving construction details are some of the approaches used to achieve this goal. In bridge construction, several alternative systems and materials compete. The prestressed girder bridge alternative is one of the most popular ones today as it offers many advantages such as ease of construction and durability. The prestressed girders are usually precast off site and transported for erection before pouring composite decks. Thus, the full continuity between adjacent girders has generally been sacrificed for the sake of ease of construction. Several methods for achieving continuity between adjacent girders have been proposed. The behavior of bridge continuity detail has been studied by several researchers. The majority of the work addresses full integration techniques as opposed to partial integration. For example, Loveall (1985) and Wasserman (1987) reported their experience with jointless bridge decks over continuous girders. Oesterle et al. (1989) published a comprehensive study on converting precast prestressed concrete girders into a continuous system. Russel and Gerken (1994) wrote about the knowns and unknowns of jointless bridges. Burke, Jr. (1992) discussed the attributes and limitations of integral bridges. He also demonstrated some of the adverse effects of full bridge integration due to the buildup of stresses in concrete pavements (2004). Alampalli and Yannotti (1998) surveyed the integral and jointless-deck bridge inventory in the State of New York, US, indicating that their performance is as designed. They recommended some new details for future projects to avoid some of the problems noted in the existing bridges. Thippeswamy et al. (2002) also evaluated the performance of in-service jointless bridges and performed analytical studies of the bridges based on which design recommendations were drawn (1995).

Documentation of bridges that have been constructed or rehabilitated using one of the mentioned approaches can also be found in the literature. Repair of the Story Bridge in Australia by eliminating construction joints were also reported by Demartini and Haywood (1991). A redecking case study where joints were eliminated was reported by Pierce (1991). The construction of a demonstration bridge with jointless decks in North Carolina, US, was reported by Caner and Zia (1998). Caner et al. (2002) also demonstrated the positive performance of bridges with jointless decks in seismic zones using existing bridges in Turkey. More recently, Wing and Kowalsky (2005) reported the results obtained from monitoring an instrumented jointless bridge with debonded link slabs that was constructed as a pilot bridge in North Carolina. Long-term effects were also investigated by several researchers (Burke, Jr. 1994; Siros and Spyrakos 1995). The results from these studies indicate that within certain limits, long-term effects may be ignored. This finding simplifies the analysis considerably. Several methods for the analysis of jointless deck systems were proposed (Caner and Zia 1998; Gastal and Zia 1989; Richardson 1989; Zia et al. 1995). Most of these methods are based on the finite element method, where researchers developed special computer code to incorporate the specifics of the jointless deck problem in the analysis. Okeil and El-Safty (2005) developed a simplified analysis method for jointless bridges, where an upper and a lower bound support configurations were

considered. Closed form expressions were derived and used to develop design tables that eliminate the need for computationally intensive finite element analysis.

Recently, NCHRP Project 12-53 investigated a positive moment continuity detail for prestressed girder bridges. The findings of the project were published in NCHRP Report 519 (Miller et al. 2004), which presents the results from the experimental program, the recommended details, and analysis method. The recommended detail calls for positive moment reinforcement to extend from the girder ends at the bottom. Thus, creating a mechanism for transferring the tensile forces that would develop at the supports of a continuous girder due to live loads at far way spans, and more importantly, due to long term effects such as creep and temperature changes as depicted in Fig. 2-1.

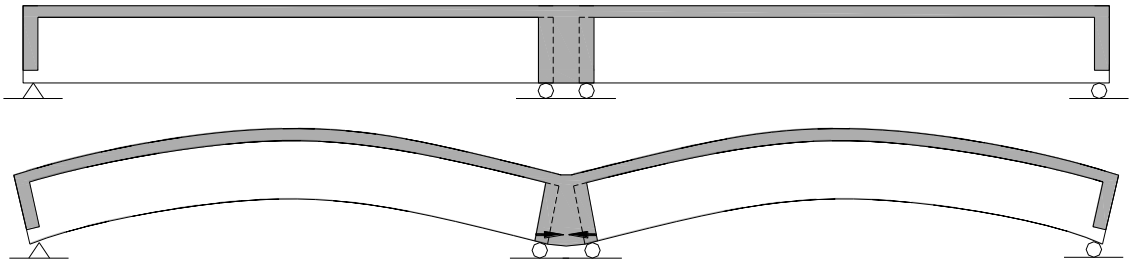

Fig. 2-1 Development of positive moment in bridge connections with continuity diaphragm due to long-term effects

In addition to allowing for the more efficient designs (longer spans, fewer strands, etc.), adequate design of the positive moment continuity may reduce the potential problems associated with continuity diaphragms such as cracking and spalling. The NCHRP Report 519 (Miller et al. 2004) recommends the use of positive moment reinforcement in the form of additional hairpin bars, or simply extending the prestressing strands out of the girder's bottom flange. Fig. 2-2 shows the two alternatives recommended in the report.

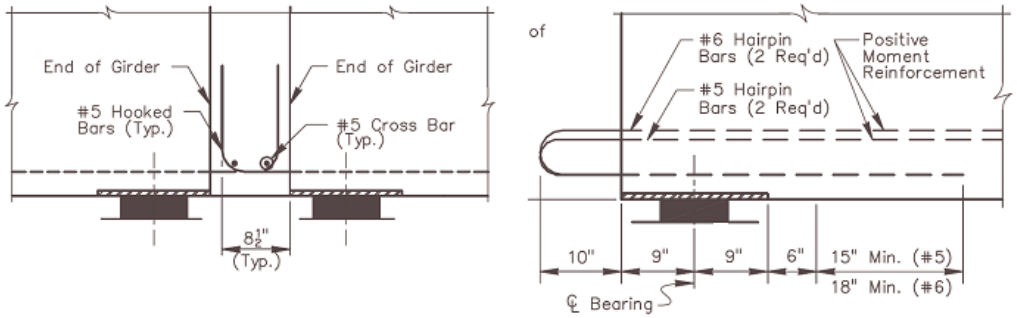

90 ° bend hooked bars or prestressing strands 180 ° bend hairpin bars

Fig. 2-2 Alternative positive moment reinforcements at the continuity diaphragm proposed by the NCHRP Report 519(Miller et al. 2004)

The newly constructed John James Audubon Bridge connects the cities of Saint Francisville and New Roads in Louisiana across the Mississippi River. The designer adopted the NCHRP 519 positive moment continuity detail with hairpin bars for the slab on prestressed concrete girder approach spans. This detail is different than the current standard used in

Louisiana Department of Transportation and Development (LA-DOTD) Bridge Design Manual. Furthermore, one of the bridges with the new detail utilizes Bulb-T girders and is skewed, which is not covered in the scope of the experimental program conducted as part of NCHRP Project 12-53. Thus, it was decided to monitor the performance of that bridge. This paper presents details of the monitoring system developed for this project. Preliminary results of strains and temperatures from the casting yard as well as from the bridge site are also presented.

2.2 Details of the Monitored Bridge

The LA-DOTD Bridge Design Section chose a segment from one of the approach bridges to the main span of the new John James Audubon Bridge for evaluating the performance of the new continuity detail. The chosen segment is part of Bridge #2, which consists of 52 spans with a total length of about 1200 m divided into 14 continuous segments. The DOTD chose a 3-span continuous span with a total length of 73.76 meters [242 feet]. The segment's middle and longest span (31.09 meters [102 feet]) is skewed to accommodate an existing railway track. As a result of the 45^{o}-skew of the middle span, the girders supporting the exterior spans ranged in length from 15.54 meters [51 feet] to 27.13 meters [89 feet]. AASHTO Bulb-T girders (BT-72) have been used for the construction of this segment of Bridge #2. This segment was chosen because of its configuration, which has not been covered by the tests conducted in NCHRP Project 12-53; namely skewed configuration and Bulb-T girders. The span and girder layout of the monitored bridge section is shown in Fig. 2-3. Only one of the identical intermediate bents (Bent 24) was chosen to monitor the performance of the new continuity detail taking advantage of the anti-symmetric layout under uniform loading conditions (e.g. long-term effects) as can be seen in Fig. 2-3.

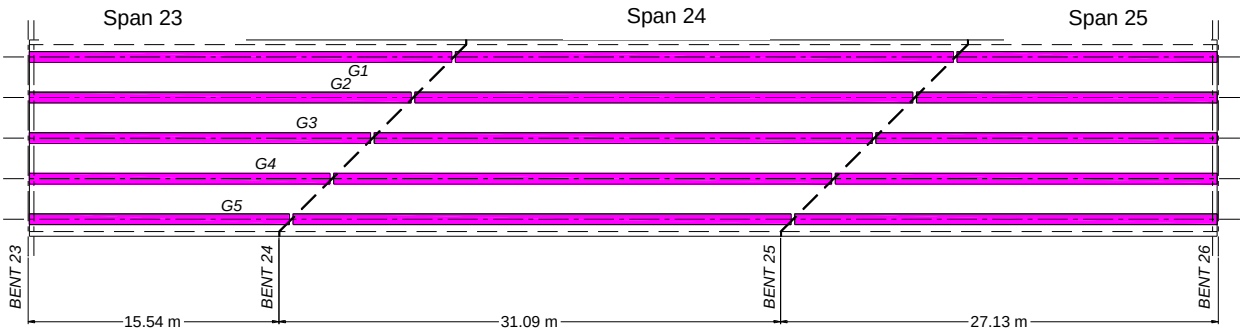

Fig. 2-3 Span and girder layout for monitored segment of Bridge #2 showing anti-symmetry

Fig. 2-4-a shows Bent 24 of the monitored segment of Bridge #2. It supports a clear roadway width of 11.58 meters [38 feet] on five prestressed BT-72 girders, spaced at 2.51 meters [8'-3"]. The 19.5-cm [7.5-inch] reinforced concrete deck was monolithically cast with the continuity diaphragm joining adjacent girders over intermediate bents. The cross-sectional dimensions of the segment are shown in Fig. 2-4-b. Positive moment reinforcement in the form of five #5 hairpin bars (see Fig. 2-4-c) extending out of the bottom flange was chosen by the designer. It should be noted that the girders are supported by rubber bearing pads over a typical pile bent supported on 61-cm [24-inch] square prestressed concrete piles.

2.3 Monitoring System

The performance measures to be used for evaluating the continuity detail were first identified prior to designing the monitoring system. Based on the similar work in literature ,it was deemed necessary that the monitoring system should be capable of capturing: (1) the tensile force in the positive moment reinforcement in the diaphragm, (2) the strain distribution at key locations (at intermediate bent and at midspan), (3) differential shrinkage between cast-in-place (CIP) deck and precast girders, (4) degree of continuity between adjacent girders, (5) the development of cracks or gaps at the continuity diaphragm, and finally (6) the corresponding temperature for each of the recorded readings.

(a) View of Bent 24 of the monitored bridge segment.

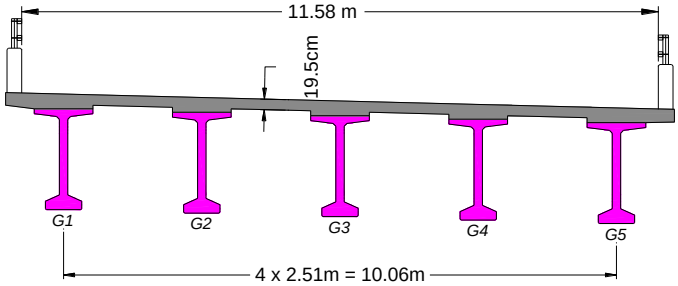

(b) Cross section of monitored bridge segment

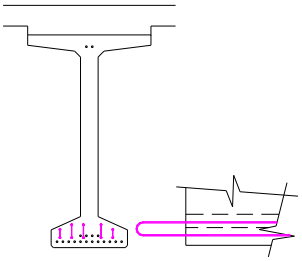

(c) Hairpin bars used for positive moment reinforcement

Fig. 2-4 Completed and sectional view of the monitored bridge (Bridge #2)

2.3.1 Sensor Types and Datalogger

In choosing the type of sensors to capture the aforementioned engineering quantities, it was kept in mind that the monitoring system should be robust such that the failure of some sensors should not jeopardize the entire project. Therefore, redundant and different sensor types were employed to capture behavioral aspects that can be used to interpret the same engineering quantity. Furthermore, because of the importance of the initial setting period for the girders prior to erection at the project site and pouring the continuity diaphragm, embedded sensors were

installed to monitor creep and shrinkage strains from the first day after casting the girders. In all, 66 sensors were chosen for the job. All chosen sensors are vibrating wire gages that are particularly suited for long-term monitoring since they do not suffer from drifting (Bordes and DeBreuille 1985; Choquet et al. 1999). Another advantage of using vibrating wire gages is that they provide temperature readings corresponding to each recorded sensor reading. Temperature is important for two reasons: (1) temperatures are needed for correction of recorded gage readings following the manufacturer's recommendations, and (2) temperature distribution within the structural elements is needed for understanding the long-term behavior of the bridge.

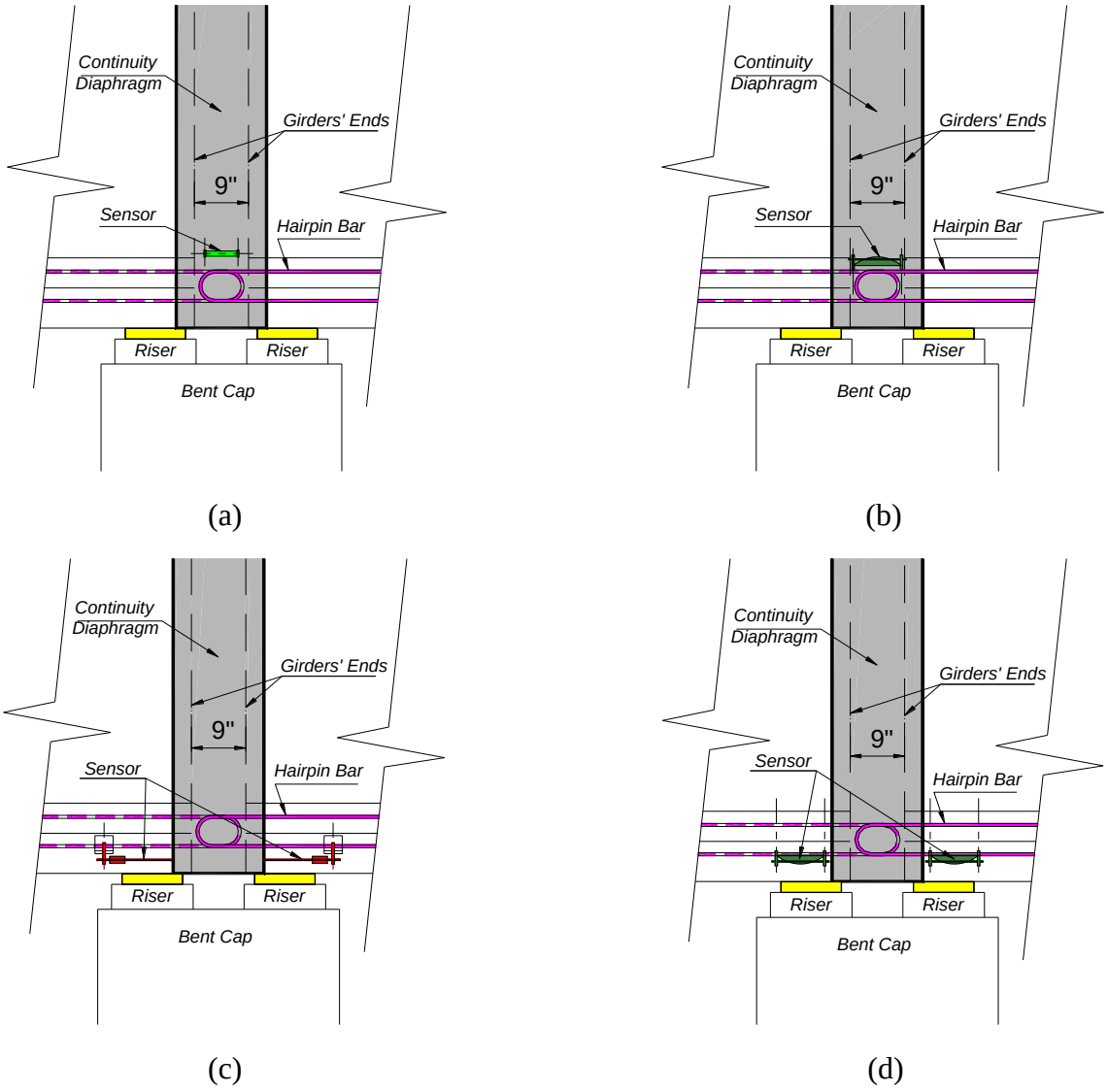

Fig. 2-5 Alternative positions for placing embedded sensors in/near continuity diaphragm

The sensors were chosen to measure strains, gap openings (displacements), and inclination angles. Three types of strain sensors were employed; two of which were embedded inside the girders and the deck and the third type was surface mounted after the bridge completion. The difference between the embedded strain sensor types lies in the way of their attachment to the structure. Strandmeters are equipped with clamps that surround reinforcing

bars or prestressing strands at two points. The gage length between these clamping points is 203 mm [8 in]. The body of the sensor is isolated from the surrounding concrete using grease-filled plastic tube, which means that only strains in the bar to which the sensor is clamped are measured regardless of the surrounding concrete movement. Sisterbars on the other hand rely on bond between the concrete and a dummy reinforcing bar to which the vibrating wire gage is installed. In other words, sisterbars measure strains in the concrete over a long gage length (about 4 feet). Therefore, it should not be used in disturbed zones such as girder ends in the vicinity of the continuity diaphragm.

All sensors were connected to a datalogger powered using a solar panel and rechargeable batteries to ensure continuous operational capabilities even in the case of power outages. The datalogger is also connected to a cellular modem that allows for remote access to the logger's data buffer through an internet IP connection using the LoggerNet utility from Campbell Scientific. It should be noted that the datalogger recorded readings from each sensor one at a time, which translated into one reading every 2.5 minutes to allow for covering all 96 channels. In other words, 24 readings per hour were recorded for each sensor, which were then averaged and stored for retrieval. The sensor wirings were bundled into six groups through six 16-channel multiplexers feeding into the datalogger. Only 66 channels out of the available 96-channel system were used (excluding 7 gapmeters that were not installed – see details in the next section), which left some open channels for future expansion of the monitoring system.

2.3.2 Sensor Locations

At the continuity diaphragm, the research team faced three alternatives for placing sensors. First, sensors could be placed in the continuity diaphragm, whether floating inside the concrete (Fig. 2-5-a) or on the positive moment reinforcement extending into the continuity diaphragm (Fig. 2-5-b), to capture straining actions as they transfer between girders from one span to another. These two locations were ruled out for three reasons: (1) the force transfer mechanisms taking place in this short distance are so complex that qualify this region to be a disturbed region (D-region) , which means that slight shifts in sensor location result in major changes in measured strains, (2) the depth of the BT-72 girders rendered that location beyond reach at the bridge site after placing the diaphragm forms, especially for the narrow width of 229 mm [9 inches] between girder ends, in addition to the impracticality of sensor installation in the casting yard prior to transportation or prior to placing the diaphragm forms because the sensors would be exposed to severe damaging transportation and site activities, and (3) the gage length for strandmeters is 203 mm [8 inches], which is longer than the straight portion of the hairpin bars extending out of the girder ends. The second alternative was to install sensors to measure the relative movement between the girder ends and the diaphragm (Fig. 2-5-c). This option is valid and the research team allocated 7 additional gapmeters to be installed when separation ensued. However, no major separations took place during the monitoring period. Hence, the gap meters were not installed as described. Finally, embedded sensors could be placed on the positive moment reinforcement inside the girders as close as possible to the girder ends (Fig. 2-5-d). This position captures strains in reinforcement at the transfer plane between the girders and the diaphragm. These strains can be directly converted into forces without the effects of the D-region inside the diaphragm. It also provides protection to the sensor during transportation and during the casting of the diaphragm. Furthermore, the research team was of the opinion that the study should focus on girder performance since cracking of prestressed girders may lead to adverse effects, especially at girder ends.

The types, numbers, and location of sensors used in this study are listed in Table 2-1. The distribution of the sensors is shown in Fig. 2-6. It can be seen from the figure that the symmetry and anti-symmetry were utilized in distributing sensors. For example, the midspan location of Girder 1 in the middle span (L = 31.09 meters [102 feet]) is identical to the midspan location of Girder 5. Therefore, sensors were installed at one of them only (Girder G5).

Table 2-1Types of sensors employed in this study

Sensor Type	Measurement	Location	Number
Sisterbars	Strain in concrete	Embedded	12
Strandmeter	Strain in reinforcement		16
Vibrating wire strain gauges	Surface strains	External	29
Displacementmeters	Girder relative movement		6
Tiltmeters	Slope		3
Gapmeter	Girder/diaphragm separation		7*
	Total:		73

* gapmeters were not installed

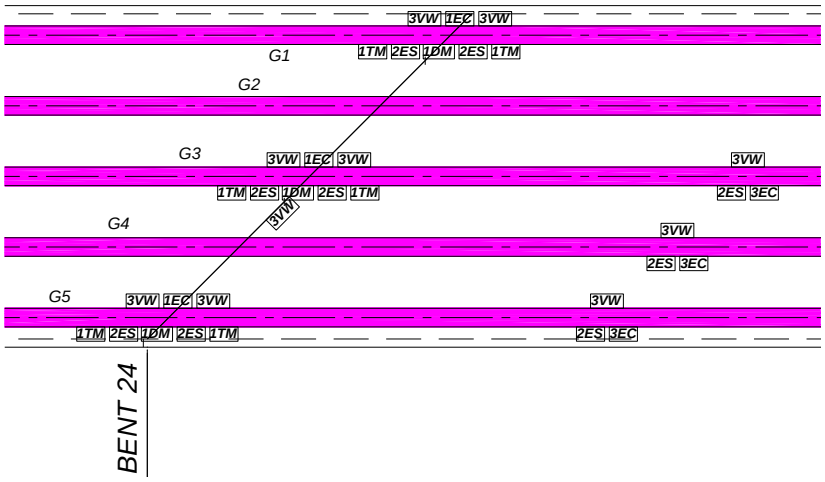

EC: sisterbar strain gage

ES: strandmeter strain gage

TM: tiltmeter

VW: external strain gage

DM: displacement meter

Fig. 2-6 Plan showing details of the monitoring system

The three monitored midspan locations (Girders G3, G4, and G5) will still provide information about a complete line across the middle span of the monitored segment. The same cannot be applied for the line at the monitored bent. Thus, Girders G1, G3, and G5 will be monitored at that location. Fig. 2-7 shows a more detailed view of the sensors employed in this study across the height of the superstructure. One of the most important performance measures is the tensile force in the positive moment reinforcement at the continuity detail (hairpin bars). Fig. 2-8 shows the placement of the embedded sensors (strandmeter) on the hairpin bars at the girder ends and on prestressing strands at midspan (sisterbar).

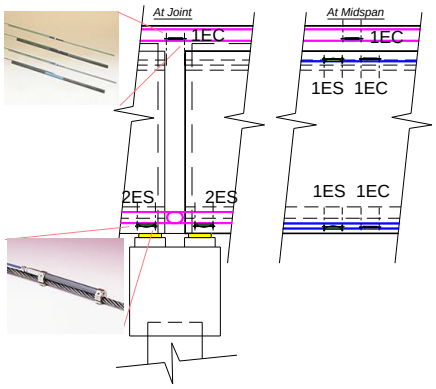

(a) Embedded sensors

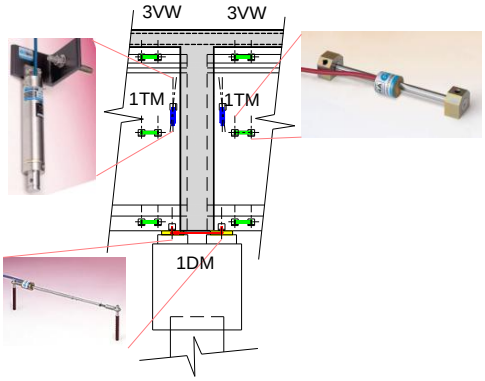

(b) External sensors

Fig. 2-7 Distribution of the employed sensors across the height of the superstructure

2.3.3 Monitoring System Protections

Because of the exposed nature of the bridge site to lighting strikes, it was deemed necessary to provide embedded sensors with surge protectors. External sensors were not treated similarly, since they are accessible and can be easily replaced in the event of a lightning strike. Furthermore, wires were protected at critical locations that are known to cause problems due to site activities. In particular, wires passing through holes in metal stay-in-place forms were protected from the sharp edges by padding the holes with special putty material. As a result of the protection measures, no sensors were damaged in this project; i.e. a 100% survival rate of embedded sensors was achieved.

2.4 Data Preprocessing

All sensor data records were manipulated through scripts specially adapted for this project's monitoring system. For any specific sensor, raw data files were first read to extract the corresponding sensor readings (e.g. strains, slopes) and sensor temperature. Before interpreting the readings, two preprocessing steps had to be carried out. These steps are namely to (1) correct reading values based on actual sensor temperature relative to user specified initial sensor temperature conditions and (2) to obtain a clean data record to remove any outliers.

(a) Strandmenter at the end of girder on hairpin bars

(b) Sisterbars at midspan on prestressing strands

Fig. 2-8 Installation of the embedded sensors (a) at the end of girder and (b) at midspan

2.4.1 Temperature Correction

The manufacturer of the vibrating wire gages used in this study recommends correcting the recorded raw data to account for temperature variations that affect the length of the vibrating wire inside the gages, and hence, affecting its readings. Temperature corrections were applied to all sensors used in this study except for tiltmeters, for which temperature correction is not highly recommended. Fig. 2-9 shows a plot of raw and temperature corrected data for a sisterbar and a strandmeter at the same location (bottom of Girder G3 in the middle of Span 24). It can be seen in Fig. 2-9-a that the recorded raw data are quite different. This is mainly due to the different characteristics of both sensors and, because of the different gage lengths. Fig. 2-9-b shows that once the temperature correction is applied, the trend and range of variations from both sensors match very well. The shift between the reading is due to the condition at the initial reference point used to generate these plots. If another datum is chosen, the shift between the relative strain recorded by both sensor types would drop substantially.

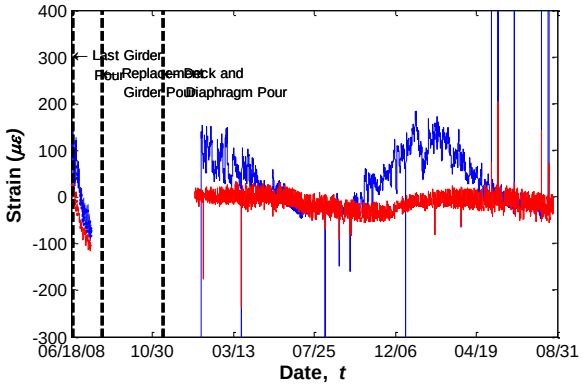

(a) raw data

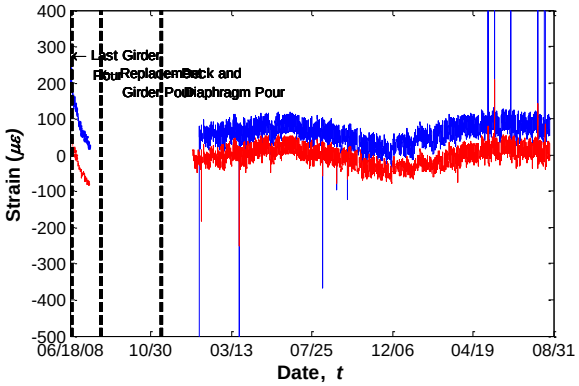

(b) temperature corrected data

Fig. 2-9 Temperature correction of sensors #89(ES) and #92(EC) in G3 (bottom) at Midspan of Span 24

2.4.2 Removal of Outliers

As stated earlier, average hourly readings are recorded during the normal operation of the datalogger. If for any reason one of the 24 readings averaged within an hour is bad (e.g. due to a lightning hit or irregular voltage supply to the datalogger), the recorded hourly average is affected and becomes an undesirable datapoint. The large size of data (66 sensors over 24 months) makes the task of removing outliers manually a daunting task. Several data cleaning scripts were tested before the research team developed its own data cleaning routine that performs the task on a global scale first before scrutinizing a smaller user-specified window for any datapoints that fall out of a user-specified range of acceptable tolerance. Fig. 2-10 shows plots of the raw and cleaned data records for Sensor #22.

2.4.3 Adjusting Reference Datum for Live Load Test

Because of the slow nature of the monitoring system, live load tests conducted for this project lasted about 6 hours. During this time period, temperature distribution changed as the bridge deck was exposed to rising sun. Fig. 2-11shows temperature readings from two groups of sensors. The first group consists of top sensors (#48, #6, #53, #47, #5) in the deck, while the second group consists of bottom flange sensors (#2, #49, #46). It should be noted that the five

deck sensors were at a depth of about 152.4 mm [6 in.] from the deck surface. Temperatures above 115ºF on the deck surface were recorded manually by the research team during site visits. It can be seen that the temperature increased at a higher rate for top sensors than for bottom sensors. As a result, the temperature gradient varied during the course of the live load test. Hence its effect should be decoupled from the total sensor reading.

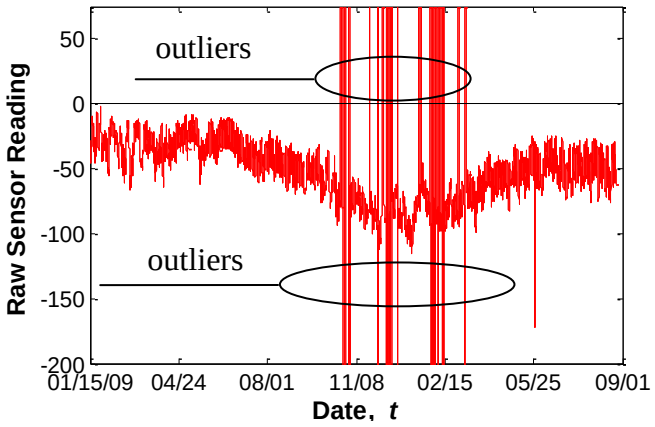

(a) raw data

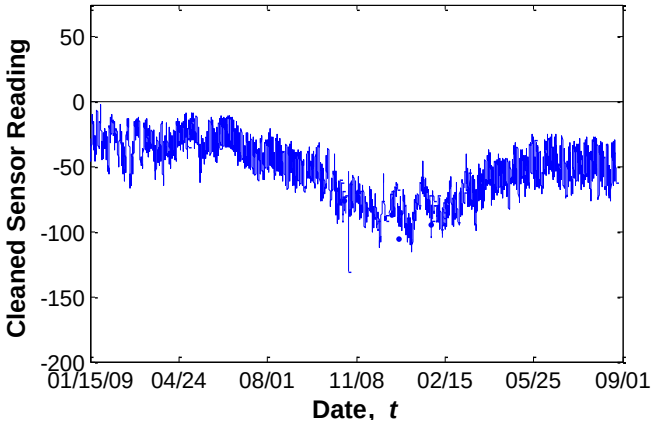

(b) cleaned data

Fig. 2-10 Removal of outliers from raw data (sensor #22 – VW on G1 (bottom) at Bent 24 in Span 23)

This was done by identifying an appropriate temperature adjusted datum from which the effect of the static live load effect is to be measured. The identified datum was determined with the help of the six periods where the trucks were driven of the bridge allowing for no-load effects. Instead of zeroing the sensor, the readings were measured from the identified temperature adjusted datum. This is illustrated in Fig. 2-12 for Sensor #50. The beginning and end times of 9 load case positions (6 positive positions P1 through P6, and 3 negative positions N1 through N3) are marked with dashed lines in the figure. Despite the fact that the entire record is positive, negative live load effects are measured for Load Case P2. A small positive strain reading is measured for Load Case P3.

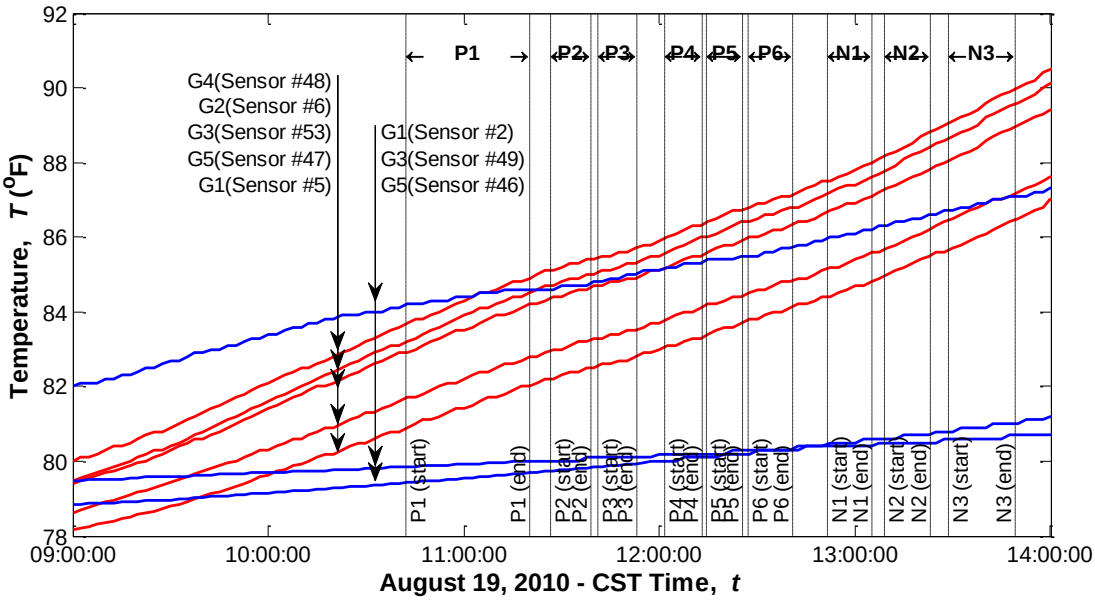

Fig. 2-11 Temperature increase during the time of conducting static load tests

2.5 Sample Data Records

In this section, sample plots of data recorded over the project period are presented. One record is presented for each sensor type. Key dates are marked on the plots (e.g. deck and diaphragm pour or establishing continuity). The records cover both the casting yard period (first phase), which started on June 18, 2008, however, it should be noted that no readings from this period exist for surface mounted sensors and embedded sensors that were not connected to the datalogger. Prior to transporting the girders to the bridge site, the casting yard datalogger had to be disconnected, which explains the blackout period between days 32 and 205 when the full monitoring system installation was completed on January 9, 2009.

The sample readings from each sensor type are presented through Fig. 2-13 through Fig. 2-17. In these figures, the abscissa represents the days from the beginning of sensor installation on June 18th, 2008. Both the relative readings and the temperatures are plotted in these figures. Fig. 2-13 represents strain readings from strandmeter (ES) located at the top of Girder G3 at midspan of Span 24. The temperature plot shows that high temperatures are recorded in the first few days following the casting of the girder, which is expected due to the additional heat caused by hydration reaction of the cement in the wet concrete. Strain readings reflect tension at the first phase, which is due to the cambering action of the girder. However, when the deck is poured the additional load causes the girder to bend downward creating compression at the top.

Fig. 2-14 represents the strain readings from a typical sisterbar (EC) located at the bottom of Girder G4 at midspan of Span 24. The temperature of the readings shows a higher trend at the first phase which can be accounted due to the hydration of the cement. However, the strain in this sensor/location shows a downward trend at the beginning. As the prestress force is transferred to the girder it causes a compression at the bottom, and when the deck is poured the additional load causes the girder to bend downward resulting a tension there. These facts are also

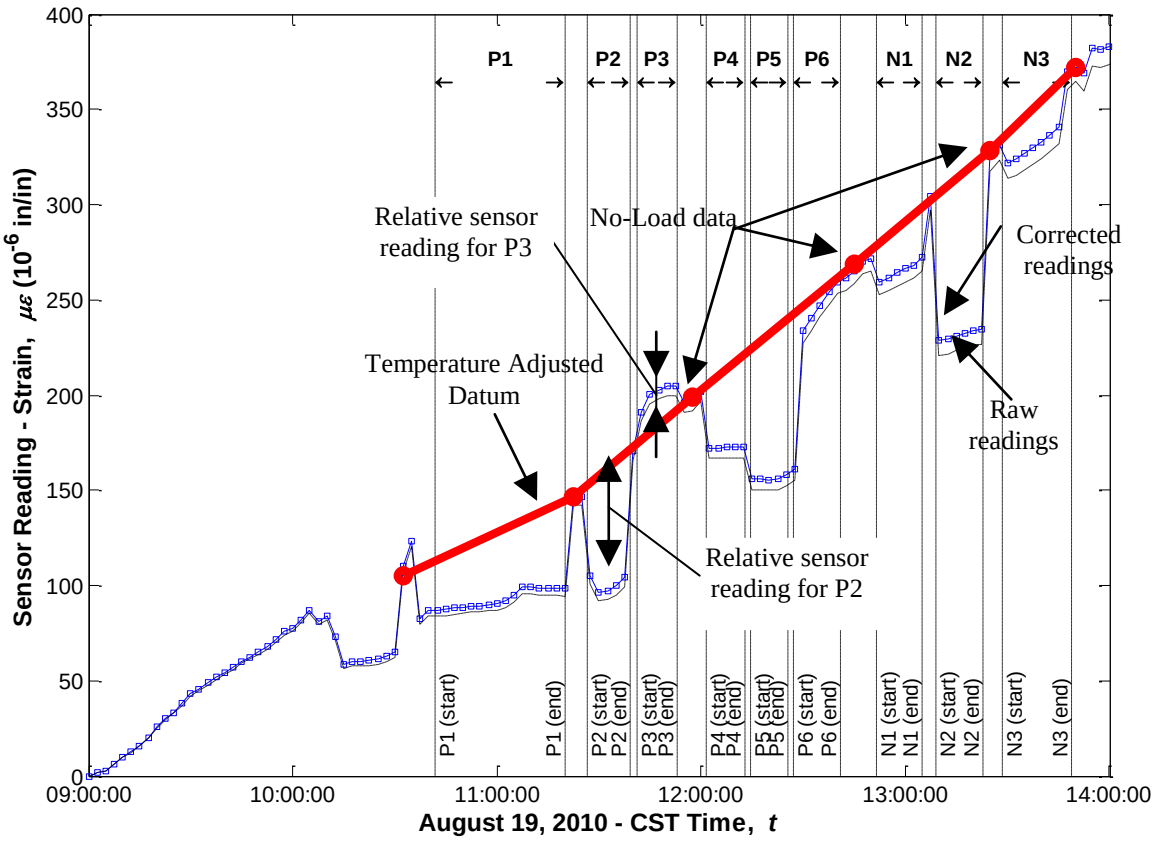

Fig. 2-12 Sample sensor reading during static live load testing (Sensor #50 – G3, Span 23, hairpin bar)

depicted in the strain reading of Fig. 2-14. Reading from a vibrating wire (VW) gauge located at the middle half of Girder G3 at the support (Bent 24) of Span 23 is shown in Fig. 2-15. This is a surface mounted sensor, which was installed at the bridge site after the deck and diaphragm had been poured. Thus there is no reading from the first phase.

The end rotation of Girder G3 of Span 23 is captured by the tiltmeter and is depicted in Fig. 2-16 along with the temperature at that sensor location. The relative displacement of the girder is very important in determining the performance of the continuity detailing. The reading from the displacement meter connected at the bottom of Girder G1 between Span 23 and Span 24 is presented in Fig. 2-17 along with the temperature at that point. It can be seen that as the temperature increases the girder elongates and a length shortening is recorded by the sensor. The temperature readings from all the sensors will help determining the actual temperature gradient, and will be available for studying its effect on the continuity moment and the performance of the new detail. It should be noted here that all the plotted data are hourly averages of numerous readings recorded by the sensors during that period.

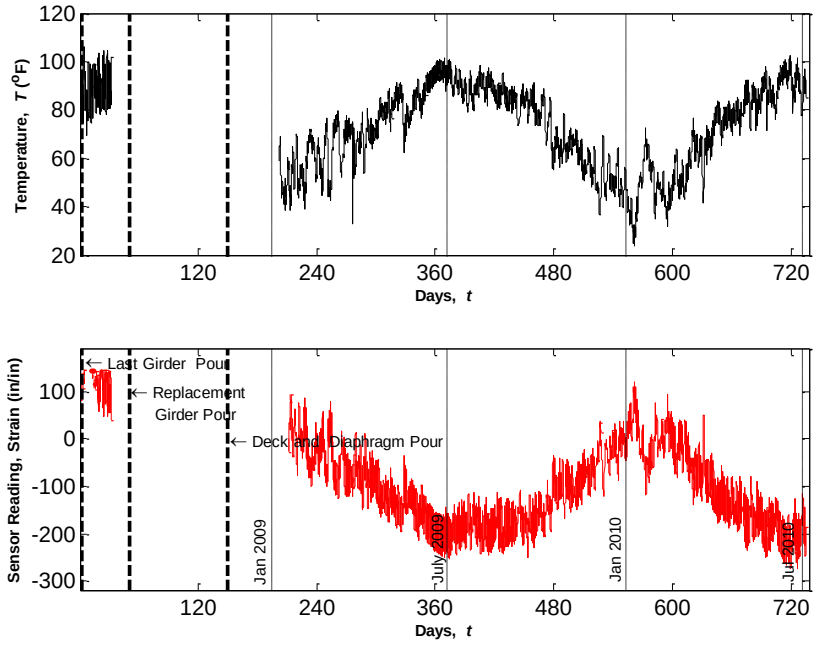

Fig. 2-13 Strandmeter readings of Girder G3 in Span 24. (top location at midspan)

2.6 Summary and Conclusions

The development of a long term monitoring system that will be used in evaluating the performance of the new NCHRP 519 positive moment continuity detail is presented. The new continuity detail calls for positive moment reinforcement to extend out of girder ends in the form of hooked prestressing strands or additional hairpin bars. Six different sensor types have been employed in the monitoring system. The completed system comprised of a total of 66 sensors. They were chosen to capture the essential behavioral aspects that will be used to interpret the structural performance of the detail. Each of the sensors will record its reading (strain, slope angle, gap) and a corresponding temperature at that location. Temperature readings are used to correct sensor readings following manufacturer's recommendation and also to obtain the temperature gradient which will then be used to assess its effects on the long-term performance of the continuity detail. The installation of the embedded and the surface mounted sensors has already been completed with a 100% survival rate. Preliminary readings from the sensors (embedded and external) were remotely downloaded over an IP connection to the datalogger which is equipped with a cellular modem. It can be said that the system is functioning as expected.

The success in developing such a monitoring system is a collaborative effort between many parties. The research team, general contractor, casting yard crew, sensor supplier and installation team, sponsoring agency had an open line of communication to plan tasks ahead of time and ensure proper installation of the sensors. The data collected for this project will be analyzed by the research team to help the Louisiana Department of Transportation and Development (LA-DOTD) in making a decision whether to adopt the new detail.

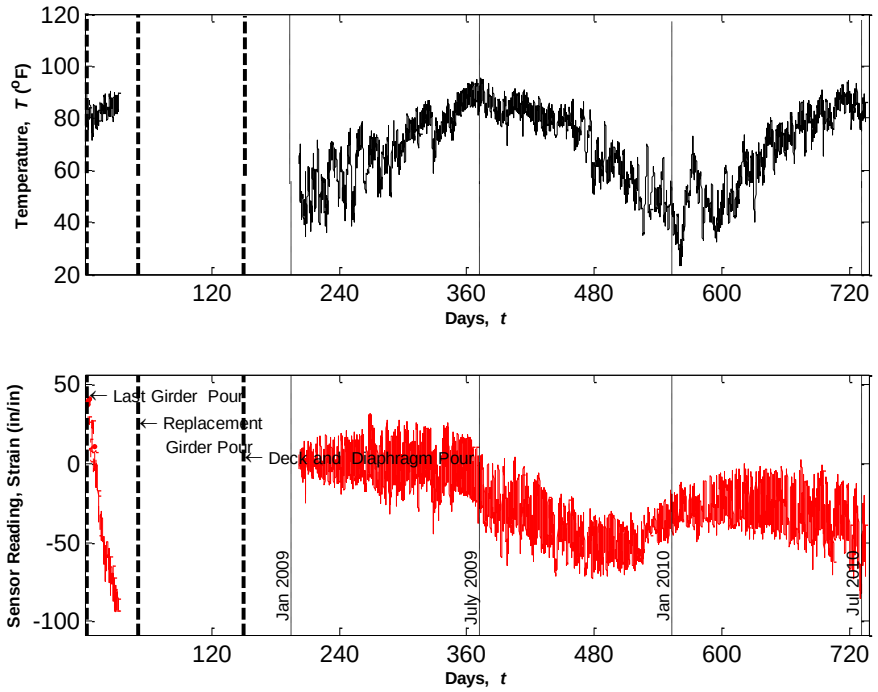

Fig. 2-14 Sisterbar reading of Girder G4 in Span 24. (bottom location at midspan)

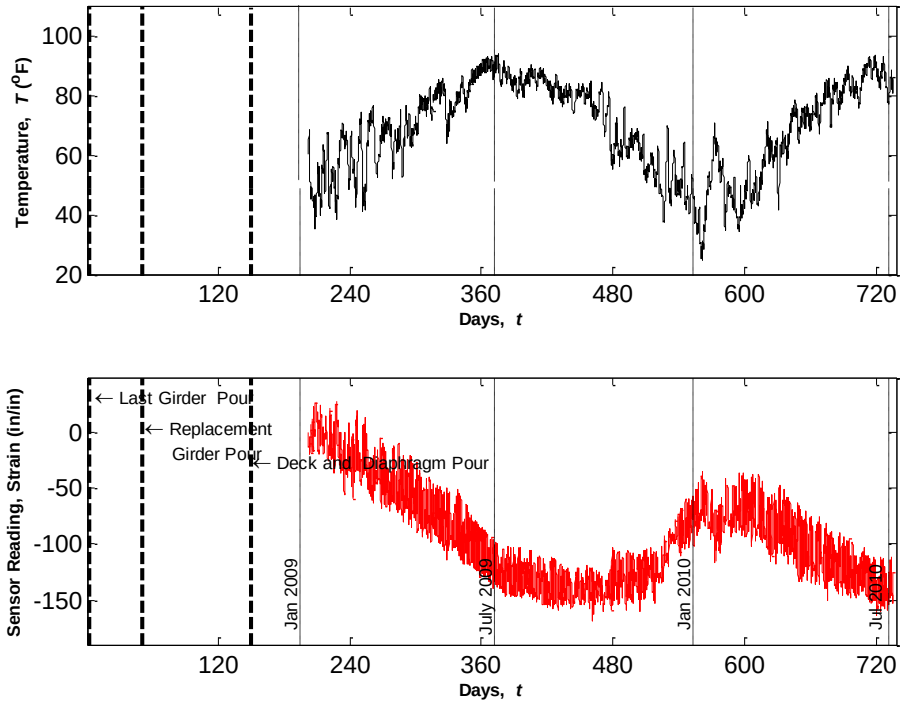

Fig. 2-15 Vibrating wire gauge reading of Girder G3 in Span 23. (midheight at Bent 24)

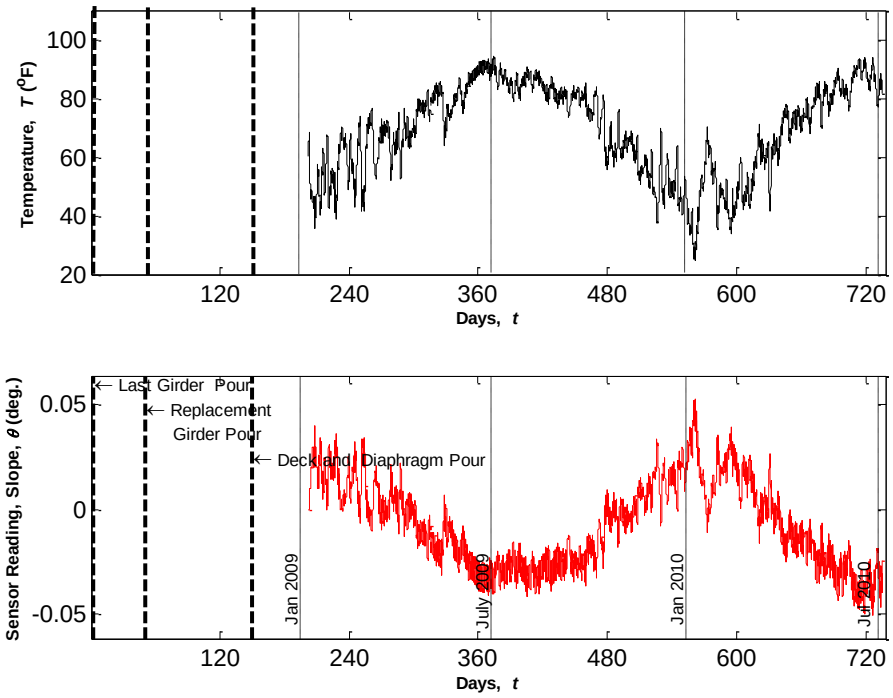

Fig. 2-16 Tiltmeter reading of Girder G3 in Span 23. (midheight at Bent 24)

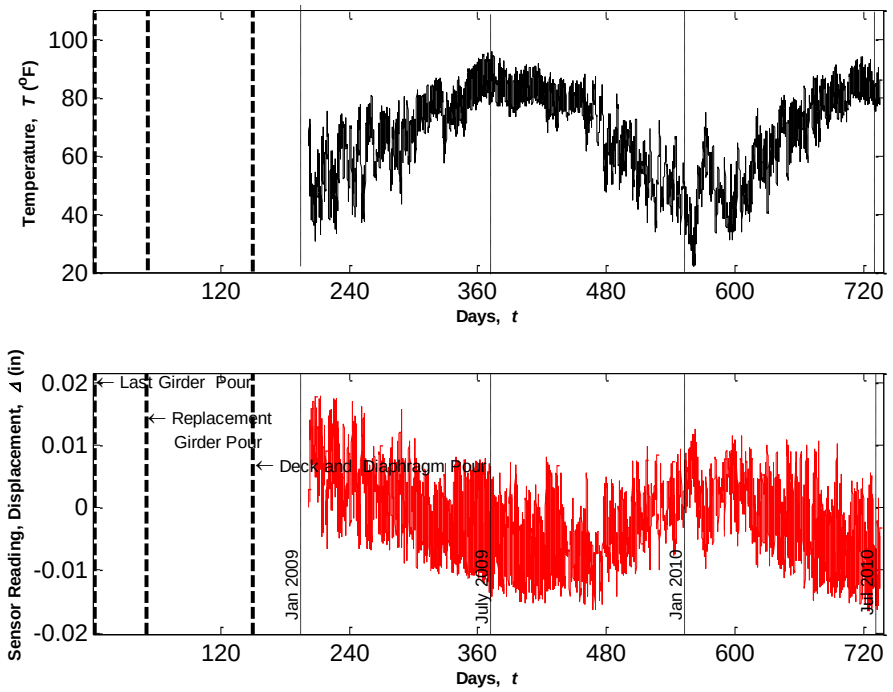

Fig. 2-17 Displacement meter reading at Girder G1. (bottom flanges at Bent 24 between Spans 23 and 24)

2.7 Reference List

Alampalli, S., and Yannotti, A. P. (1998). "In-Service Performance of Integral Bridges and Jointless Decks." *Transportation Research Record*, 1624, 1-7.

Bordes, J. L., and DeBreuille, P. J. (1985). "Some Facts About Long-Term Reliability of Vibrating Wire Instruments." *Transportation Research Record*, Natl Research Council, Transportation Research Board, Washington, DC, USA, 20-27.

Burke, M. P., Jr. (1992). "Integral Bridges: Attributes and Limitations.".

Burke, M. P., Jr. (1994). "Semi Integral Bridges: Movements and Forces." *Transportation Research Record*, 1460, 1-7.

Burke, M. P., Jr. (2004). "Reducing Bridge Damage Caused By Pavement Forces." *Concrete International*, 26(2), 83-89.

Caner, A., Dogan, E., and Zia, P. (2002). "Seismic Performance of Multisimple-Span Bridges Retrofitted with Link Slabs." *Journal of Bridge Engineering*, 7(2), 85-93.

Caner, A., and Zia, P. (1998). "Behavior and Design of Link Slabs for Jointless Bridge Decks." *PCI Journal*, 43(3), 68-80.

Choquet, P., Juneau, F., DeBreuille, P. J., and Bessette, J. (1999). "Reliability, long-term stability and gage performance of vibrating wire sensors with reference to case histories." 49-54.

Demartini, C. J., and Haywood, R. J. (1991). "Repair of the Southern Approach to the Story Bridge by Elimination of the Contraction Joints." 357-370.

Gastal, F., and Zia, P. (1989). "Analysis of Bridge Beams with Jointless Decks." 555-560.

Loveall, C. L. (1985). "Jointless Bridge Decks." *Civil Engineering*, 55(11), 64-67.

Miller, R. A., Castrodale, R., Mirmiran, A., and Hastak, M. (2004). "Connection of Simple-Span Precast Concrete Girders for Continuity." *Rep. No. NCHRP Report 519*, Transportation Research Board, Washington, D.C.

Oesterle, R. G., Glikin, J. D., and Larson, S. C. (1989). "Design of Precast Prestressed Bridge Girders Made Continuous." *Rep. No. NCHRP Report No. 322*, Transportation Research Board, Washington, D.C.

Okeil, A. M., and El-Safty, A. K. (2005). "Partial Continuity in Bridge Girders with Jointless Decks." *Practice Periodical on Structural Design and Construction*, 10(4), 229-238.

Pierce, P. (1991). "Jointless Redecking." *Civil Engineering*, 61(9), 60-64.

Richardson, D. R. (1989). "Simplified Design Procedures for the Removal of Expansion Joints from Bridges Using Partial Debonded Continuous Decks." M.Sc., North Carolina State University.

Russell, H. G., and Gerken, L. J. (1994). "Jointless Bridges- the Knowns and the Unknowns." *Concrete International*, 16(4), 44-48.

Siros, K. A., and Spyrakos, C. C. (1995). "Creep Analysis of Hybrid Integral Bridges." *Transportation Research Record*, 1476, 147-154.

Thippeswamy, H. K., and GangaRao, H. V. S. (1995). "Analysis of In-Service Jointless Bridges." *Transportation Research Record*, 1476, 162-170.

Thippeswamy, H. K., GangaRao, H. V. S., and Franco, J. M. (2002). "Performance Evaluation of Jointless Bridges." *Journal of Bridge Engineering*, 7(5), 276-289.

Wasserman, E. P. (1987). "Jointless Bridge Decks." *AISC Engineering Journal*, 24(3), 93-100.

Wing, K. M., and Kowalsky, M. J. (2005). "Behavior, Analysis, and Design of an Instrumented Link Slab Bridge." *Journal of Bridge Engineering*, 10(3), 331-344.

Zia, P., Caner, A., and El-Safty, A. (1995). "Jointless Bridge Decks." *Rep. No. Research Report No. FHWA/NC/95-006*, Center for Transportation Engineering Studies.

3 FIELD MONITORING OF POSITIVE MOMENT CONTINUITY DETAIL IN A SKEWED PRESTRESSED CONCRETE BULB-T GIRDER BRIDGE

3.1 Introduction

The precast prestressed concrete girder bridge alternative is considered one of the most economical construction choices. Erecting precast PSC girders eliminates the need for cumbersome and costly formwork, which usually negatively impacts daily activities around the construction site. As a result, construction speed benefits from the use of PSC girder construction, especially since the girders are only erected after being cured in the casting yard. Precast elements are separate by definition and therefore are not monolithically connected by default. Therefore, many of the existing precast PSC girder bridges are constructed as simply supported spans as can be seen in Fig. 3-1.

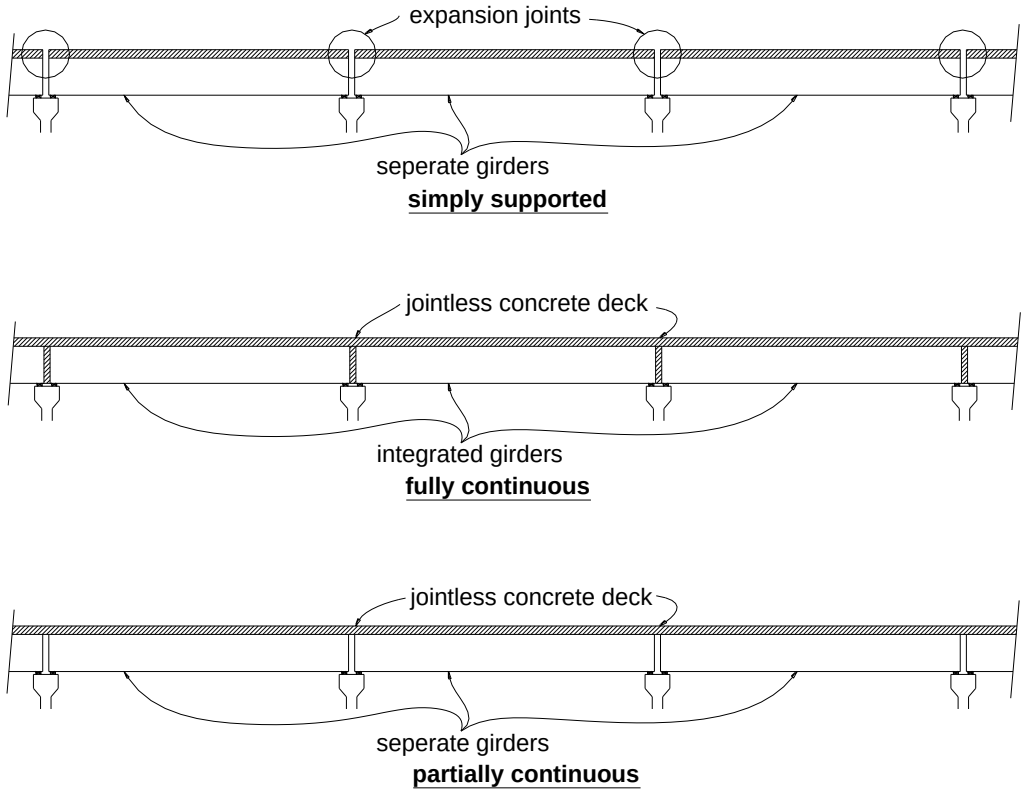

Fig. 3-1 Typical continuity conditions in precast PSC girder bridges (Okeil and El-Safty 2005)

Expansion joints between spans are known to cause serious problems (e.g. joint maintenance and deterioration of elements in their vicinity). Elimination of joints avoids many of these problems. Several continuity details have been used over the years in the bridge industry for slab-on-girder bridges with the goal of avoiding the aforementioned maintenance issues and reaping the benefits of continuity without the drawbacks of introducing it in large structures such

as bridges (e.g., thermal movements). Two major categories of continuity solutions are commonly used, namely *full integration* details and *partial integration* details. Full integration details (Fig. 3-1) result in a fully continuous structure (both deck and girders) that can resist the bending moments that develop at the supports due to long term, thermal, and live load effects. Alternatively, partial integration (Fig. 3-1), where the expansion joints are eliminated by casting a continuous deck over the support while allowing adjacent girders movement with respect to each other, relieves some of the continuity effects (Caner and Zia 1998; Okeil and El-Safty 2005)

Researchers have investigated the behavior of continuous bridge superstructures (Burke, Jr. 1994; Siros and Spyrakos 1995). Continuity details have to resist moments that develop as a result of establishing continuity. Negative moments develop due to live loads and superimposed dead loads. Positive moments develop mainly due to long-term effects such as creep, shrinkage and thermal variations. The existence of deck reinforcement over continuity diaphragms makes resisting negative moments an easy task. Conversely, special arrangements need to be made for resisting positive moments. Extending reinforcement from girder ends for development in continuity diaphragm is a common solution. In 1989, the National Cooperative Highway Research Program (NCHRP) published the findings from Project 12-29 in Report 322 (Oesterle et al. 1989), which is a comprehensive study on converting precast prestressed concrete girders into a continuous system. More recently, NCHRP sponsored Project 12-53 to investigate the performance of bridges made continuous and make recommendations. The recommendations were published in NCHRP Report 519 (Miller et al. 2004), which were adopted by the designer of a major project in Louisiana. The John James Audubon Project connects the cities of Saint Francisville and New Roads across the Mississippi River in Louisiana. Many of the spans of its eight bridges utilize hairpin bars to establish continuity between adjacent girders. Fig. 3-2 shows the adopted hairpin detail, which is different than the Louisiana standard continuity diaphragm detail also seen in Fig. 3-2. In addition to the lack of positive moment reinforcement, the Louisiana detail calls for a bond breaker to allow girder ends to move freely with respect to the diaphragm.

The LA-DOTD seized the unique opportunity offered by the construction of the John James Audubon Project and called for an investigation into the performance of this new detail on a full scale bridge to assess its long-term performance. One of the constructed bridges included a skewed segment with Bulb-T girders. Both attributes were not within the scope of the experimental program covered in Project 12-53 that produced NCHRP Report 519. The segment was therefore chosen for the study that lasted over two years. A structural health monitoring approach was used in the investigation. This paper presents the results from the study which includes monitoring data from a period of over 24 months. Also, results from a live load test are presented.

3.2 Monitored Bridge and Monitoring System

The monitored bridge segment is a three span continuous superstructure, 242-ft (73.76 m) long with a skewed layout. It constitutes Spans 23, 24, and 25 of Bridge No. 2. Five AASHTO Bulb–T girders (BT-72) were used to support a a deck with 38 ft of clear width. The deck was 7.5 in. (19.5 cm) thick cast-in-place (CIP) reinforced concrete. Because of the bridge's symmetry, only one of the identical intermediate bents (Bent 24 and Bent 25) was monitored. This segment was chosen because of its configuration, which has not been covered by the tests conducted in NCHRP Project 12-53; namely skewed configuration and Bulb-T girders. The

bridge girders were supported on bearing pads over typical pile bents. More details about the bridge can be found elsewhere (Okeil and Cai 2009).

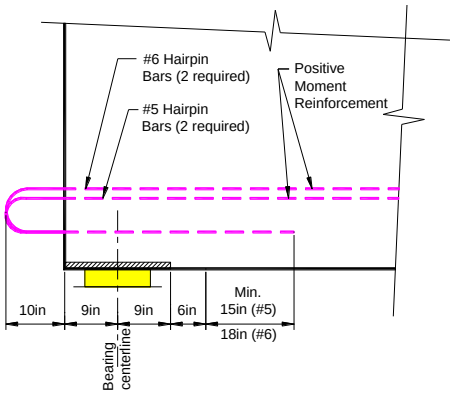

NCHRP 519 detail with hairpin bars (Miller et al. 2004)

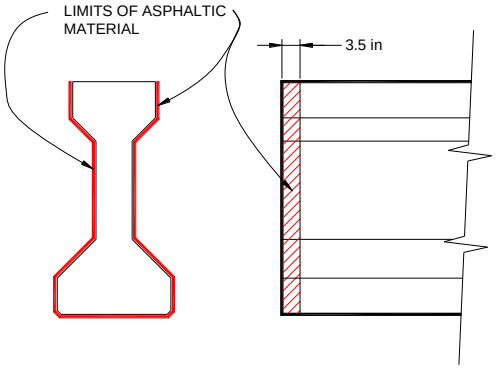

Louisiana DOTD standard continuity detail

Fig. 3-2 Different continuity diaphragm details (Note: 1 in.=25.4 mm)

A 96-channel monitoring system was designed to record essential performance measures to be used for evaluating the continuity detail. Several sensor types were chosen to measure strains, rotations, crack widths and gaps. All sensors utilized the vibrating wire technology which is known to be more suitable for long-term monitoring projects as they do not suffer from drifting (Bordes and DeBreuille 1985; Choquet et al. 1999). Embedded as well as surface-mounted sensors were employed. In all six types of sensors were utilized and the monitoring system included 66 active sensors. The sensors were strategically located at midspan and on both sides of the continuity diaphragm. Fig. 3-3 shows a schematic of the sensor locations. More details the bridge can be found elsewhere (Okeil and Cai 2009).

3.2.1 Temperature Data

Fig. 3-4 shows the temperatures at midspan sections of one of the girders (G3) in Span 24 at three locations, namely deck, top girder flange, and bottom girder flange. It can be seen that the seasonal changes cause huge temperature fluctuations from a minimum of about 20ºF to 115ºF. The highest temperatures are always recorded in the deck because of the direct exposure to sunlight. Sunlight exposure also causes larger daily variations in the deck than the other sensors as evident by comparing the range of daily amplitude from deck and girder flanges. It should also be noted that the deck sensors were installed on the bottom mesh of the deck reinforcement to protect them during concrete casting. This position was at least 4 inches (102 mm) below the deck surface. The research team checked the temperature on the deck surface and compared it to those recorded by the deck sensors, which showed a difference of between 10-15ºF.

Fig. 3-5 and Fig. 3-6 shows a plot of the measured temperatures across the midspan section of Girder G3 in Span 24, which does not benefit from any shading to the deck offered by the barriers. Also shown in the figure is the design gradient as per AASHTO-LRFD specifications (AASHTO 2010). Two representative dates were picked to illustrate the severity of the temperature gradient.

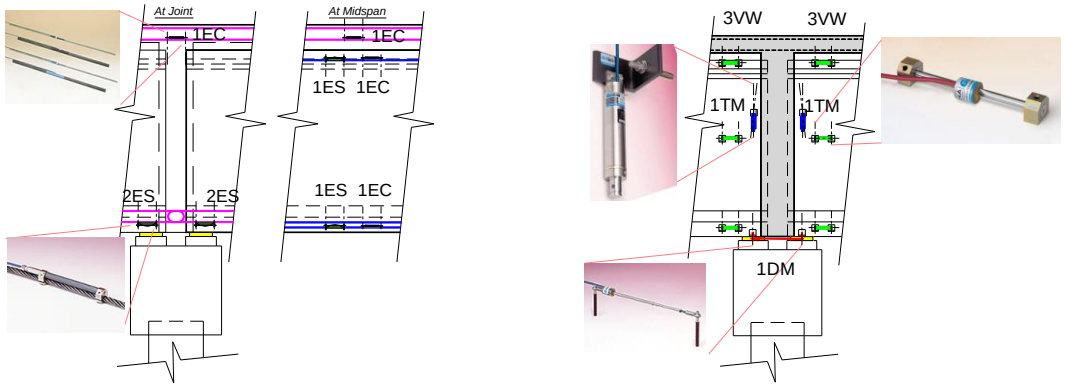

embedded sensors surface-mounted sensors

Fig. 3-3 Distribution of sensors at each monitored location. (EC=sisterbar, ES=strandmeter, TM=tiltmeter, VW=vibrating wire strain gage, DM=gapmeter)

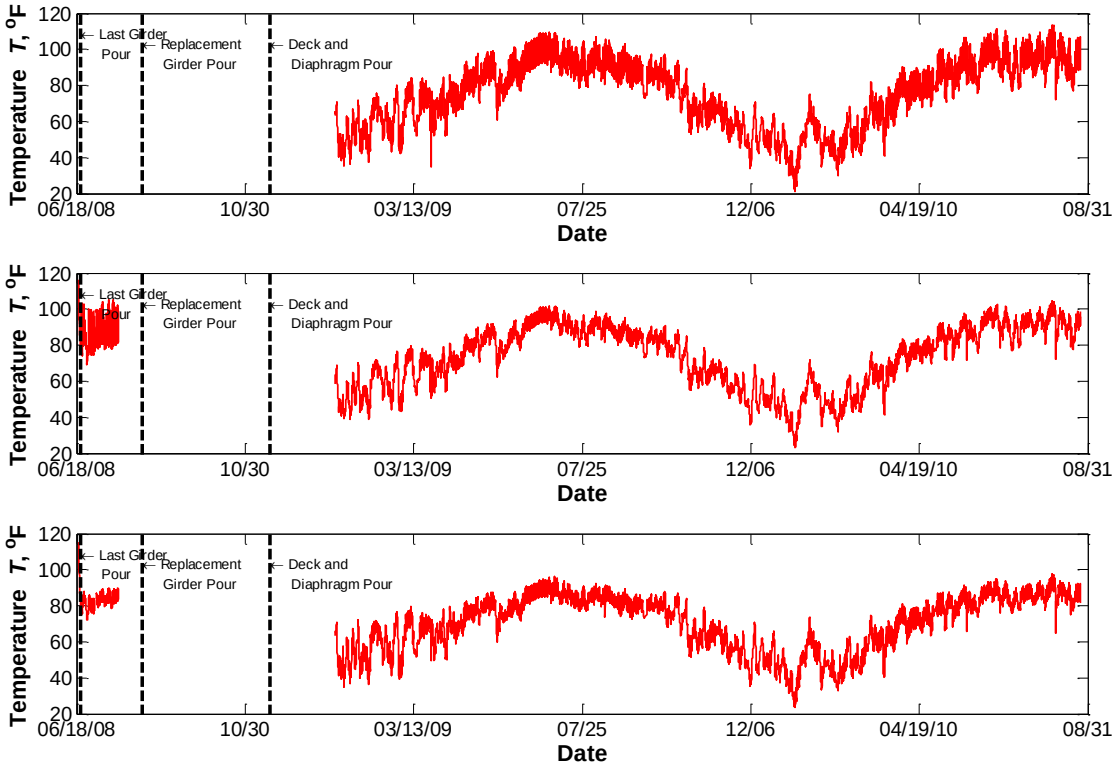

Fig. 3-4 Temperature readings in deck, top, and bottom girder flanges (Girder G3 – Span 24)

In hot summer months (Fig. 3-5), the difference between the top recorded temperature and the bottom one is in the order of 18-20ºF not accounting for the higher deck surface temperature discussed earlier. Overnight in winter time (Fig. 3-6), the temperature gradient is almost nonexistent. It can be seen that the design gradient matches the measured temperatures well. The shown temperatures cover the entire height of the girder and deck, albeit only to where the sensors are located. In other words, the higher temperatures at the very top of the deck were not captured by the monitoring system because of the position of the deck sensors as discussed earlier. These results give confidence that designing precast PSC girder bridges using AASHTO-LRFD specified temperature gradient is adequate. It will be shown later that the temperature gradient effect has a significant impact on the performance of continuous precast PSC girder bridges.

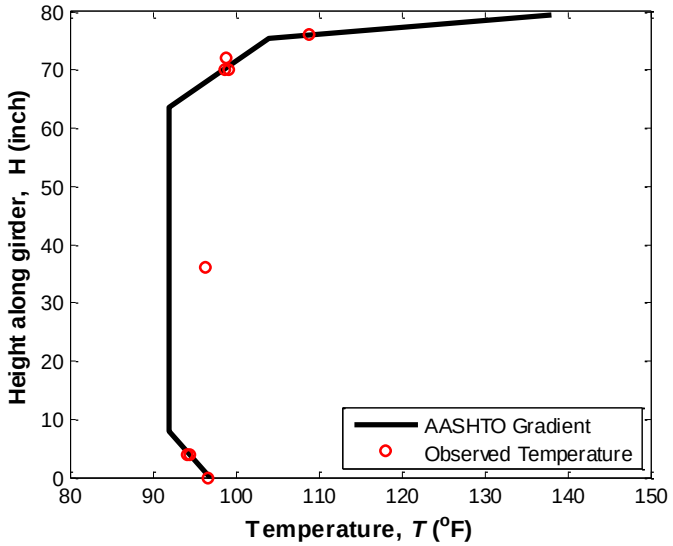

Fig. 3-5 Measured temperature gradient for Girder G3 at Midspan 24 at 3:00 PM on August 10, 2010

3.2.2 Hairpin Strain Data

Strain sensors installed on the hairpin bars on both sides of the diaphragm (see Fig. 3-3) revealed a lot of important information about the performance of the continuity detail. Seasonal and daily temperature variations are clear to impose strains on the hairpin bars. By comparing strain readings shown in Fig. 3-7 for Girder G3 at two similar dates (e.g. 01/2009 and 01/2010), it seems that permanent residual strains take place due to creep effects. It should be noted that continuity was established after 101 days after the casting of Girder G3, which is more than the required 90-day period required by AASHTO-LRFD specifications (AASHTO 2010) if the designer opts to ignore creep effects on the detail.. As a result, the creep effect is small and seems to diminish with time. The more interesting observation from these strain plots is the daily strain variations. It is clear that the hairpin bars are subjected to large strains especially during summer months. This is due to the temperature gradient effect discussed in the previous section. Hundreds of microstrains are recorded as daily strain fluctuations. These strains are capable of initiating cracking in the vicinity of the continuity diaphragm, especially if combined with other sources of tension (e.g. creep and live load effects). It is therefore concluded that temperature

gradient effects should be considered in the design of continuous precast PSC girder bridges. Finally, Fig. 3-7 shows that strains on both sides of the continuity diaphragm seem to mirror each other, which is an indication of force transfer between adjacent girders. This observation will be corroborated by readings obtained from the live load test discussed later in the paper.

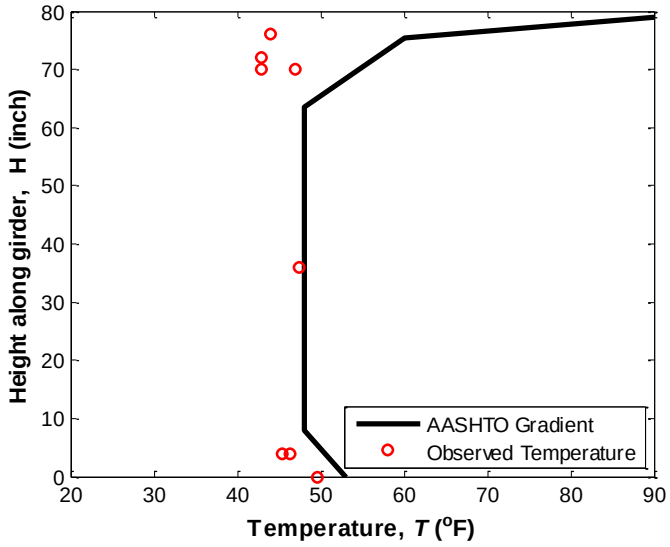

Fig. 3-6 Measured temperature gradient for Girder G3 at Midspan 24at 1:00 AM on January 21, 2009

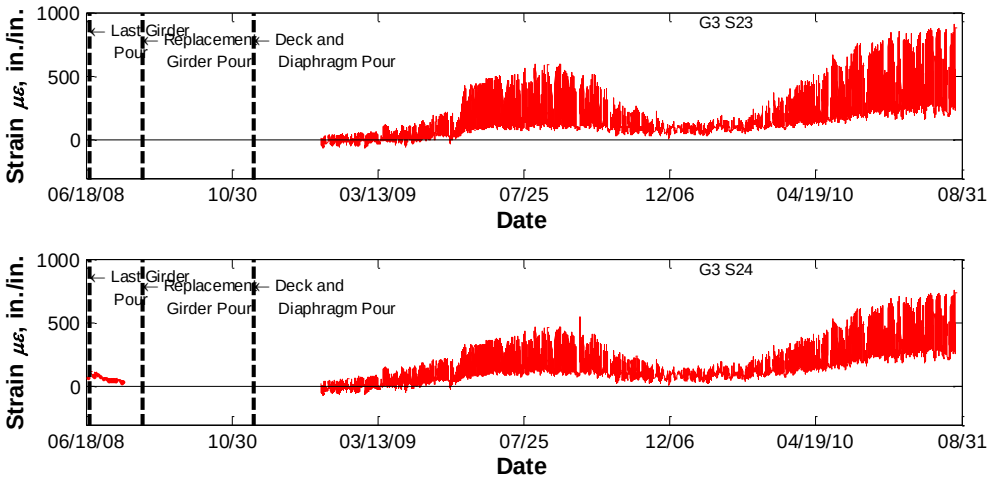

Fig. 3-7 Strains in hairpin bars at both sides of continuity diaphragm (Girder G3)

3.2.3 Relative Movement Between Adjacent Girders

The relative movement between the bottom flanges at the ends of the adjacent girders on both sides of the continuity diaphragm was investigated using the gapmeters installed at Girders G1, G3, and G5. Positive displacements imply that the distance between the bottom flanges have increased, i.e., the girders are applying tension on the diaphragm, and vice versa. Fig. 3-8 shows a plot of the temperature corrected readings from all three gapmeters, which were installed on Girders G1, G3, and G5 across the continuity diaphragm at Bent 24. It can be seen from the

figure that Girders G1 and G5 experienced far less seasonal and daily changes than Girder 3 due to the smaller temperature gradients experienced by G1 and G5 because of their vicinity to the barrier which shades the deck over these girders. Quantitatively, the gage lengths for these extended DM gages were 46.0 in., 43.0 in., and 45.5 in (1168 mm, 1092 mm, and 1156 mm). for Girders G1, G3, and G5, respectively. This means that if a joint was cast monolithic with the girders, the resulting daily strain changes would have been equal to about 0.0150/46=326 $\mu\varepsilon$, 0.0325/43=756 $\mu\varepsilon$, and 0.0175/45.5=385$\mu\varepsilon$ for Girders G1, G3, and G5, respectively. It should also be noted that the daily changes are less in the cold months (December through February) than in the summer. This is due to the smaller temperature gradients during cold months, which in turn reduces girder rotations at the joint.

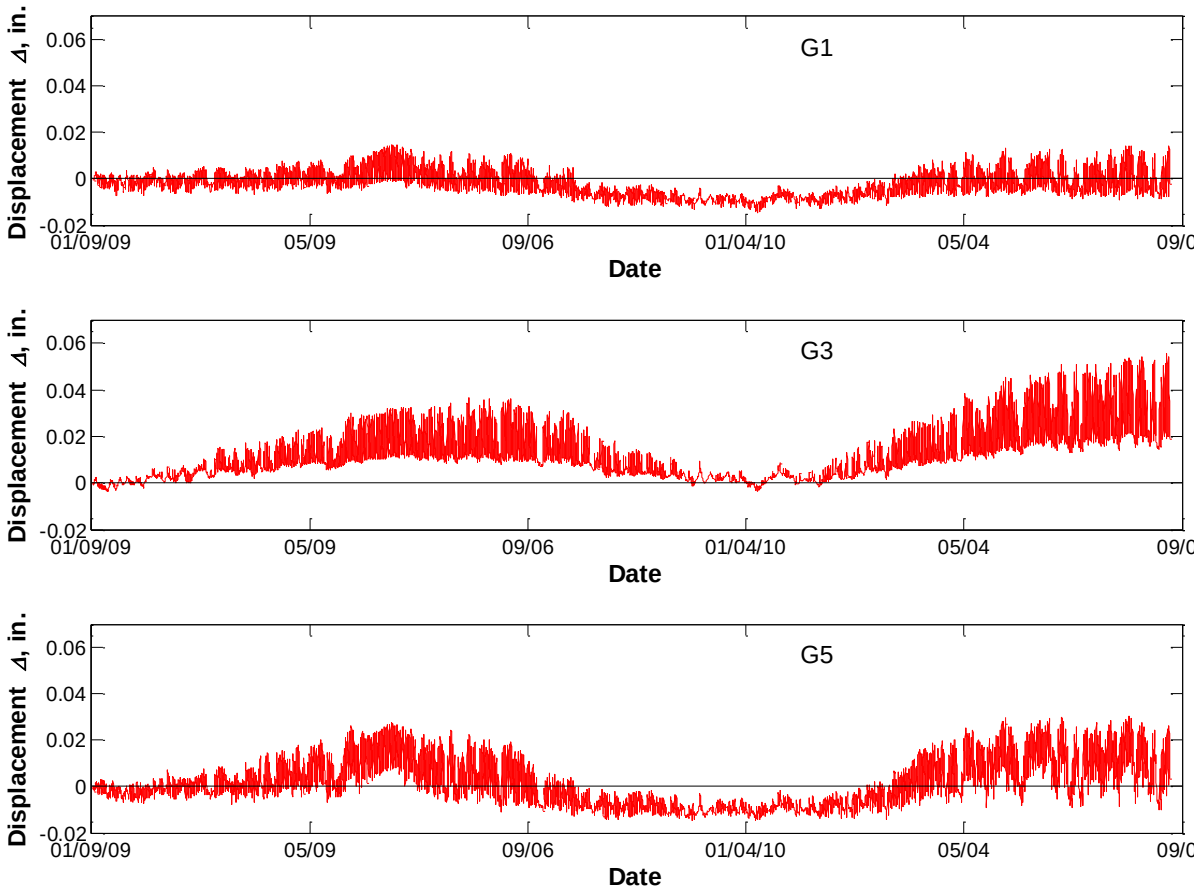

Fig. 3-8 Gapmeter displacements for Girders G1, G3, and G5

3.2.4 Girder End Rotations

Fig. 3-9 shows a plot of the recorded rotations from the tiltmeters installed on the webs at Girder G3 ends on both sides of the monitored continuity diaphragm (Bent 24). It can be seen from the plot that rotations on both sides of the continuity diaphragm follow the same trend. This means that the girders are rotating in the same direction, which indicates that the continuity diaphragm is doing its job of providing continuity between the girders.

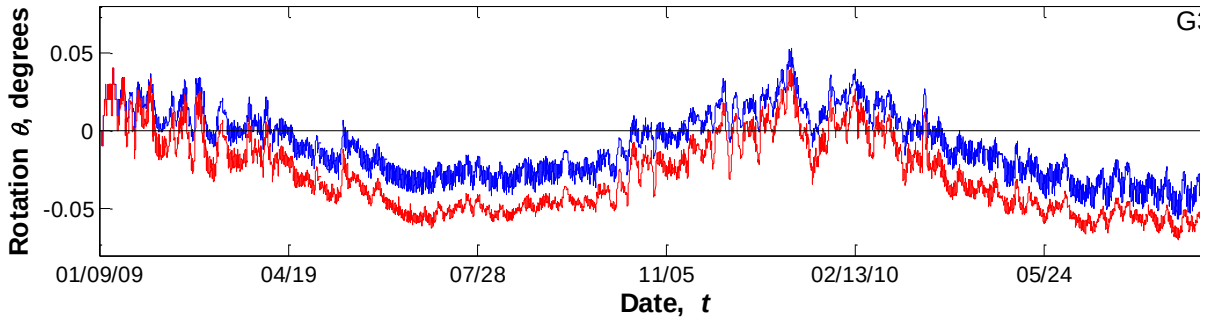

Fig. 3-9 Rotation of girder ends for G3

3.3 Live Load Test

A live load test on the monitored segment was conducted to assess the continuity detail's performance under truck loads. Two dump trucks weighing 54.1 and 57.0 kips (241 and 254 kN) were used to load the bridge in 9 static loading cases. The trucks were positioned in tandem for 6 side-by-side midspan positive moment positions (P1 through P6) and 3 truck train negative moment positions at Bent 24 (N1 through N3) as can be seen in Fig. 3-10. Details of the truck positions, which were determined using finite element analyses of a full bridge model, can be found elsewhere (Okeil et al. 2011). Due to the slow nature of the installed long-term monitoring system, the rate of data recording was 24 readings per hour, which were then averaged and stored for retrieval. This rate translated into one reading every 2.5 minutes. To ensure that more than one data point was collected for each static load position, the trucks remained at each position for a period equal to or longer than 11 minutes. During this period, at least three and probably four readings were recorded for each loading case. In between loading positions (P1 and P2, P3 and P4, P6 and N1, N1 and N2, and N2 and N3), the trucks were driven of the tested bridge segment to help determine a reference datum for the recorded readings. Fig. 3-11 shows the actual trucks in two of the static loading positions, namely P1 and N1.

As can be expected, not all sensors were highly strained by all loading positions because of their locations with respect to the position of the trucks. Therefore, a minimum threshold strain was set to discard readings that were too small to be considered reliable. The results were compared to analytical results from the Global FE model. Fig. 3-12shows a plot of the vertical displacement contours for the P5 load case. P5 is a case that causes positive moments in Span 24 (middle span). The two trucks were positioned over Girder G1, G2, and G3. As a result, downward deformations at this location could be seen in Fig. 3-12. At the same time, upward movement of girders in adjacent spans (23 and 25) took place.

One interesting observation was that the hairpin strain records confirmed that forces were transferred from Span 25 (loaded span) to Span 23 (monitored span) for load positions P3 and P6. These two cases caused positive moments on the monitored continuity detail. Fig. 3-13 shows the magnitude of the strains, which are larger for Girder G3 than G1.

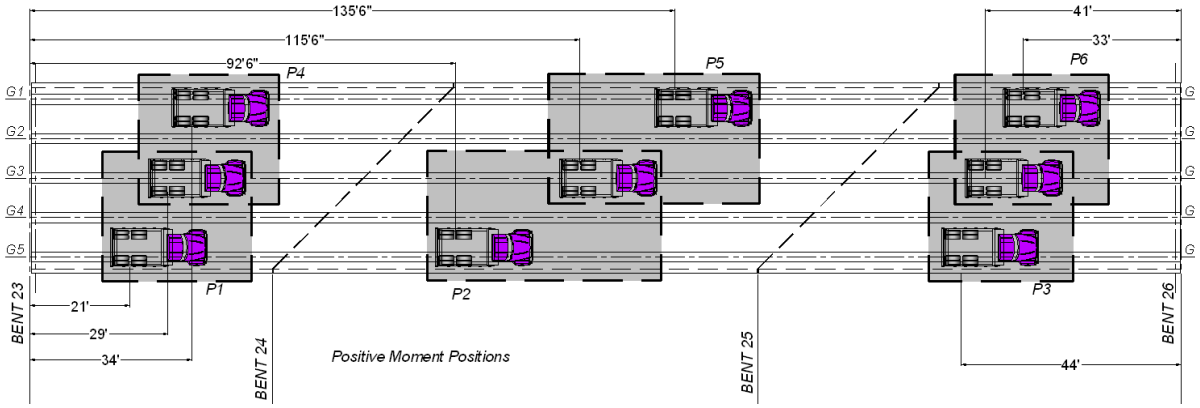

Positions for positive moment at midspans

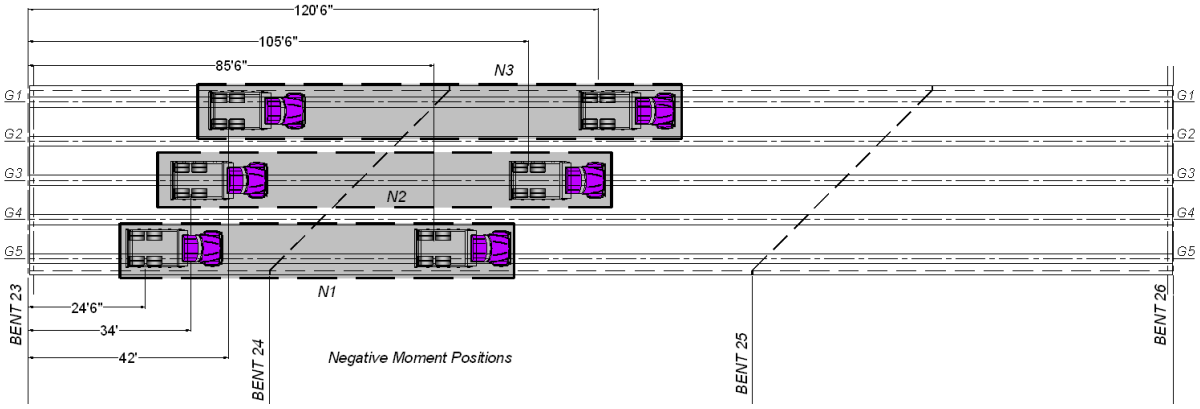

Positions for negative moment at Bent 24

Fig. 3-10 Load test truck positions (distance with reference to middle of rear drive axle – Note: 1ft = 0.305 m)

Position P1 Position N1

Fig. 3-11 Loading trucks in position for two of the nine static load positions

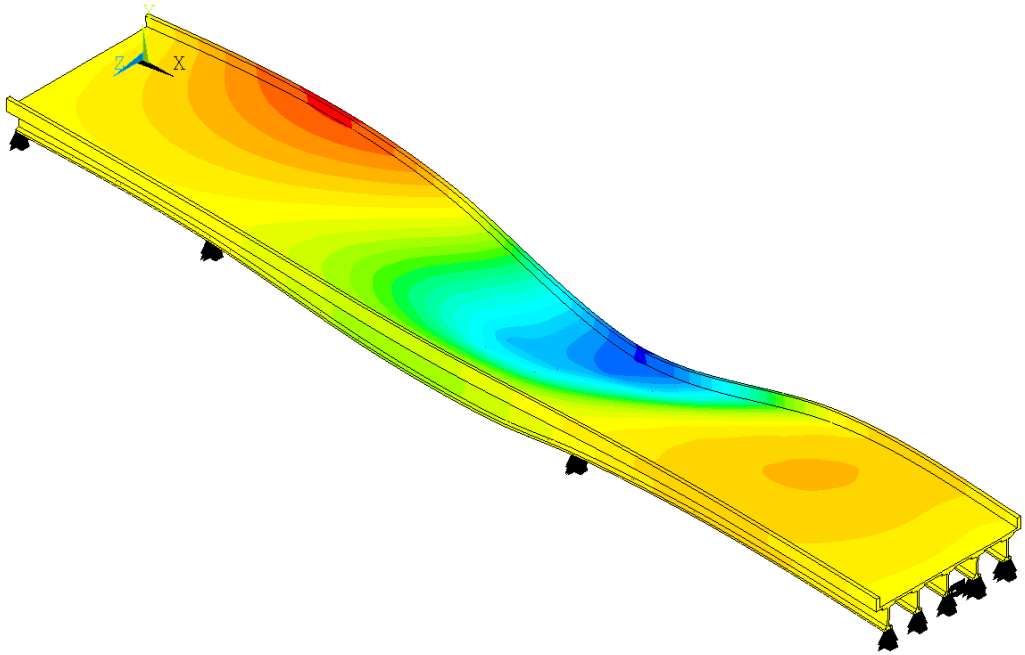

Fig. 3-12 Contours of vertical displacement (Case P5)

A similar observation was related to the recorded negative strains for load positions P2 and P5. Both were load cases that target positive moment in the middle of Span 24. Therefore, trucks were positioned over Span 24. The trucks would, however, apply negative moments on the continuity diaphragm if it performed as intended. In both load positions (P2 and P5), the hairpin bars experienced negative strains that were, as expected, higher than the positive strains discussed earlier. Like the P3 and P6 load cases, the sensors were in one span and the loads acted on another for these two cases. Hence, the ability of the new detail to transfer forces between spans was confirmed. It should be noted that results from Girders G1 and G3 were only presented since Girder G5 was not instrumented on the hairpin bars in Span 23 and, therefore, a plot was not provided.

3.4 Conclusions

Based on the presented results, it can be concluded that:

- Positive moments develop in bridges employing the new continuity detail. They are caused by long-term effects such as girder creep and thermal variations.

- The continuity detail has the ability to transfer forces from one girder end to the adjacent girder end across the continuity diaphragm as evidenced by the recorded data under long-term effects as well as live load effects.

- Seasonal and daily temperature variations can cause large restraint moments in the bridge, especially temperature gradients. The level of restraint moment due to the combined seasonal and daily temperature is probably the most important factor in the design of this detail, since the designer has no influence on the temperatures at the bridge site. The other positive-moment causing factor, i.e., girder creep caused by prestressing

forces, can be greatly reduced by not introducing continuity until a large portion of the creep takes place prior to pouring the diaphragm.

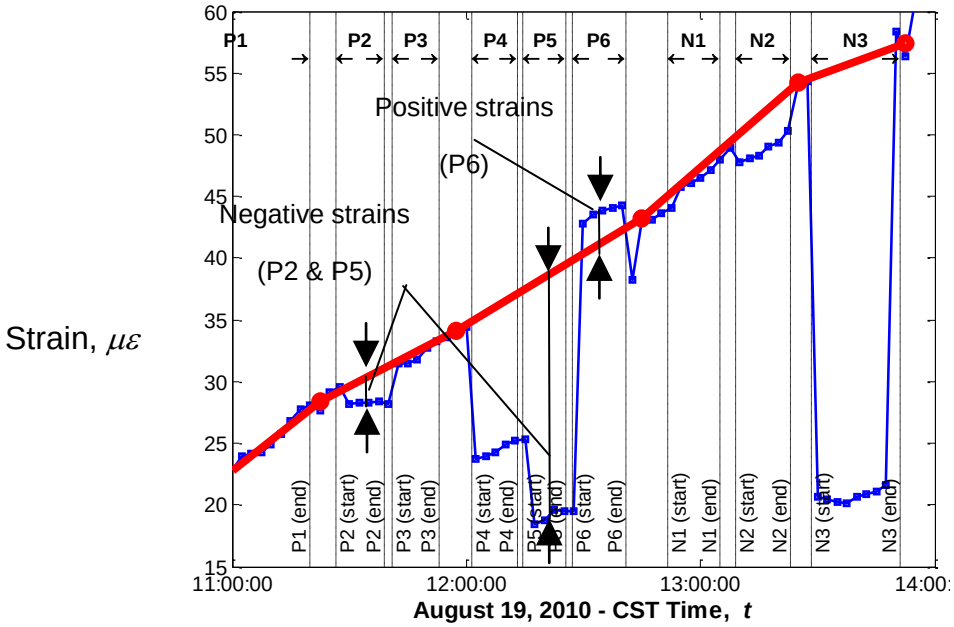

Girder G1 – Span 23 –Sensor #3

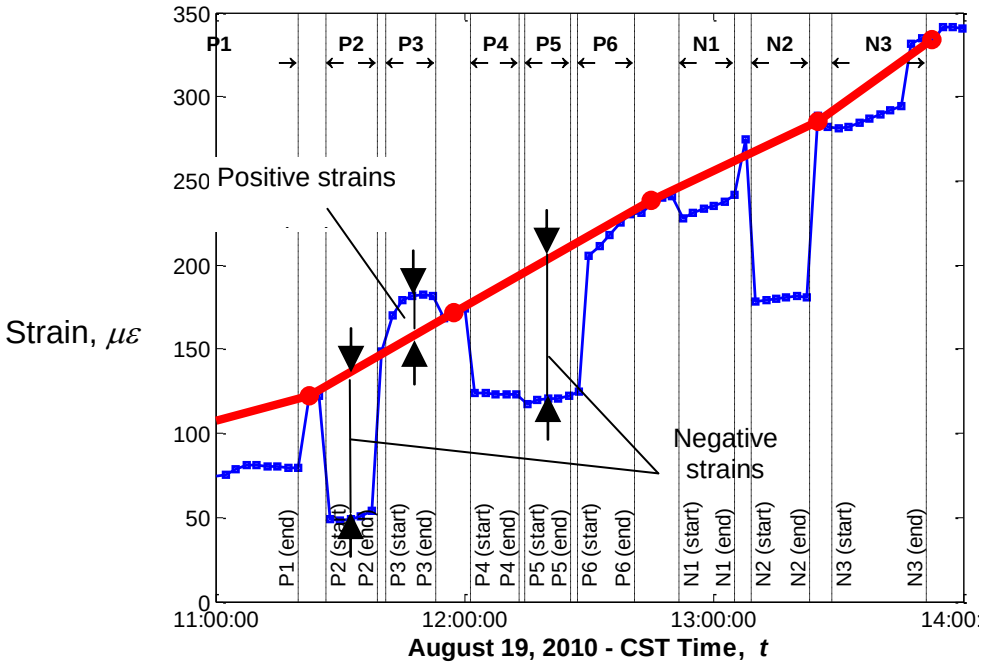

Girder G3 – Span 23 –Sensor #51

Fig. 3-13 Strains in hairpin bars showing positive values for faraway load cases

- Positive restraint moment can cause cracking in the diaphragm and/or girder ends if the total effect of positive moment causing factors are not considered in the design; i.e. creep in addition to thermal gradient. Girder cracking may have adverse effects on the durability and on the shear capacity of the girders. Therefore, special care should be

given to the level of positive restraint moment during design. The authors are of the opinion that temperature gradient effects need to be considered in the design regardless of girder's age at establishment of continuity.

- The live load test revealed that the continuity detail transferred negative and positive moments across the diaphragm. The strains from the live load test were much lower compared to other long-term effects. Even if the actual design load were to be applied (approximately twice the test live load), the strains would still be small. Therefore, the live load case should be considered in the design; however, it is not the most demanding action on the detail.

- The monitored segment was skewed. Skewed configurations cause additional straining actions that do not develop in non-skewed bridge configurations. Therefore, the skew effect may have exacerbated the straining actions on the continuity detail. However, this hypothesis will need to be explored further through analytical or field investigations before it is confirmed.

Discussions with the precaster and the contractor revealed that construction cost of the detail is not substantial. Nevertheless, the precaster would rather build girders without the detail. The contractor's critique of the new detail was stronger than that of the precaster. The contractor is of the opinion that the continuity diaphragm, especially for skewed bridge configurations, is cumbersome and adds to the construction time mainly because of the diaphragm's formwork. Simpler details that require less formwork would expedite the construction of slab-on-girder bridges.

3.5 Reference List

AASHTO (2010). "LRFD Bridge Design Specifications." American Association of State Highway and Transportation Officials, Washington, D.C.

Bordes, J. L., and DeBreuille, P. J. (1985). "Some Facts About Long-Term Reliability of Vibrating Wire Instrument." *Transportation Research Record*, Natl Research Council, Transportation Research Board, Washington, DC, USA, 20-27.

Burke, M. P., Jr. (1994). "Semi Integral Bridges: Movements and Forces." *Transportation Research Record*, 1460, 1-7.

Caner, A., and Zia, P. (1998). "Behavior and Design of Link Slabs for Jointless Bridge Decks." *PCI Journal*, 43(3), 68-80.

Choquet, P., Juneau, F., DeBreuille, P. J., and Bessette, J. (1999). "Reliability, long-term stability and gage performance of vibrating wire sensors with reference to case histories." 49-54.

Demartini, C. J., and Haywood, R. J. (1991). "Repair of the Southern Approach to the Story Bridge by Elimination of the Contraction Joints." 357-370.

Miller, R. A., Castrodale, R., Mirmiran, A., and Hastak, M. (2004). "Connection of Simple-Span Precast Concrete Girders for Continuity." *Rep. No. NCHRP Report 519*, Transportation Research Board, Washington, D.C.

Oesterle, R. G., Glikin, J. D., and Larson, S. C. (1989). "Design of Precast Prestressed Bridge Girders Made Continuous." *Rep. No. NCHRP Report No. 322*, Transportation Research Board, Washington, D.C.

Okeil, A. M., and El-Safty, A. K. (2005). "Partial Continuity in Bridge Girders with Jointless Decks." *Practice Periodical on Structural Design and Construction*, 10(4), 229-238.

Okeil, A. M., and Cai, S. C. S. (2009). "A Monitoring System for Long-term Performance of Positive Moment Continuity Detail in Prestressed Girder Bridges." National Academies, Washington, DC, United States.

Okeil, A. M., Cai, S. C. S., Chebole, V., and Hossain, T. (2011). "Evaluation of Continuity Detail for Precast Prestressed Girders." *Rep. No. 477*, Louisiana Transportation Research Center, Baton Rouge, LA.

Siros, K. A., and Spyrakos, C. C. (1995). "Creep Analysis of Hybrid Integral Bridges." *Transportation Research Record*, 1476, 147-154.

Wing, K. M., and Kowalsky, M. J. (2005). "Behavior, Analysis, and Design of an Instrumented Link Slab Bridge." *Journal of Bridge Engineering*, 10(3), 331-344.

4 ANALYTICAL AND FIELD MEASURED TEMPERATURE PROFILE AND ITS STRUCTURAL EFFECTS ON A CONTINUOUS GIRDER BRIDGE

4.1 Introduction

The behavior of bridge structures subjected to complex thermal stresses due to temperature variations has been a subject of interest for researchers for many years. Thermally induced stresses in a bridge are the result of differential daily and yearly temperature variation. If the cross section of the bridge is large, the variation of the temperature along the section is significant, which leads to thermally induced stresses. Statically indeterminate structures, such as continuous bridges, experience higher thermally induced stresses because of the added restraints to system deformations. Hambly (1978) presented a visual appreciation of temperature distributions within bridge decks throughout a day. Temperature distribution is considered as a superposition of a steady state average heat flow between top and bottom surfaces and an hourly changing variation near the surfaces. The National Cooperative Highway Research Program (NCHRP) published a comprehensive report (Report 276) on thermal effects in concrete bridge superstructures (Imbsen et al. 1985). The report includes stresses resulting from variations in average bridge temperatures and variations in temperature due to temperature gradients within the superstructures. The report states that average bridge temperature varies seasonally and/or diurnally primarily because of ambient temperature fluctuations, and if the resulting expansion and contraction of the bridge is restrained, internal stresses would developed. Radiation heat loss, or gain, results in a nonlinear distribution of temperature along the bridge height or width, and can create distortion or induced stresses.

The variation of the temperature of the bridge structure depends on many factors. The geographical location of the bridge and its orientation, the climatological condition, the bridge structure's material, surface condition and its surroundings are the primary factors affecting the temperature variation (Elbadry and Ghali 1983). The cross section of the bridge is also an important factor. The distribution of temperature over a bridge cross section is nonlinear in general and produces stresses both in the longitudinal as well as in the transverse direction (Elbadry and Ghali 1986). Dilger et al. (1983) showed that there is a significant temperature variation along a section of a concrete box girder bridge, and recommended that this variation should be taken into account in the design. Heat generation during hardening of concrete will also cause early temperature rise. Therefore, high curing temperatures during fabrication may affect the level of prestress because the strand length is fixed and the coefficient of thermal expansion of concrete and steel are different (Barr et al. 2005). If the volume movement of the concrete due to this increase in temperature is restrained, thermal stresses would develop and may results in early age thermal cracking as reported by (Du et al. 2011). An experimental study by Batla et al. (1985) indicates that a substantial temperature differential exist between the top flange and bottom portion of a concrete box girder superstructure due to the daily and seasonal variations of the surrounding atmospheric temperatures. The variation of the temperature along a concrete bridge section causes differential thermal strain and if not considered adequately, concrete cracks and durability of the structure is reduced. Furthermore, if the variation of the stress exceeds the fatigue stress, fatigue cracks may appear and the life of the structure is shortened. Realizing the importance of temperature effects, AASHTO-LRFD Bridge Design Specifications (AASHTO 2008) offers an idealized temperature gradient along the vertical

section of a bridge for consideration in the design when needed, which may be included in various load combinations.

In this study, the temperature variation at a particular bridge segment of the recently completed John James Audubon Project in Louisiana is investigated analytically and through a field study. The case study segment is part of Bridge #2, which is a precast prestressed concrete girder bridge built using standard Bulb-T girders (BT-72). A monitoring system has been installed on this bridge to study the effectiveness of a newly proposed continuity detail. All of the installed sensors are based on the vibrating wire technology and are capable of measuring the physical strain as well as the temperature at each monitored point (Okeil et al. 2011). The temperature readings from these sensors are used for validation of the analytical method. A computer program *RadTherm* (RadTherm2009) has been used in this study to predict the temperature at different locations of the girder which is then compared with the observed temperature from the installed sensors. The temperature gradient at different locations was determined using data from the installed sensors at different times of the year, and the results were compared to AASHTO-LRFD specified design temperature gradient. Finally, an analytical procedure to calculate the restraint moment resulting from the temperature gradient is also presented in this study. The primary and secondary stresses across the girder height that would develop from this temperature gradient are quantified and discussed.

4.2 Bridge Description

The subject of the current study is a segment of Bridge #2 of the John James Audubon Project, which is located in Pointe Coupe Parish, Louisiana. The bridge extends Route LA-10 across the Mississippi River connecting the cities of St. Francisville and New Roads. The project, which includes the longest cable stayed bridge in North America, was recently completed and opened to traffic. Spans 23, 24 and 25 of Bridge #2 were chosen to study the performance of a new continuity detail by employing a monitoring system (Okeil and Cai 2009). The new detail relies on positive moment reinforcement extending from girder bottom flanges, which develop inside the continuity diaphragm to transfer tension forces between adjacent girders (Miller et al. 2004). The monitored segment consists of five AASHTO Bulb-T girders, and the bent is skewed by 45° to accommodate an existing railway track. The monitoring system was built using vibrating wire gages, which have a built-in thermistor. Each gage recorded a reading (e.g. strain, slope) and a corresponding temperature, which will be used in the current study to investigate the temperature profile along with the associated thermal stresses that would develop from the existence of a temperature gradient. A top view of the monitored bridge segment can be seen in Fig. 4-1. Fig. 4-2 displays the cross section of the studied bridge.

4.3 Temperature Profile

The variation of temperature of a bridge structure depends on many factors. Geographical location of the bridge, its orientation with respect to the solar radiation, climatological condition, materials of the structure, and surroundings of the structure all play important roles in temperature variation (Elbadry 1986). Temperature not only varies diurnally, but also seasonally as the position of the sun changes with time and season due to the earth rotation around the sun. Depending on the earth's position with respect to the sun, the solar radiation can be theoretically calculated. The value of the solar radiation for different times of the day and year can then be used as an input parameter along with the other parameters in a finite element model to predict

the temperature profile of a bridge structure. This section describes the theoretical background of solar radiation calculation along with the finite element prediction of temperature profile at certain locations of the studied bridge.

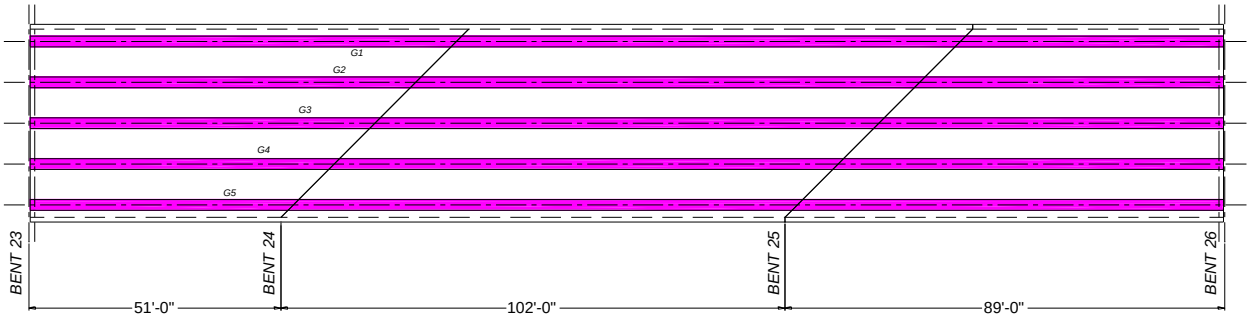

Fig. 4-1 Plan view of Bridge #2 showing different girders and spans

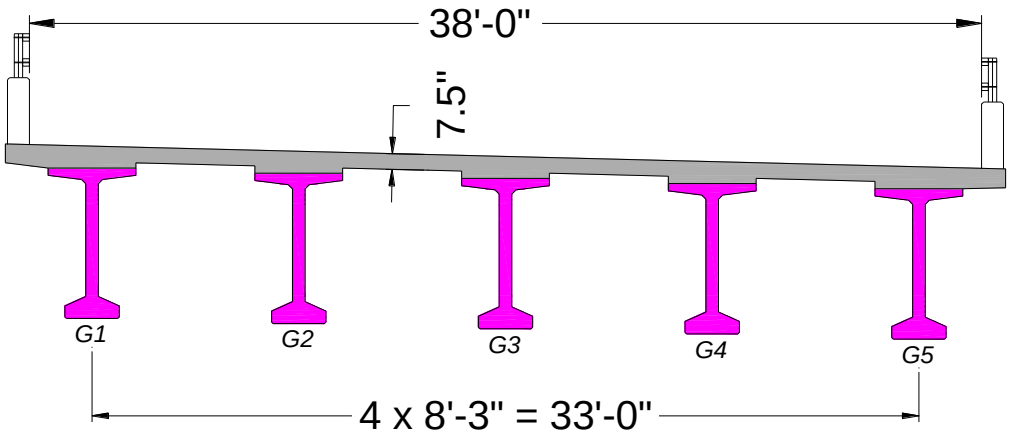

Fig. 4-2 Cross section of Bridge #2

4.3.1 Solar Radiation Calculation

The solar radiation incident on the outer side of earth's atmosphere is known as the extraterrestrial radiation and has an average value of 1367 Watts/m^2. As the earth orbits the sun; this value changes by about ±3% (Watt Engineering Ltd. 1978). To account for this orbital effect, the extraterrestrial radiation is given as:

$$I_0 = 1367 \times \left({R_{av}}/{R} \right)^2 \ w/m^2 \qquad (4\text{-}1)$$

where R_{av} is average sun-earth distance and R is the actual sun-earth distance. According to (Paltridge and Platt 1976) an approximate equation for the sun-earth distance is given as:

$$\left({R_{av}}/{R}\right)^2 = 1.00011 + 0.034221 \times \cos(b) + 0.001280 \times \sin(b)$$

$$+0.000719 \times \cos(2b) + 0.000077 \times \sin(2b) \qquad (4\text{-}2)$$

where $b = 2\pi n/365$ radians and n is the day of the year. The earth axis is tilted around 23.45º with respect to earth's axis around the sun. The angle between a plane perpendicular to a line between the earth and sun and the earth's axis is known as the angle of declination. Duffie and Beckman (1991) proposed an approximate formula for the angle of declination as:

$$d = {23.45\pi}/{180} \times \sin\left(2\pi \times {(284+n)}/{365}\right) \qquad (4\text{-}3)$$

where n is the number of the day of a year. The relationship between the solar time and the local time is required to describe the position of the sun. The solar time depends on the exact longitude of the position. The solar time is slightly different from the local time due to the earth's movement around the sun. The time difference is called the equation of the time; an important factor for solar energy calculation. An approximate formula for the equation of time is given as:

$$\left.\begin{aligned} E_{qt} &= -14.2 \times \sin\left(\pi \times \tfrac{(n+7)}{111}\right) && 1 \le n \le 106 \\ E_{qt} &= 4.0 \times \sin\left(\pi \times \tfrac{(n-106)}{59}\right) && 107 \le n \le 166 \\ E_{qt} &= -6.5 \times \sin\left(\pi \times \tfrac{(n-166)}{80}\right) && 167 \le n \le 246 \\ E_{qt} &= 16.4 \times \sin\left(\pi \times \tfrac{(n-247)}{113}\right) && 247 \le n \le 365 \end{aligned}\right\} \qquad (4\text{-}4)$$

where n represents a particular day of the year. The relationship between the local time and solar time can be estimated as a function of E_{qt} and the local time, T_{local} as:

$$T_{solar} = T_{local} + \frac{E_{qt}}{60} + \frac{(Long_{sm} - Long_{local})}{15} \qquad (4\text{-}3)$$

where $Long_{sm}$ represent the longitude of the standard meridian and $Long_{local}$ represents the longitude of the local time zone. The solar time can then be used to estimate the hour angle in radians, w as:

$$w = \frac{\pi(12 - T_{solar})}{12} \qquad (4\text{-}4)$$

When the sun ray makes an angle θ with the normal of the surface, the solar radiation I then can be expressed as;

$$I = I_0 cos\theta \qquad (4\text{-}5)$$

The angle θ can be determined in terms of several angles defining the position of the sun relative to the observer on the earth (Elbadry and Ghali 1983) as:

$$\cos(\theta) = \sin(d)\sin(l)\cos(T) - \sin(d)\cos(l)\sin(T)\cos(g) + \cos(d)\cos(l)\cos(T)\cos(w) + \cos(d)\sin(l)\sin(T)\cos(g)\cos(w) + \cos(d)\sin(T)\sin(g)\sin(w) \quad (4\text{-}6)$$

where l is the latitude of the location of which north being the positive, d is the solar declination angle, T is the angle between the horizontal and the surface, g is the angle of rotation from the north-south axis, and w is the hour angle in radians.

In this study, the computer program *Radtherm* (RadTherm2009) has been used to simulate the thermal conditions at the bridge site. *Radtherm* is a full featured heat transfer analysis software for system level applications. The program is capable of computing the temperature of a structure from the natural weather environment. The natural weather option uses the sky radiance and solar emissions to calculate the cooling or heating that takes place on a structure. The geographical location of the structure is input in terms of the latitude and longitude along with the local time zone. The weather data of a particular day are required as input and are described by eight different parameters in addition to the time of the day. The weather input values are represented by the diurnal air temperature variation, the solar irradiance, the wind speed, its humidity relative to the saturation level and direction, the long wave infrared radiation, and the rain fall. Finally, the cloud cover, which also affects the weather condition by influencing the solar radiation in the atmosphere, is given as input on a scale from 0 to 10; Zero being the clear sky while 10 represents a total overcast. Once the material property of the structure and the boundary conditions are set, the program then can calculate the temperature field for a particular time of a day from the input weather file and geographic information.

4.3.2 Input Parameters for Analyzed Girder

In this study Girder G3 of Span 24 of Bridge #2 has been selected. The temperature profile was analyzed at the bottom and mid-height of girder as well as at the deck. Two particular days of the year were chosen; namely 21st of January 2009 and 21st of June 2009. The months of January and June were selected to represent winter and summer conditions, respectively. The location of the bridge was determined using mapping software to be a latitude of $30^{\circ}44'$ and longitude of $-91^{\circ}23'$. These values are used as input parameters in the Radtherm program. The bridge is modeled as solid material of concrete with a unit weight of 2400 kg/m^3. The thermal conductivity of the material is taken as 1.5 W/m℃, and the specific heat as 960 J/kg℃. The data for the weather input file in the *Radtherm* program such as the diurnal air temperature, humidity, cloud cover, wind speed and direction, rain rate are taken for a particular day of the year from the National Oceanic and Atmospheric Administration (NOAA) and their minimum and maximum bounds are listed in Table 4-1.

4.3.3 Thermal Analysis

The thermal analysis was conducted using *Radtherm*, from which the temperature distribution across the girder section was extracted. The results are discussed in the next section and are compared to field data from the monitoring system installed on this bridge segment for the purpose of assessing a new continuity detail. Fig. 4-3-a shows the calculated and measured temperature variations at the top of Girder G3 in Span 24 at midspan during 18 consecutive hours starting at 6:00AM on 21st January 2009. The peak temperature occurred at around 4:00

PM as can be seen from the plot. The difference between the calculated and measured temperatures is highest during the peak hours. This variation is due in part to the fact that the calculated results are displayed for a point in the middle of the bridge deck. The embedded sensors, however, were installed on the lower mesh of deck reinforcement with is lower than that mid-deck location. It is known that the temperature is highest at the deck surface and drops rapidly in the first 4 inches as will be discussed later. The slightest deviation from the middeck location leads to a significant drop in temperatures. Furthermore, the rapid rise and drop of the temperature may be affected by the exact conditions at the bridge site, which may be slightly different from those obtained from the closest weather station. Fig. 4-3-b and Fig. 4-3-c show the temperature variation at the mid height and soffit of the same girder at the same location during the same time period. The peak temperature occurs around 3:00 PM after which the temperature starts to decline. As for the girder top, the measured and calculated temperature followed the same trend with some variations around peak hours due to the offset in calculated and measured locations. One observation from these plots is that the difference between the top and bottom temperature values is small (less than 10^{o}F). This indicates a low temperature gradient during winter months in Southern Louisiana.

Table 4-1 Input parameters for thermal analysis

	Time	Temperature (^{o}C)	Solar Irradiance (Watts/m^2)	Wind Speed (m/s)	Humidity (%)	Cloud Cover	LWIR, (Watts/ m^2)	Wind Direction, (degree)	Rain Rate (mm/hr)
Maximum	12:00 AM to 11:00 PM	10.0	952	13	82	7	0	170	0
Minimum		0.0	0	0	38	0	0	0	0

During summer months, the recorded temperatures are much higher (exceeding 100^{o}F). Fig. 4-4 display the temperature profile at the same location for June 21st, 2009. The calculated and measured temperatures follow similar trends with more variations in the calculated values due to abrupt input value changes from the weather station record.

4.4 Temperature Gradient

As can be observed from the previous results, temperature distribution in a bridge girder is not uniform as the girder top gets exposed to higher solar radiation in comparison with the girder parts under the deck. The difference of temperature between girder's top and bottom is often referred to as *Temperature Gradient*. AASHTO-LRFD (AASHTO 2008) specifies a generic temperature profile for use in the design of bridges. Fig. 4-5 shows the multilinear temperature gradient from AASHTO, which differs slightly from between concrete and steel girder structures. In this section, the midspan of Girder G3 in Span 24 is chosen to compare the measured and AASHTO specified temperature gradients.

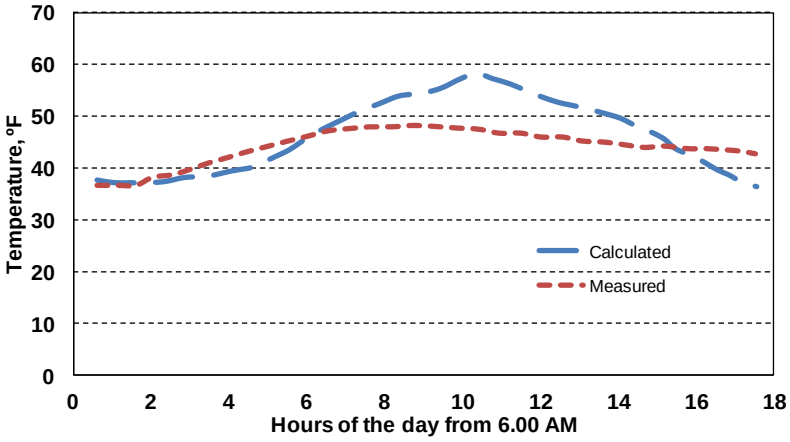

(a) girder top

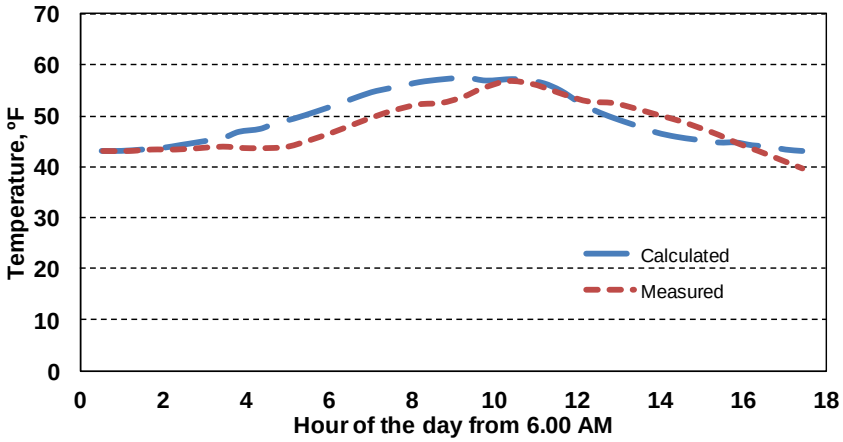

(b) girder mid-height

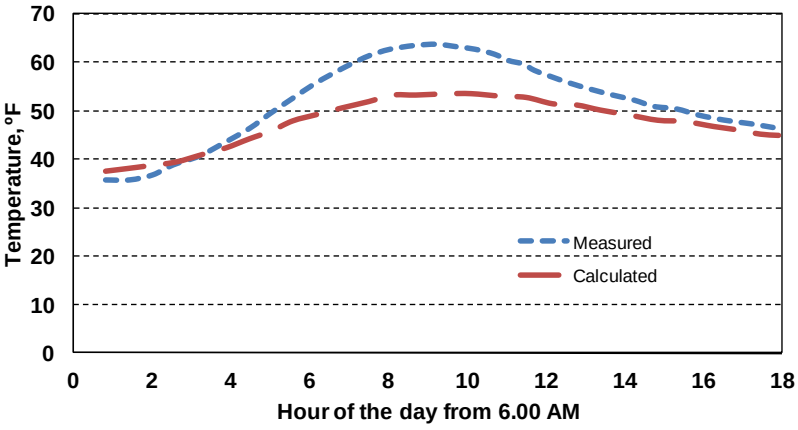

(c) girder soffit

Fig. 4-3 Daily temperature variation in Girder G3 at midspan on January 21, 2009 (Span 24)

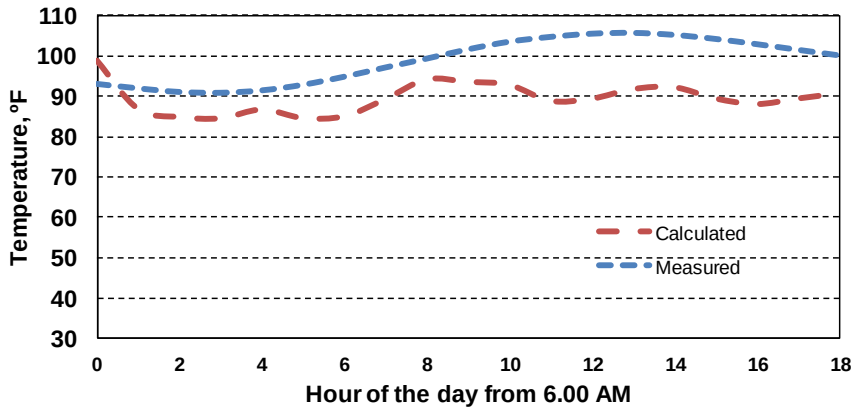

(a) girder top

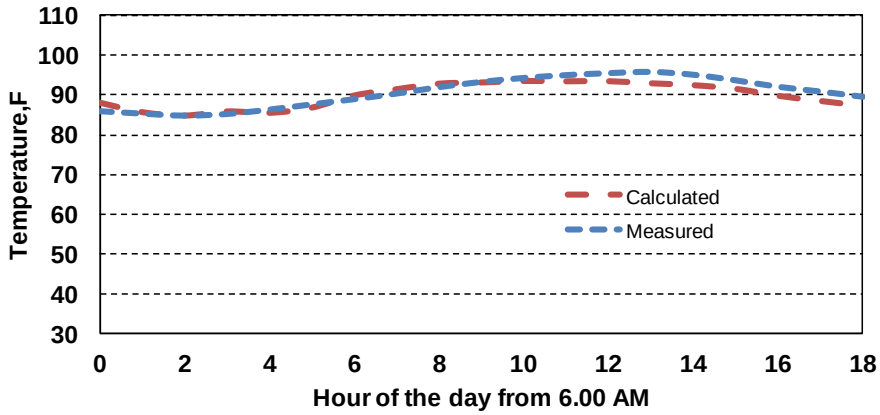

(b) girder mid-height

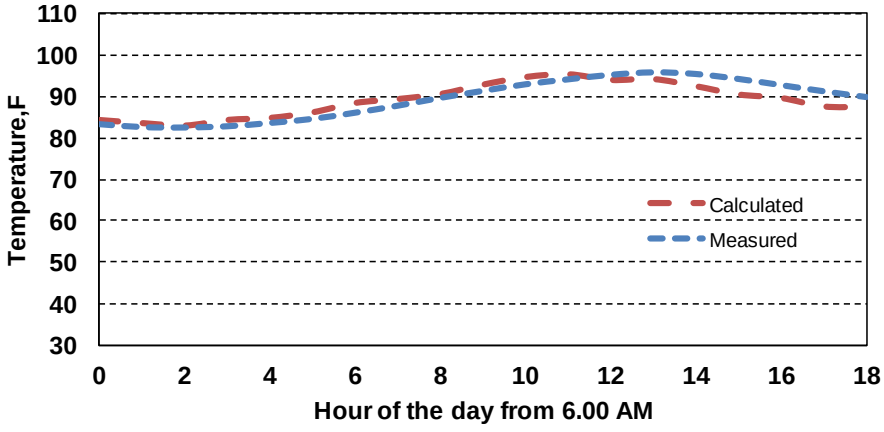

(c) girder soffit

Fig. 4-4 Daily temperature variation in Girder G3 at midspan on June 21, 2009 (Span 24)

At the chosen location, eight sensors were installed across the height of the girder (Okeil and Cai 2009). As stated earlier, the installed sensors had built in thermistors, and therefore recorded a temperature reading along with the main reading of the sensor (e.g. strain, slope) at a particular point. A typical day of May 10th, 2010 was chosen to investigate the daily variation of temperature gradient and temperature across the girder height was measured at 6:00 AM and at 3:00 PM to represent the coolest and hottest time of the day respectively. The measured temperature gradient was also compared with the AASHTO specified design gradient. Fig. 4-6 shows the temperature gradient of girder at 6.00 AM in the morning of May 10th, 2010. Ambient temperature for that time was taken from the NOAA recorded data. It can be seen from Fig. 4-6 that the measured temperature gradient is in good agreement the design gradient. The steep temperature increase for the first 4 inches in the design gradient were not captured in the sensor readings because the topmost sensor was below that depth. Sporadic measurements with a hand device revealed that the deck surface temperature is 10-15ºF higher than at the closest embedded deck sensor. Fig. 4-7 shows a plot of the temperature gradient at the same location, but at 3.00 PM in the afternoon of the same day. As expected, the plot shows that the temperatures rose in the afternoon,; however, the gradient still follows the AASHTO-LRFD design gradient. The higher value of temperature at the girder's soffit compared to its mid-height may be attributed for the heat radiation from the surrounding terrain which is also accounted for in the design gradient.

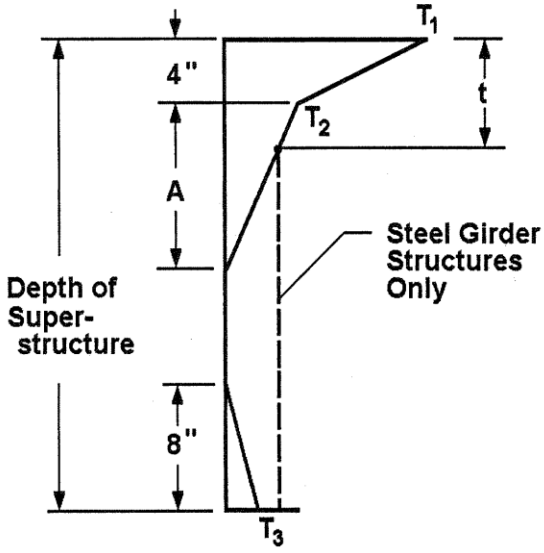

Fig. 4-5 Design temperature gradient in AASHTO LRFD Specifications (AASHTO 2008)

The seasonal effects on temperature gradient are investigated by comparing two typical days in the year; namely August 10th 2010 and December 12th 2009 which represent the summer and winter season, respectively. Fig. 4-8 displays the temperature gradient at the same location for August 10th 2010 at 3:00 PM in the afternoon. It can be seen here that the difference between the top and bottom temperature is about 18ºF. This large gradient does not take into account the higher deck surface temperature, which can add another 10-15ºF for a total difference between the top deck surface and the girder of about 28-33ºF. During the winter season, the temperature gradient on December 12th 2009 at 3.00 PM is plotted in Fig. 4-9 for the same location. As can be seen the difference between the top and bottom temperatures is almost negligible. This trend is typical of a cloudy day, when the effect of solar radiation is minimal. As a result, a uniform

temperature distribution is expected across the girder height. In summary, it can be said that the temperature gradient is much pronounced during the summer season than during the winter season temperature.

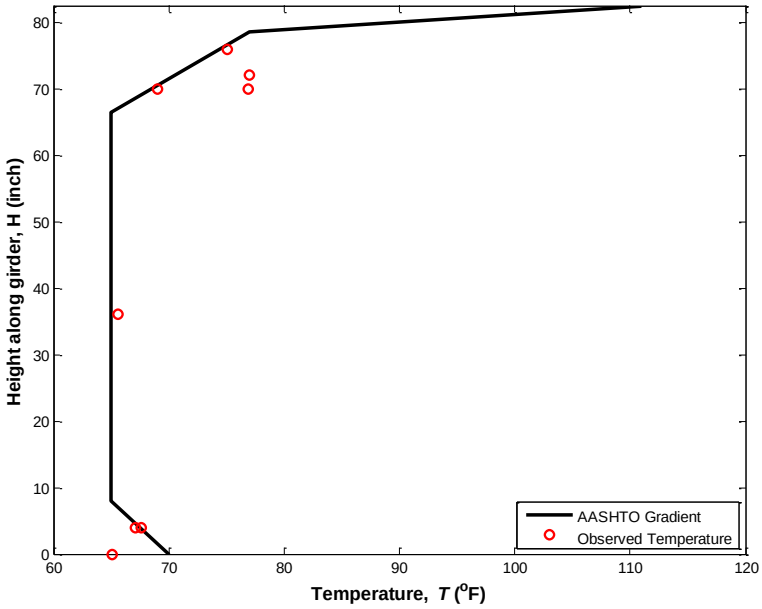

Fig. 4-6 Measured temperature gradient at the midsection of girder G3 span 24 at 6.00 AM of 10th May 2010

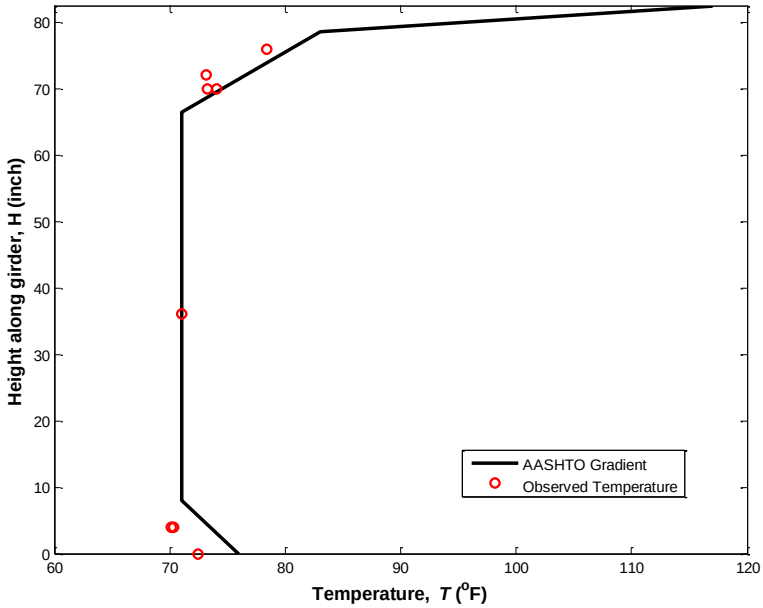

Fig. 4-7 Measured temperature gradient at the midsection of girder G3 span 24 at 3.00 PM of 10th May 2010

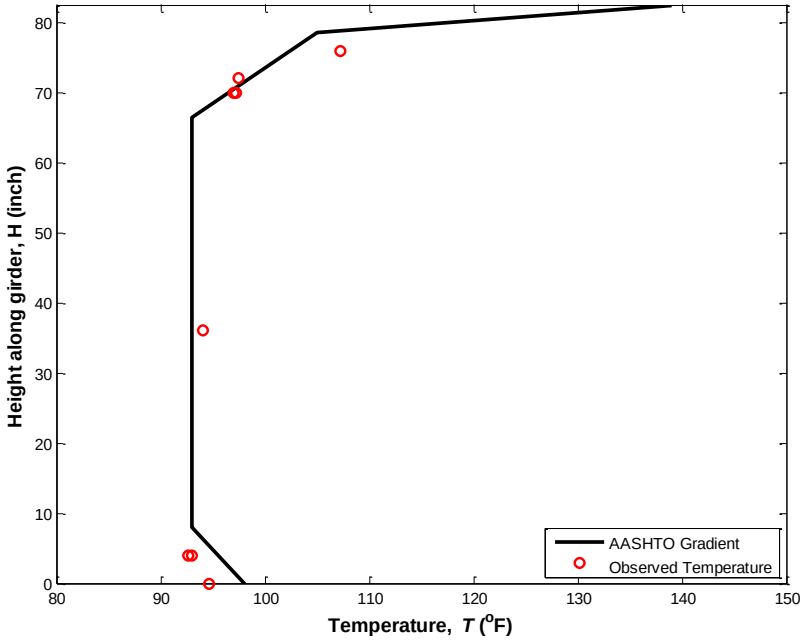

Fig. 4-8 Measured temperature gradient at the midsection of girder G3 span 24 at 3.00 PM of 10th August 2010

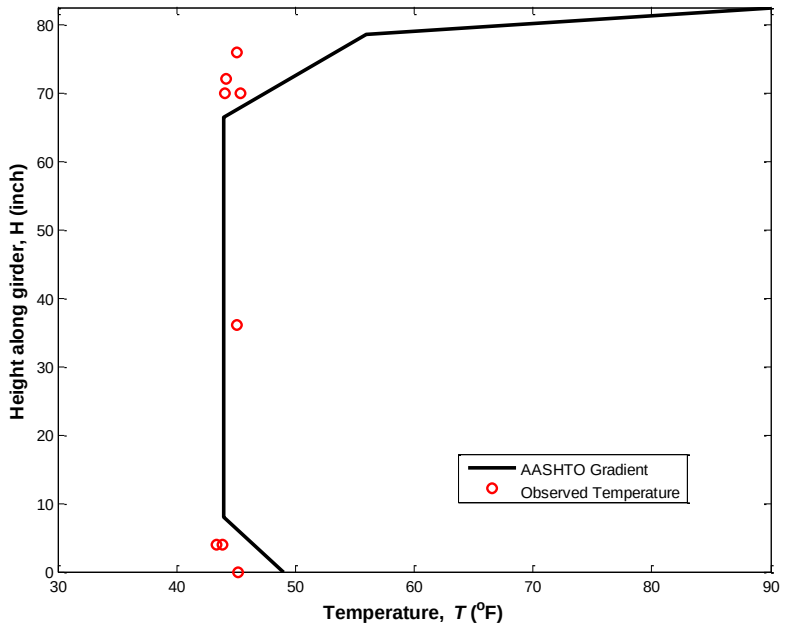

Fig. 4-9 Measured temperature gradient at the midsection of girder G3 span 24 at 3.00 PM of 12th December 2009

It should be noted that one of the girders experienced a negative temperature gradient; i.e. bottom flange temperature higher than deck temperature. This was observed during winter months when the sun shifts to the south exposing the bottom flange exterior girder to solar

radiation while the barrier and overhang shade the deck and top flange as can be seen in Fig. 4-10. This behavior was not of interest to this study since the continuity detail is capable of resisting the negative moments that develop from such negative temperature gradients.

Fig. 4-10 Solar radiation exposure for exterior girder on south side during winter months

4.5 Thermally Induced Stresses

Thermally-induced stresses are a common problem in the response of a continuous linear structure (e.g. bridge superstructure). Additional restraint exacerbates the effect of thermally induced stresses as it restricts the ability of the structure to move freely when temperatures change. Thermally-induced stresses are of two types; namely primary thermal stresses and secondary thermal stresses. Primary thermal stresses develop due to the nonlinear distribution of temperature across the height of structure whereas the secondary thermal stresses develop in statically indeterminate structures as a result of the compatibility to maintain the boundary conditions. The sum of these two stresses results in the total stress induced by temperature. Priestly (1985) presented an analysis method for estimating the thermal stresses induced by temperature gradient. These equations are based on fundamental mechanics principles in addition to some assumptions such as, material properties are independent of temperature, materials are homogenous and isotropic, plane section remains plane after thermal loading and temperature profile can be defined throughout the intended structure.

4.5.1 Primary Thermal Stresses

The primary thermal stress is calculated based on the assumption that plane sections remain plane. This assumption leads to the following equation:

$$f_{p(y)} = E_c\left(\varepsilon_y - \alpha_c \theta_{(y)}\right) \qquad (4\text{-}7)$$

where E_c is the modulus of elasticity of concrete, ε_y is the linear strain distribution, α_c is the coefficient of thermal expansion of concrete and $\theta_{(y)}$ is the change in temperature. Integrating Equation 9 over the section depth d results in the internal axial force. The equation can also be used to calculate the corresponding internal bending moment due to the primary thermal stresses. Since for primary thermal, the structure is made determinate by removing sufficient redundancies, therefore axial force and moment cannot develop and assumed as zero. This leads to the following equations:

$$P = E_c \int \left(\varepsilon_y - \alpha_c \theta_{(y)}\right) b_y dy = 0 \quad (4\text{-}8)$$

$$M = E_c \int \left(\varepsilon_y - \alpha_c \theta_{(y)}\right) b_y (y - n) dy = 0 \quad (4\text{-}9)$$

where b_y is the net section width at height y, n is the distance between the neutral axis and any arbitrary datum, and y is the height at which net section width is taken. The equation for the assumed linear strain distribution can be written as:

$$\varepsilon_y = \varepsilon_0 + \psi y \quad (4\text{-}10)$$

where ε_0 the final is strain at $y = 0$ and ψ is the final curvature. The curvature and strain equations can then be calculated by substituting for ε_y into the force and moment equation:

$$\psi = \frac{\alpha_c}{I} \int \theta_y b_y (y - n) dy \quad (4\text{-}11)$$

$$\varepsilon_0 = \frac{\alpha_c}{A} \int \theta_y b_y dy - n\psi \quad (4\text{-}12)$$

where A and I are the cross section's area and moment of inertia, respectively. Since most cross-sectional geometries will not be amenable for expressing their relations in the form of equations suitable for integration, it is more suitable to express the curvature and strain in summation form as:

$$\psi = \frac{\alpha_c}{I} \sum_{i=1}^{m} \theta_i (y_i - n) dA_i \quad (4\text{-}13)$$

$$\varepsilon_0 = \frac{\alpha_c}{A} \sum_{i=1}^{m} \theta_i dA_i - n\psi \quad (4\text{-}14)$$

where the section is discretized into m elements, θ_i and y_i are the average temperature change of the i-th fiber element of area dA_i, and centroid located a height y above the datum respectively. Once the strain and curvature is known, the primary thermal stress induced by θ_i is then calculated as:

$$f_{py} = E_c \left(\varepsilon_0 + \psi y - \alpha_c \theta_y\right) \quad (4\text{-}15)$$

4.5.2 Secondary Thermal Stresses

Secondary thermal stresses also develop in continuous bridge structures due to temperature changes. The secondary stresses are calculated using the fixed end moment produced by curvature, ψ. This is done conducting a statically indeterminate structural analysis where the redundancies in the system are first removed and then the compatibility equations are solved. Fig. 4-11 illustrates two ways for solving the problem. The restraint moment can be either negative or positive depending on the sign of curvature, which depends on whether the temperature gradient is positive or negative. The fixed end moment is calculated from the flexural rigidity of the section, $E_c I$, and the curvature, ψ:

$$M = E_c I \psi \quad (4\text{-}18)$$

The final moment M' is then calculated based using any structural analysis method (e.g. the moment distribution theorem), from which the secondary stress can be calculated:

$$f_{sy} = \frac{M'(y-n)}{I} \quad (4\text{-}19)$$

The total thermal stresses due to the temperature gradient can now be calculated as the summation of primary and secondary stresses as:

$$f_{ty} = E_c(\varepsilon_0 + \psi y - \alpha_c \theta_y) + \frac{M'(y-n)}{I} \qquad (4\text{-}20)$$

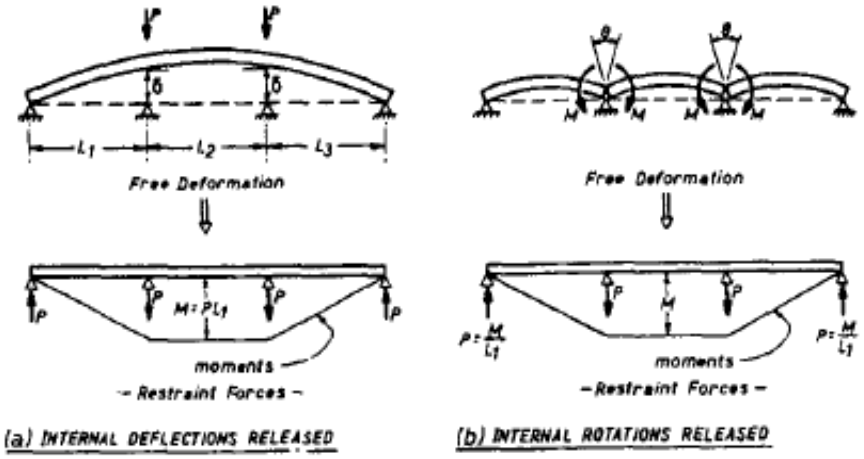

Fig. 4-11 Schematic representation of obtaining restraint moment developed due to temperature gradient

4.6 Thermal Stresses in Bridge #2

In this section, thermally induced stresses are assessed for the monitored segment of Bridge #2 that was described earlier. AASHTO specified design temperature gradient (see Fig. 4-5) as it was found that it provides an acceptable representation of actual field data. Girders G1, G2 and G3 of the monitored segment of Bridge #2 (see Fig. 4-1) were chosen for this study. The coefficient of thermal expansion was taken as $5.5\text{x}10^{-6}$/°F. The modulus of elasticity, E_c, was calculated for the deck and the girder based on the actual concrete strength obtained from cylinder tests, which were found to be 6.5 ksi and 11.5 ksi, respectively. Because of the difference in E_c for the deck and girder concretes, it was necessary to transform the deck and girder into one system based on the modular ratio. The cross section was discretized into 52 elements as can be seen from Fig. 4-12. As can be seen, the discretization was not uniform through the thickness. To improve the accuracy of the summations in Equations 15 and 16, more layers were considered where the gradient rate of change was higher (deck and girder flanges). The temperatures used in this study were $T_1 = 46$°F , $T_2 = 12$°F and $T_3 = 5$°F.

The primary thermal stress for girder G3 can be seen in Fig. 4-13. It can be seen for all the girders that at the top of deck and bottom flange of girder experience compression and web of girders experience tension force. In order to calculate the secondary stresses that develop due to restraining the global movement of the continuous structure, it is necessary first to calculate the restraint moment at the intermediate supports. This is done using a transformed section based on the elastic moduli of the deck and girder concretes. Once the restraint moment, M, is calculated using Equation 4-18, the final moment, M', is then obtained through moment distribution analysis. The restraint moment and the final moments for girder G1, G2 and G3 are summarized in Table 4-2. Fig. 4-14 shows the secondary stress distribution for girder G3.

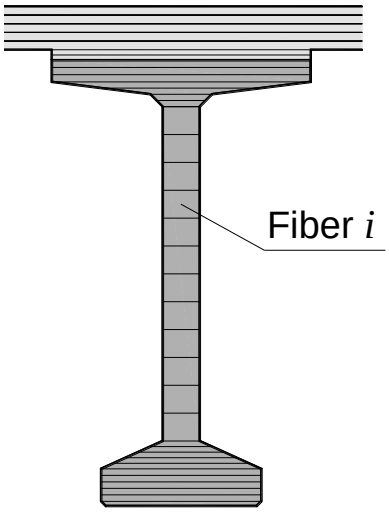

Fig. 4-12 Schematic of girder discretization for temperature induced stress calculation

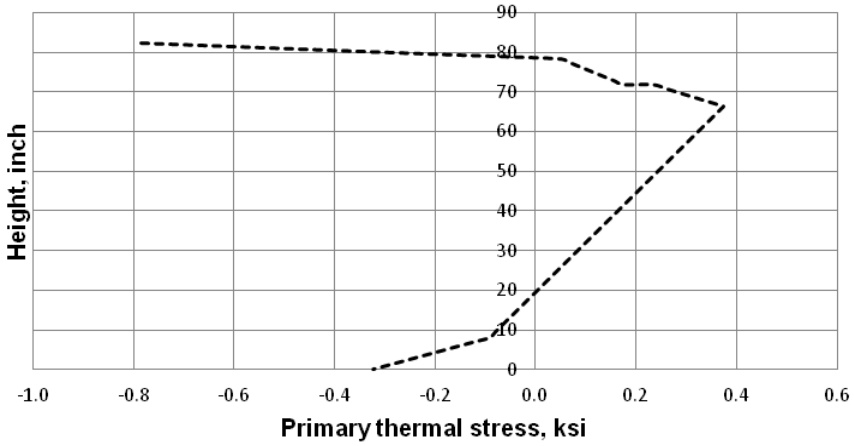

Fig. 4-13 Primary thermal stress for girder G3

Table 4-2 Comparison between the cracking moments and temperature induced restraint moments for different girders

Girder	Cracking Moment, M_{cr} (kip-in.)		Restraint Moment, M' (kip-in.)	
	At diaphragm	At girder end	At Bent 24	At Bent 25
G1	14799	20260	11057	10135
G2	14751	20967	11020	10553
G3	14751	20967	10833	10833

The total thermal stress at any point across the section height is obtained by summing the primary and secondary thermal stresses (Equation 4-20). Fig. 4-15 displays the total thermal stress for girder G3. It can be seen that the temperature gradient subjects the girder top to compressive stresses that may reach 1 ksi. The corresponding maximum total tensile thermal stress can reach about 0.37 ksi and takes place 9 in. above the girder's soffit. The total thermal stresses for Girder G1 and Girder G2 were also calculated in a manner similar to that used for Girder G3. The results can be seen in Fig. 4-16 and Fig. 4-17, respectively. For these girders, two lines are plotted in each figure. Each of the plotted lines represents one of the intermediate supports which are subjected to different moment levels unlike Girder G3 where symmetry leads to equal restraint moment at both intermediate supports. From Fig. 4-16 and Fig. 4-17, it can be said that the thermal stress distribution and magnitudes are almost identical with some minor variations due to the geometric differences between girders.

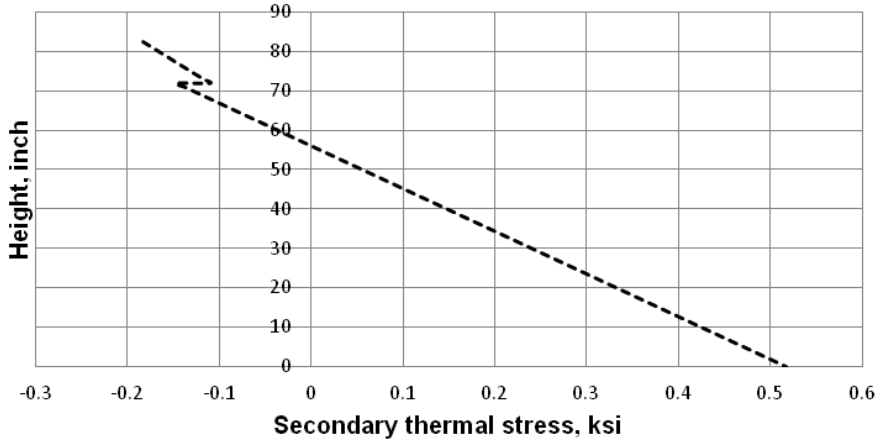

Fig. 4-14 Secondary thermal stress for Girder G3

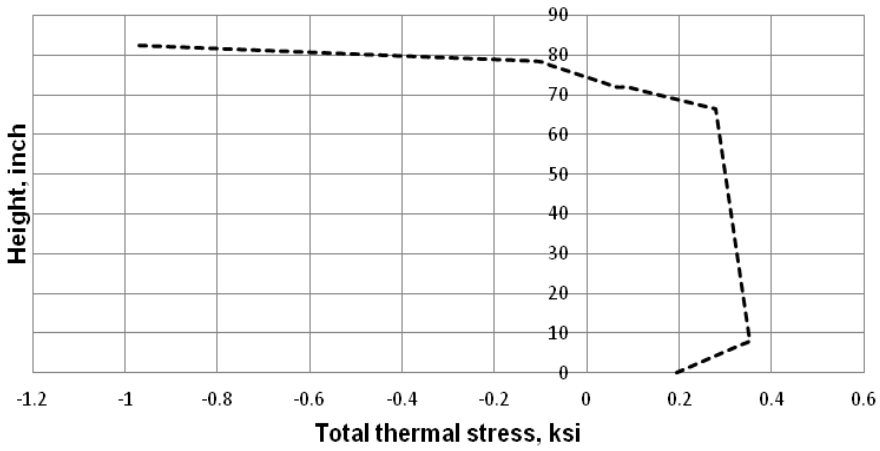

Fig. 4-15 Total thermal stress for Girder G3

4.7 Cracking Moment

The potential for cracking at the intermediate supports of continuous girder bridges will now be assessed by comparing the thermally induced restraint moment to the cracking moment at the critical locations. The modulus of rupture, f_r, is first calculated following AASHTO-LRFD provisions:

$$f_r = 0.24\sqrt{f_c'} \qquad (4\text{-}21)$$

where $f_c^{'}$ is the compressive strength of concrete in ksi. The modulus of rupture is then used to calculate the cracking moment using the following equation considering diaphragm cracking:

$$M_{cr} = \frac{I_g f_{r/diaphragm}}{y_t} \qquad (4\text{-}22)$$

where y_t is the distance from the neutral axis to the tension surface; i.e. girder soffit, and I_g is the gross moment of inertia of girder. The cracking moment at the girder end can be calculated as:

$$M_{cr} = \left(\frac{f_{r/girder} I_g}{y_t}\right) + \left(\frac{P_e I_g}{A_g y_t}\right) + P_e e \qquad (4\text{-}23)$$

where A_g is the area of girder, P_e is the effective prestressing force at the critical section, which is taken at the face of the diaphragm, and e is the eccentricity of the prestressing strands. The effective prestress force in was calculated assuming linear transfer stress (Nilson 1987) at a distance of 4 in. from the girder end, i.e. at the face of the diaphragm. Table 4-2 shows the comparison between the calculated cracking moment of the diaphragm and girders with the moment that develops from the temperature gradients. From the results, it can be seen that in all the cases temperature gradient induced restraint moment is below the cracking moment of diaphragm and decks. It should be noted that the positive moment reinforcement is the only mechanism for transferring the tension force between adjacent girder ends through the diaphragm. As a result, this continuity detail is considered a disturbed region (Schlaich et al. 1987), which implies that the tensile force will be transferred through the concrete areas around the reinforcement only and not the entire section. According to St. Venant's principle, it can be

said that the localization effect of the reinforcement becomes small after a distance equal to about the section's depth after which it can be assumed that the entire section resists the straining actions. This means that higher stresses than those calculated from basic principles are to be expected at girder ends. Furthermore, additional positive moments also develop at intermediate supports due to other factors (e.g. creep and some live load positions). Therefore, the superposition of all these effects may subject the girders to high tensile stresses leading to cracking at girder ends or in continuity diaphragms. Visual inspection of the monitored segment revealed a bottom flange crack at 4 in from the girder end. The crack was first noticed after the first heat wave during in May 2009.

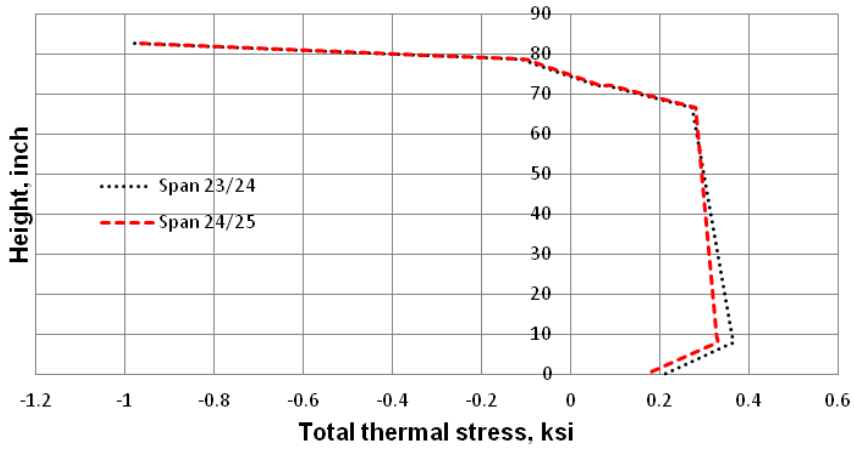

Fig. 4-16 Total thermal stress for Girder G1

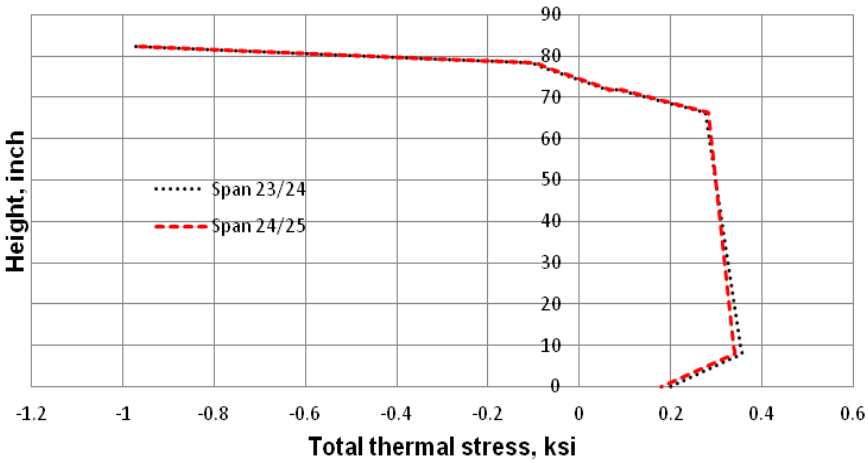

Fig. 4-17 Total thermal stress for Girder G2

4.8 Conclusion

In this study, Bridge #2 of the John James Audubon project was analyzed for temperature effects. Estimation of temperature at different parts of the structure due to solar radiation is first performed with the aid of a computer program using the geographical as well as atmospheric data. Seasonal and diurnal temperature were estimated and compared with the measured values from an existing monitoring system. The temperature gradient across the superstructure was then

studied and thermally induced stressed were calculated. Based on the results, the following conclusions can be drawn:

- Good agreement between analytical and field temperature data was observed. This implies that analytical models for complex structures can be used to predict thermal conditions, which can then be used in design.
- Field temperature data revealed that the AASHTO LFRD design temperature gradient is adequate for design of girder bridges as it matched the recorded temperature gradient across the superstructure from the monitoring system.
- The primary and secondary thermal stresses that develop due to the temperature gradient can cause high tensile stresses due to the restraint moment at intermediate supports of continuous structures. While estimates of the cracking moment were above the calculated restraint moments, stress concentrations in disturbed regions may still cause cracking to occur as was observed in the field especially since other long-term effects (e.g. creep) may cause additional tensile stresses.

Based on these conclusions, it is recommended that temperature effects be considered in the design of continuous bridges.

4.9 References

AASHTO (2008). *LRFD Bridge Design Specifications*. American Association of State Highway and Transportation Officials, Washington, D.C.

Barr, P. J., Stanton, J. F., and Eberhard, M. O. (2005). "Effects of Temperature Variations on Precast, Prestressed Concrete Bridge Girders," *Journal of Bridge Engineering*, American Society of Civil Engineers, Vol. 10, No. 2, pp. 186-194.

Batla, F. A., Reisnour, P. R., and Pathak, D. V. (1985). "Deformations and Stresses in Flanged Concrete Structures due to Temperature Differentials." *Deflections of Concrete Structures*, American Concrete Inst, Phoenix, AZ, USA, pp. 395-406.

Dilger, W. H., Ghali, A., Chan, M., Cheung, M. S., and Maes, M. A. (1983). "Temperature Stresses in Composite Box Girder Bridges," *Journal of Structural Engineering*, Vol. 109, No. 6, pp. 1460-1478.

Du, J., Luo, X., Ng, P. L., and Au, F. T. K. (2011). "Early age temperature rise and thermal stresses induced in concrete bridge pier." *2011 International Conference on Structures and Building Materials, ICSBM 2011, January 7, 2011 - January 9, 2011*, Trans Tech Publications, Guangzhou, China, pp. 2731-2737.

Duffie, J. A., and Beckman, W. A. (1991). *Solar Engineering of Thermal Processes*. John Wiley & Sons, New York.

Elbadry, M. (1986). "Thermal Stresses and Cracking of Concrete Bridges," .

Elbadry, M., and Ghali, A. (1986). "Thermal Stresses and Cracking of Concrete Bridges," *Journal of the American Concrete Institute*, Vol. 83, No. 6, pp. 1001-1009.

Elbadry, M. M., and Ghali, A. (1983). "Temperature Variations in Concrete Bridges," *Journal of Structural Engineering*, Vol. 109, No. 10, pp. 2355-2374.

Hambly, E. C. (1978). "Temperature Distributions and Stresses in Concrete Bridges," *Structural Engineer*, Vol. 56 A, No. 5, pp. 143-148.

Imbsen, R. A., Vandershaf, D. E., Schamber, R. A., and Nutt, R. V. (1985). "Thermal Effects in Concrete Bridge Superstructures." *NCHRP Report No. 276*,

Miller, R. A., Castrodale, R., Mirmiran, A., and Hastak, M. (2004). "Connection of Simple-Span Precast Concrete Girders for Continuity." *NCHRP Report 519*, Transportation Research Board, Washington, D.C.,

Nilson, A. H. (1987). *Design of Prestressed Concrete*. John Wiley & Sons Inc.

Okeil, A. M., and Cai, S. C. S. (2009). "A Monitoring System for Long-term Performance of Positive Moment Continuity Detail in Prestressed Girder Bridges." *88th Annual Meeting of the Transportation Research Board*, National Academies, Washington, DC, United States.

Okeil, A. M., Cai, S. C. S., Chebole, V., and Hossain, T. (June 2011). "Evaluation of Continuity Detail for Precast Prestressed Girders." *477*, Louisiana Transportation Research Center, Baton Rouge, LA, p. 198.

Paltridge, G. W., and Platt, C. M. R. (1976). *Radiative processes in meteorology and climatology*. Elsevier Scientific Pub. Co..

Priestley, M. J. N. (1985). "Long Term Observations of Concrete Structures. Analysis of Temperature Gradient Effects," *Materials and Structures/Materiaux et Constructions*, No. 106, pp. 309-316.

RadTherm (2009).Theory Reference.

Schlaich, J., Schäfer, K., and Jennewein, M. (May 1987). "Toward a Consistent Design of Structural Concrete," *PCI Journal*, PCI, Vol. 3, No. 3, pp. 74-150.

Watt Engineering Ltd. (1978). *On the Nature and Distribution of Solar Radiation*.

5 CALIBRATED FINITE ELEMENT MODELING OF CREEP BEHAVIOR OF PRESTRESSED CONCRETE BRIDGE GIRDERS

5.1 Introduction

Concrete in prestressed girders remains under compressive stress in service load conditions, and therefore it deforms plastically, which is known as creep. Creep is a material property and is defined as the deformation of a material subjected to sustained loads. Estimation of creep in a prestressed concrete girder bridge is very important as it affects the girder's camber, loss of prestress in prestressing strands, and also causes restraint moments if the girders were made continuous by casting a diaphragm between the ends of adjacent girders. The rate of creep not only depends on the material properties but also on the age of concrete maturity when the load is applied and on the magnitude of the applied stress. According to a report published by American Concrete Institute (ACI) Committee 209 on the subject(ACI 1992), the amount of concrete creep is proportional to the applied stress if it is about 40% of the concrete strength at the time of loading. Other researchers(Shams and Khan 2000) suggested that the creep strain is proportional to the applied stress for stresses up to 60% of the compressive stress of the concrete at the time of loading. The load and resistance factor design (LRFD) bridge design specification(AASHTO 2008) also imposes a limit on the compressive stress as 60% of the concrete strength at the time of loading.

Concrete creep has been the focus of many researches for quite some time who introduced several models for its estimation. ACI Committee 209(1992) proposed a method for determining the three parameters needed for estimating long-term deformations of concrete structures; namely, creep coefficient, shrinkage strain and total strain. The creep coefficient is defined as the ratio of creep strain to the elastic strain and its ultimate value is determined from the properties and mix proportions of the concrete. Once the ultimate creep coefficient is determined, it can then be adjusted to predict the desired creep coefficient at any point in time. The PCI-BDM(1997) recommends two methods of estimating the creep coefficient and shrinkage strain. The first method is the same as the one recommended by ACI-Committee 209(ACI 1992) and is applicable to concrete with compressive strengths ranging from 20.7 to 34.5 MPa (3 to 5 ksi), while the second method is based on the modifications by Hou(1997) of these recommendations and is applicable to concrete with compressive strengths ranging from 27.6 to 82.7 MPa (4 to 12 ksi). The European model (also known as the CEB-FIP-90 model) proposed a creep coefficient and shrinkage strain for concrete with compressive strength ranging from 11.7 to 80.0 MPa (1700 to 11600 psi)(Comite Euro-Internationale Du Beton (CEB) 1990). The proposed coefficient is applicable to members subjected to a compressive stress limit of 40% of the concrete compressive strength at the time of loading. This model for estimating creep strain is applicable to cases where humidity is in the range of 40 to 100% and the average temperature ranges from 41 to 86ºF.

AASHTO LRFD(2008) specifications allows the use of ACI-209 and CEB-FIP-90 methods in estimating the creep coefficient and shrinkage strain. It should be noted that AASHTO LRFD specifications adopts a modified ACI-209 model based on the more recent experimental data and the research by Collins and Mitchell(1991) for determining the creep

coefficient and shrinkage strain. Despite the fact that there is a difference between the creep behavior for normal strength concrete and high performance concrete (HPC), provisions in AASHTO-LRFD specifications do not differentiate between these two categories of concrete strength. Therefore, Shams and Khan(2000) proposed a modification to the AASHTO LRFD provisions for creep and shrinkage to address the lower creep strain observed for HPC. The proposed modifications include the stress-to-strength ratio at the time of loading, length of moist curing and concrete maturity at the time of loading. The factors for concrete strength and concrete maturity were also modified. Tadros et al.(2003) proposed another model for estimating the creep coefficient and shrinkage strain for high strength concrete (HSC) which is a modified version of ACI-209 model. Le Roy et al.(1996) developed a creep model also known as AFREM model that is particularly suited for HSC. This model helps the designer in predicting the creep strain during the design phase and depends on the elastic modulus of concrete at 28-days rather than the concrete modulus at the time of loading. The B3 model which was developed at Northwestern University by Bazant and Baweja(Bazant and Xi 1989; Bazant and Baweja 1995) takes into account the diffusion process of concrete, and is considered as the most theoretically-based model available to compute creep and shrinkage strain. This model does not compute creep strain from the traditional creep coefficient. Alternatively, the model computes the creep strain using a *"creep compliance function"* that depends on the concrete properties. Gardener and Lockman(2001) developed another model, GL2000, for estimating creep strains in concrete. The advantage of this model is that all the information used as input parameters for creep strain calculation are available to the engineer during the design phase such as the mean compressive strength, relative humidity, type of cement, age of loading, volume to surface ratio and the stress being applied.

All of the aforementioned creep models have their own limitations in estimating creep strains over time. A thorough experimental work carried out by Waldron(2004) on normal as well as high strength concrete revealed that most of these models tend to overestimate the creep strain while a few models underestimate it. Overestimating creep strains results in uneconomical overdesign of the members whereas underestimating may result in adverse effects (e.g. excessive deflections or cracking) even under service loads. Waldron(2004) also noted that time step methods for estimating creep strain usually consider simple span girders, while in reality prestressed concrete girder are in many cases built to be continuous by placing a diaphragm between the adjacent girder ends to benefit from the inherent advantages of continuity over simple span construction. Waldron(2004) also suggested considering continuity effects on the creep behavior in the design of bridges. Furthermore, the construction sequence also plays a vital role on creep strain because the applied load on the concrete girders causes major changes to the most important factor affecting creep; i.e. magnitude of sustained stress, in every construction stage. As a result, the long-term deformations are greatly affected by the construction sequence.

In general, the creep strain is estimated at the centroid of the prestressing strands and at the midspan of the girders. Estimation of creep strains by considering the varying stress state at different sections and locations along the span is computationally expensive and time consuming. Therefore, a robust method for estimating creep deformations of prestressed girder bridges is needed which not only includes the effect of continuity and construction sequence, but also should be able to determine creep deformation at any place and any location in the bridge. Finite element modeling of long term deformation of prestressed girder bridges offers all these advantages. In this paper, a finite element (FE) model for simulating long-term creep behavior of

a prestressed concrete girder from a full scale continuous bridge using the finite element software ANSYS is presented. The girder is part of Bridge #2 from the John James Audubon Bridge Project, which adds a new traffic artery across the Mississippi River between the cities of New Roads and Saint Francisville in Louisiana. The project was bid as a design and build contract and the designer chose to use one of the positive moment continuity details recommended in NCHRP Report 519 (Miller et al. 2004) which can be seen in Fig. 5-1. To evaluate the performance of this continuity detail, a structural health monitoring system was installed and data were collected for a period of almost two years. Monitoring data from the initial period of the girder life while being stored as a simply supported girder at the casting yard were first used to calibrate the creep model in ANSYS. The model was then used to predict the creep response during the first 1000 days of the girder life, which includes periods when the girder was integrated in the bridge's continuous superstructure. Finally, the FE model was used to estimate the restraint moment and comparisons between these estimates at different girder ages at the time of establishing continuity and other model estimates are presented.

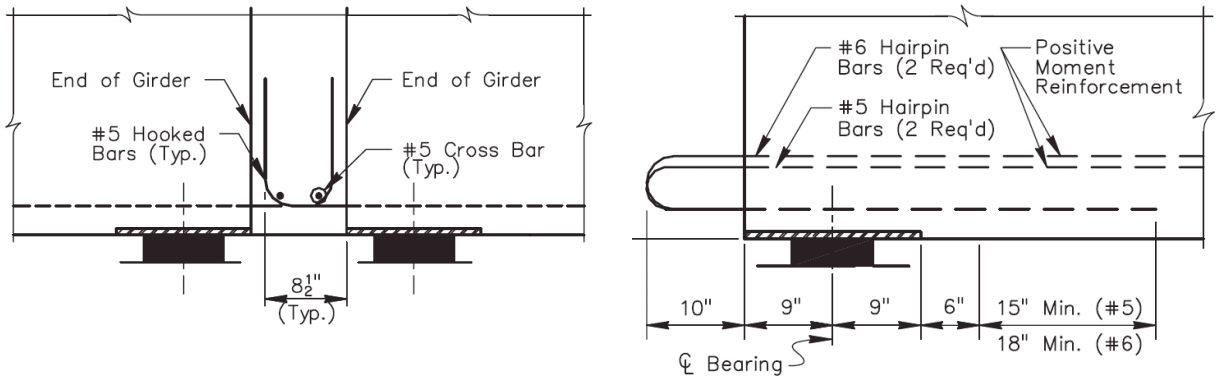

(a) hooked bars or prestressing strands (b) hairpin bars

Fig. 5-1 Alternatives for positive moment reinforcement

5.2 Bridge Description

The recently completed John James Audubon Project adds a new transportation artery across the Mississippi River between the cities of New Roads and Saint Francisville in Louisiana. The project consists of eight bridges including a major cable-stayed span across the river. Bridge #2 is the subject of the current study, which consists of 52 spans for a total length of about 1200 m (4000 ft) that are divided into 14 continuous segments. The LA-DOTD chose a 73.76 m (242 ft) segment of this bridge to monitor the performance of a newly adopted positive moment continuity detail (see Fig. 5-1) that was one of the recommendations in the National Cooperative Highway Research Program (NCHRP) Report 519(Miller et al. 2004) resulting from NCHRP Project 12-53. Fig. 5-2 shows the plan view of Bridge #2 which crosses an existing rail line. The longest span (31.09 meters (102 ft)) of this bridge segment is skewed by 45º to accommodate the railway track, and as a result, the girders in both exterior spans ranged in length from 15.54 meters to 27.13 meters (51 ft to 89 ft). The five girders are denoted as Girder G1 through G5; Girder G1 and G5 being the exterior girders and Girders G2 through G4 the interior ones. The three spans are denoted as Span 23, Span 24, and Span 25. Fig. 5-3 shows the

cross section of the monitored bridge segment, which supports a clear roadway width of 11.58 meters (38 ft) on five pretensioned Bulb-T (BT-72) girders spaced at 2.51 meters (8.25 ft). A 19.5 cm (7.5-inch) reinforced concrete deck is monolithically cast with the continuity diaphragm joining the adjacent girders over the intermediate bents. A 50 mm (2-inch) haunch is provided between the deck and girders to compensate for the cambering of the prestressed girders. Hairpin bars were embedded in the girder ends and extended 203 mm (8 in) into the continuity diaphragm to provide positive moment reinforcement. The girders are supported on bearing pads over typical pile bents. Expansion bearing pads were provided at Bents 23 and 26, whereas fixed bearing pads were provided at Bents 24 and 25.

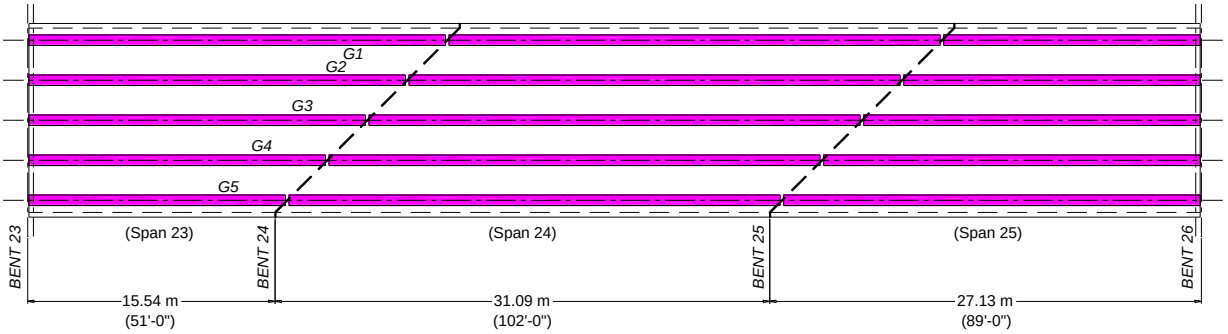

Fig. 5-2 Plan view of Bridge #2 showing different girders and spans

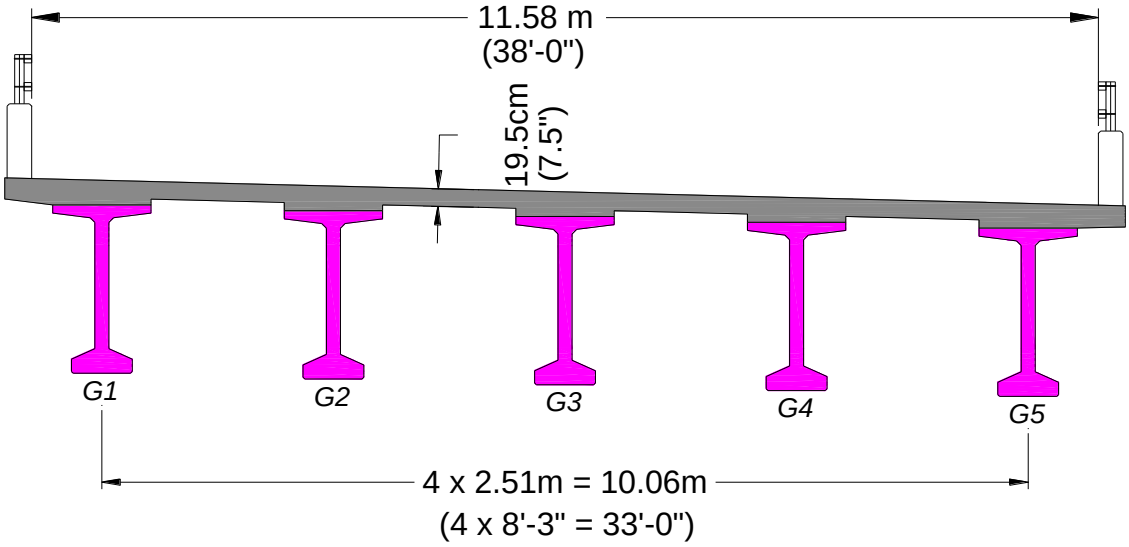

Fig. 5-3 Cross section of Bridge #2

5.3 Health Monitoring System

The research team designed a health monitoring system to capture the long-term behavior of the chosen continuous segment. The focus of the monitoring effort was mainly on the tensile force that develops in the positive moment reinforcement, the strain levels and distribution at the key locations such as over intermediate bents and at midspans, the differential shrinkage between cast-in-place deck and precast girders, and the degree of continuity between adjacent girders. Embedded (sisterbars and strandmeters) as well as surface-mounted (gapmeter, tiltmeter and

vibrating wire strain gages) sensors were used in the study. All of the employed sensors were based on the vibrating wire technology, which is well suited for long term monitoring as they do not suffer from drifting (Bordes and DeBreuille 1985; Choquet et al. 1999). Embedded sensors were installed during casting of the girders in the casting yard and also in the deck during deck casting at the bridge site. Surface mounted sensors were installed after casting the deck and diaphragm, and continuity was established. All the employed sensors have built-in thermistors and can record the temperature at the sensor location in addition to its main reading (e.g. strain or slope). A complete description of the number and location of the sensors can be found elsewhere(Okeil et al. 2011).

Data monitoring consisted of two phases. The first phase (Phase 1) took place at the casting yard, and the second phase (Phase 2) took place at the bridge site. Phase 1 started on June 18, 2008 after the last girder was cast and continued for almost 32 days. The datalogger was then disconnected to allow for girder transportation to the bridge site. Data collection resumed on January 9, 2009 after installing the surface-mounted sensors. At that day all the wires from the both types of sensors were connected to the 96-channel datalogger. Phase 2 of data recording continued for almost two years until the project was completed on December 27, 2010. Fig. 5-4-a shows the temperature reading of a typical sensor located at the bottom flange of Girder G4 of Span 24 at the midspan. The seasonal and daily temperature fluctuations are evident in the plot. Fig. 5-4-b shows the strain readings for the same sensor over the entire monitoring period. Strain readings from the sensor were temperature corrected as per the manufacturer's recommendation to eliminate the effect of temperature variations on sensor readings(Okeil et al. 2011). Nevertheless, it can be seen that strain readings fluctuated despite the fact that the bridge was not open to traffic during the plotted monitoring period. These seasonal and daily strain fluctuations are due to the aforementioned temperature variations which cause thermal deformations in the girder. Therefore, it can be said that the recorded strains are total strains relative to a reference datum and are caused by temperature, creep and shrinkage effects combined. The zoomed-in plot (insert in Fig. 5-4-b) illustrates that daily strain variations take place. The highest daily strain is usually recorded in the afternoon when the temperature effect is greatest. Overnight, the difference in temperature between the deck and the girder bottom are at a minimum due to lack of solar radiation, and hence the thermally-induced restraint moment drops, which causes a drop in strain readings (Hossain et al. 2012). Connecting the highest and lowest daily readings gives the upper and lower bounds of strain readings as can be seen in the figure. It can be seen that during the casting yard period when the girder is simply supported and the bottom flange is not fully shaded, the difference between the upper and lower bounds of the recorded strains are smaller than during later stages when the girder is integrated in the bridge superstructure, thus acting as part of a statically indeterminate structure and thermally induced secondary restraint moments develop.

5.4 Finite Element Modeling

Creep analysis is highly nonlinear in nature and requires substantial amount of time and computational resources. Thus, instead of analyzing a 3-dimensional (3D) model of the full bridge, a three span line model of Girder G3 was built using commercially available finite element software ANSYS(ANSYS 2008). Two types of elements from the ANSYS library were used in building the model; namely SOLID45 and LINK8. The SOLID45 element is an 8-node brick element with three translational degrees of freedom at each node. This element was used to model the girder, deck, haunch, diaphragm and the bearing pads. SOLID45 was chosen over

other elements in the ANSYS library due to its ability to model implicit creep, which is the primary focus of the current study. This element also has the capability of birth and death, which is an important feature for modeling the construction sequence. Two concrete types were used in constructing the bridge; one for the precast girders and the other for the cast-in-place parts; i.e. deck, haunches and diaphragms. Therefore two sets of materials properties were obtained from the laboratory tests of control cylinders rather than the specified design material properties, which can be found elsewhere(Okeil et al. 2011).

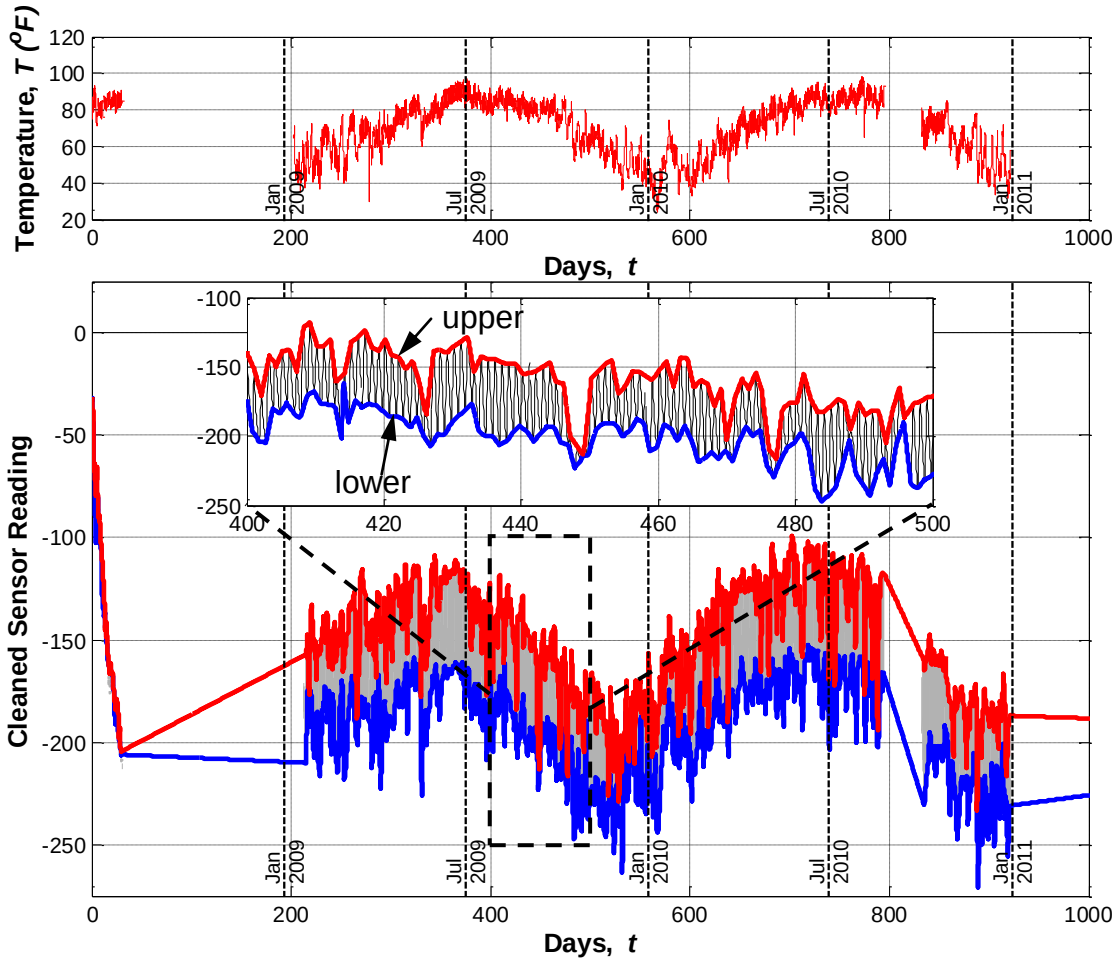

Fig. 5-4 Temperature and corresponding strain response of a typical sensor (Girder G4 - Span 24 - bottom)

Girder ends at the continuity diaphragm were embedded 102 mm (4 inches) into the continuity diaphragm. Prestressing strands were modeled using 3D spar elements from the ANSYS library (LINK8), which also has three translational degrees of freedom at each of its two nodes. The prestress was applied to the LINK8 strand elements as an initial strain based on data extracted from information on the actual girder fabrication sheet. In pretensioned concrete

construction, prestressing forces transfer to the concrete from the strands through bond actions, and as a result a sufficient length of the strands is required from girder ends to transfer the full prestressing force to the concrete. This length is known as the *Transfer Length*(Nilson 1987). In the FE model, the transfer length of the prestressing strands was modeled by incrementally increasing the initial strain in subsequent elements from the girder ends up to an initial strain equivalent to the full pretensioning force. The length over which the increase in initial strains was distributed was taken following the expression in Equation 1

$$l_t = \left(\frac{f_{pe}}{3}\right) d_b \qquad (5\text{-}1)$$

where d_b is the prestressing strand diameter and f_{pe} is the effective prestress. Hairpin bars were also modeled using LINK8 elements; albeit without any initial strains. The hairpin bars extend 8 inches from the end of the girders and were embedded into the diaphragm. The bearing pads were modeled using the SOLID45 element with varying thicknesses to distinguish between the fixed and expansion bearing pads. A shear modulus of 95 psi was assumed for the bearing pads, which falls at the lower end of the AASHTO LRFD specified values for the bearing pads. Symmetry of Girder G3's span configuration was taken advantage of to reduce the computational resources and time demands required for creep analyses. Fig. 5-5 shows a reduced one fourth model of the Girder G3 line. The boundary conditions were applied to mimic the actual bridge configuration. Fig. 5-6-a and Fig. 5-6-b show the finite element model used in the current study which employed 26,671 element, 33,403 nodes, and 97,577 degrees of freedom.

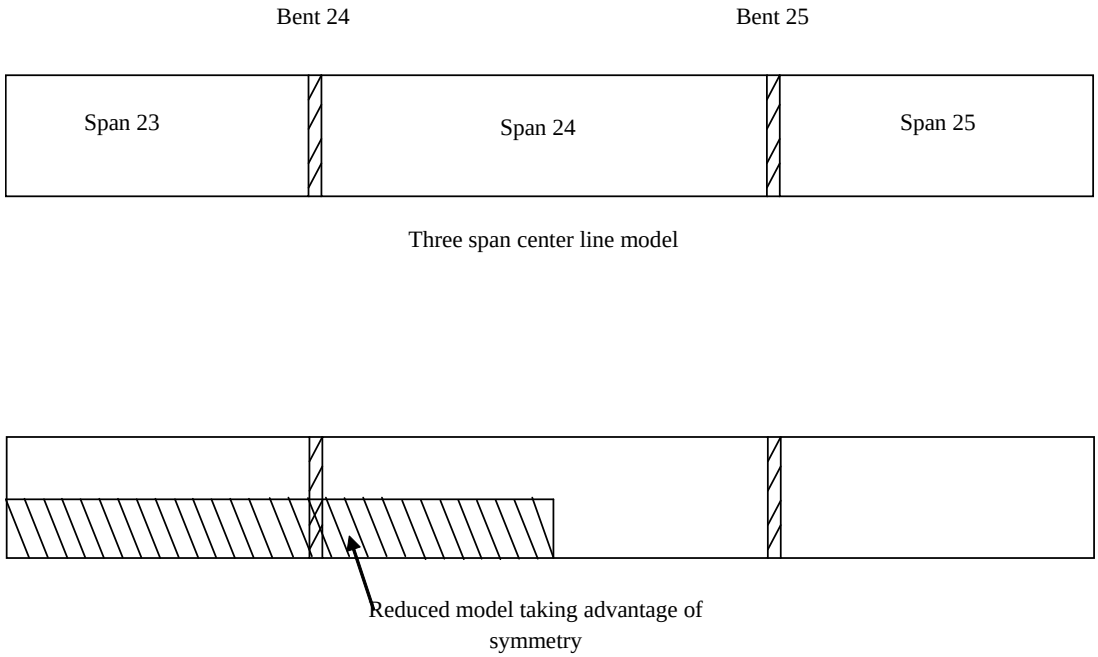

Fig. 5-5 Center line model and one-quarter symmetric model

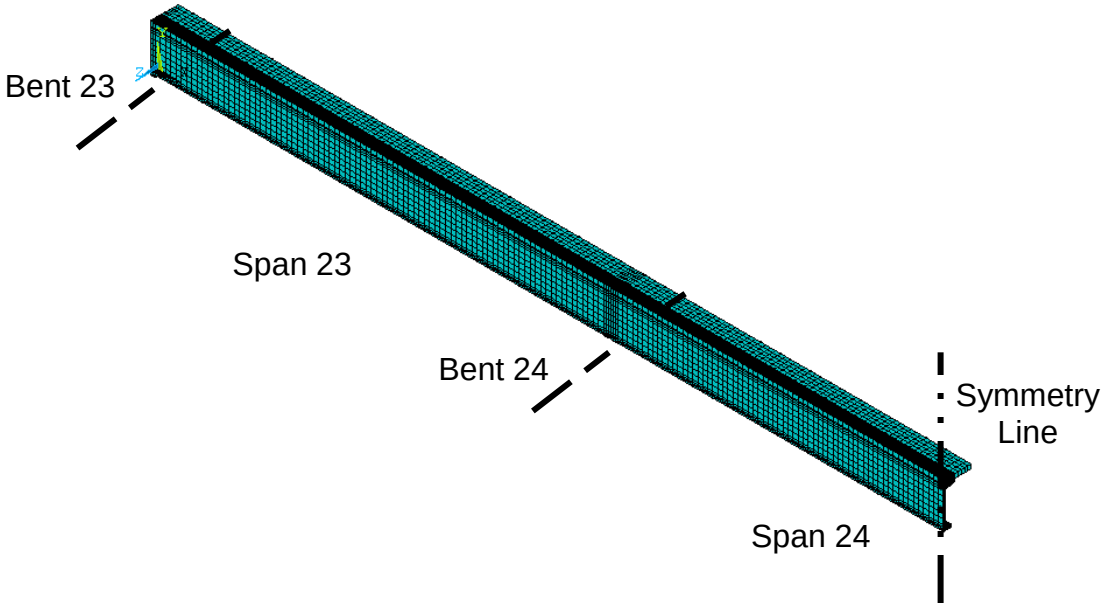

(a) Finite element model of the symmetric center line girder

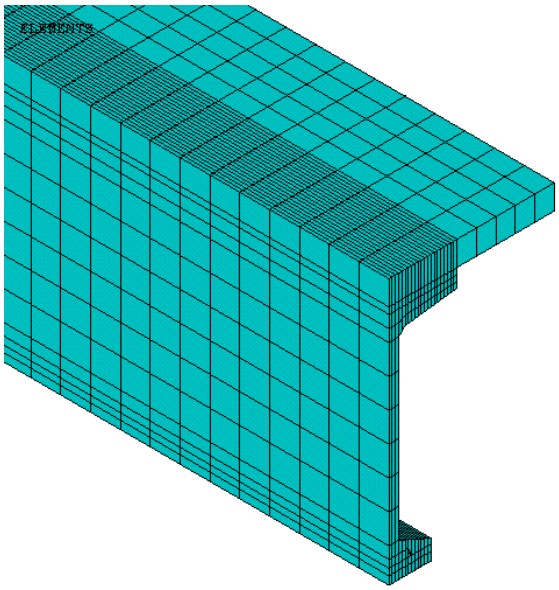

(b) Enlarged cross section

Fig. 5-6 Elements of the reduced center line model

5.4.1 Creep Model

Creep is highly nonlinear in nature, and a typical creep response consists of three parts; namely primary, secondary and tertiary creep. ANSYS is capable of simulating the primary and the secondary creep components. Tertiary creep is not important as it implies impending failure. Implicit and explicit time integration methods are available in ANSYS for creep analysis, and both are suitable for static as well as transient analyses. In the current study, the implicit integration method was chosen for the creep analysis of Girder G3. Implicit creep analysis is

fast, accurate, robust and recommended for the general use; especially where large creep strain and deformation is expected. ANSYS offers 13 creep equations that can model the primary as well as secondary creep. The choice of a particular equation depends on the user and the input parameters. The modified time hardening equation was used in the current study after attempting other equations with less success. The expression for the modified time hardening is given as:

$$\varepsilon_{cr} = \frac{C_1 \sigma^{C_2} t^{C_3+1} e^{-C_4/T}}{C_3+1} \qquad (5\text{-}2)$$

where ε_{cr} is the equivalent creep strain, σ is the equivalent stress, T is the absolute temperature, t is the time at the end of the substep, and e is the natural logarithm base. The coefficients C_1 through C_4 are dependent on the material properties and can be determined from experimental data. Due to the lack of laboratory creep tests on specimens from the same concrete used in casting the girders, the monitoring data from the casting yard days (Phase 1) for a bottom flange sensor embedded in Girder G3 at the middle of Span 24 were used for the calibration of the creep model. The obtained creep coefficients were considered as an initial guess that was subsequently fine tuned manually. It is to be noted these coefficients obtained from the calibration step correspond to the total long-term strain response as a result of using the monitoring data in the regression analysis in ANSYS that fits the data with the selected equation since it was not possible to decouple the creep and shrinkage records. Furthermore, the focus of this study was on creep and temperature effects were not accounted for, and therefore, it was assumed that C_4 was equal to zero. The other coefficients were found to be C_1 = 4.397635219E-6, C_2 = 0.22817, C_3 = −0.754335285.

5.4.2 Modeling of Construction Sequence

The sequence of construction plays an important role in any time history analysis. Therefore, the finite element model needs to mimic the actual construction sequence that took place from the casting yard to the bridge site. The actual construction sequence started on June 18, 2008, by casting the girders. The following steps summarize the actual construction sequence which was also mimicked in the FE model:

- The prestressing force was released one day after casting the girder causing the girder to camber up. As a result both the self weight of the girder and the prestressing force become fully activated. It is to be noted that the girders were placed on wooden blocks 1.07 m (3.5 ft) from girder ends in the casting yards after the prestressing force was transferred.
- The girder was then stored at the casting yard for 90 days during which the girder was subjected to the long-term effects; i.e. creep, shrinkage and temperature, only.
- The prestressed concrete girder was then transported to the bridge site and placed on the bearing pads over the bents. The bearing pads were placed at the end of girders as per the design plans. Thus, the span length of the girder increased to 30.78 m (101 ft) at this step compared to a span length of 28.65 m (94 ft) in Step 1, which results in an increase in the positive moments at the midspan of the girder.
- The girder initially behaved as a statically determinate simply supported beam because continuity was not yet established. This step lasted for 11 days during which the contractor built the construction forms and placed the deck and diaphragm reinforcement. The weight of the wet deck and haunch concrete was supported by the noncomposite girder section since no shoring was provided during constructions.

The following step lasted for 2 days, after which it was assumed that the deck and haunch concrete reached sufficient structural strength to behave compositely with the girder in resisting any additional superimposed loads. Furthermore, hardening of the continuity diaphragms converts the girders into a continuous structure that is capable of carrying live load as designed.

Simulating the actual construction sequence in the FE model is achieved by using the birth and death feature of SOLID45 elements representing the concrete deck, haunch and continuity diaphragm. First, the girder line model was built with all components; i.e. e.g. deck, girder, haunch, continuity diaphragms, bearing pads, and prestressing strands. Then, before the first analysis step in the solution process the deck, haunch and diaphragm elements were selected and deactivated (or killed) in the model. The boundary conditions were applied at a distance of 1.07 m (3.5 ft) from the girder ends. The self weight of the girder and the prestressing force (initial strains) were applied in a short time step. In the second analysis step, the boundary conditions were kept the same as in the first analysis step for a period of 90 days during which creep was allowed to take place as a result of the stress state in the girder. The initial boundary conditions were removed and bearing pad elements were activated in the following step (Analysis Step 3) leading to an increase in the girder's span length from 28.65 m to 30.78 m (94 ft to 101 ft). The girders still acted as simply supported beams until the end of this analysis step; i.e. 101 days. In the fourth analysis step, an equivalent load equal to the weight of the wet deck and haunch concrete was applied, and the girder was kept as simply supported until the end of the analysis step; i.e. 103 days. In the final analysis step, deck, haunch and diaphragm elements were activated, and continuity was established. The activated elements contributed to the structural response with an initial strain equal to zero while other elements that were active in previous steps were stressed. This analysis step lasted until Day 1000.

5.5 Results and Discussion

The FE model was analyzed for 1000 days and results were compared with the available monitoring data. Axial strain readings in the middle of Span 24 were used in the calibration of the creep model. Four sensor reading records were used in the comparison between simulated and monitoring strain. These sensors were located in the deck, top flange, mid height of the web, and bottom flange. All of the sensors were embedded ones except for the midheight sensor which was surface mounted. The total bottom flange strain response at the midspan of Girder G3 in Span 24 is plotted in Fig. 5-7 for 1000 days. The plotted total strain is the summation of the elastic strain and the creep strain in the longitudinal direction of the girder. Fig. 5-7 also shows the key construction steps discussed earlier. In the first step, instantaneous compression strains take place as a result of applying the self weight of girder and the prestressing force simultaneously. The resulting compressive stresses at the girder's bottom flange cause the girder to camber upward. During the subsequent period when the girder is stored at the casting yard, no additional forces were applied and only long-term effects took place. It can be seen that compressive strains increased due to creep with a higher rate during the first few days than at the later stage. In the following analysis step, the compressive strain decreased due to the additional positive moment resulting from the increase in span length when the girder was erected on the bearing pads over the bent at the bridge site. The compressive strain continued to increase for the next 11 days girders simulating the period of deck reinforcement placement. A load equivalent to the deck concrete weight is applied in the third step simulating unshored construction, which results in another increase in the positive moment of the simply supported girder leading to a

decrease in compressive strain. In the fourth step, the deck, haunch and diaphragm elements were activated and the bridge was converted into a continuous structure with zero initial strain. These elements were, therefore, only subjected to the subsequent long-term creep effects. The continuous girder section continues to deform due to creep resulting in an increase in the compressive strain as can be seen in Fig. 5-7 until the end of the analysis at 1000 days.

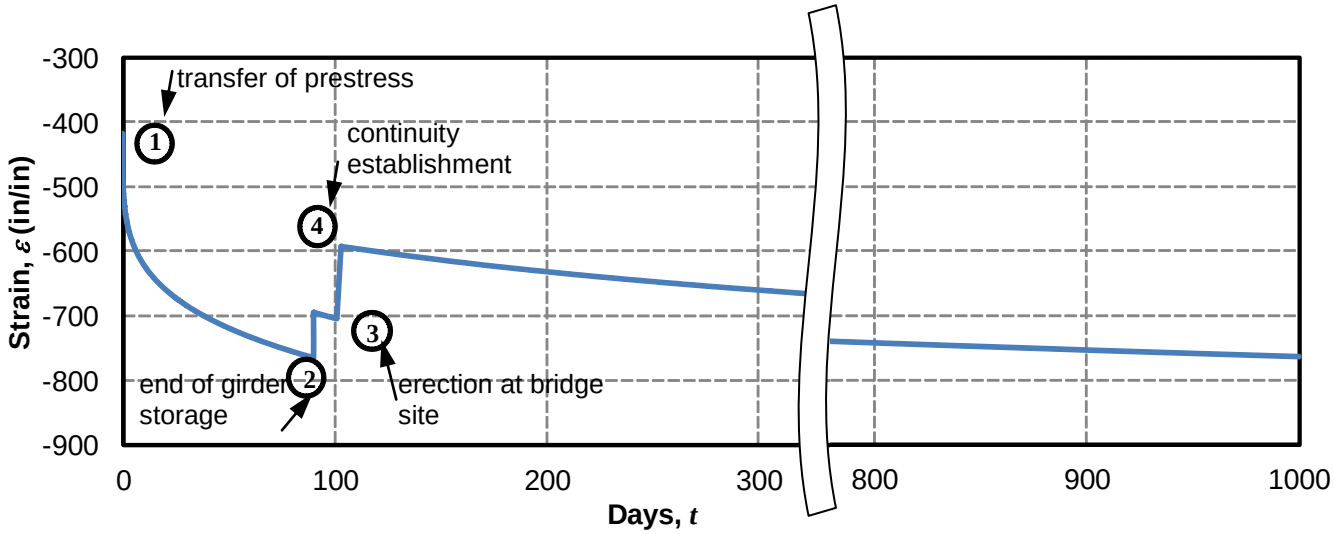

Fig. 5-7 Steps of construction sequence and the corresponding total strain response

5.5.1 Comparison between FE results and Field Data

Fig. 5-8-a, b, c, and d show a comparison between the FE results and the data of the axial strain for Girder G3 in the middle of Span 24 at the deck, girder top flange, girder mid height, and girder bottom flange, respectively. It should be noted that the plotted results (field data and FE results) were adjusted relative to the first available data point. For example, the first available data point was recorded 17 hours after girder casting for the bottom flange location (Fig. 5-8-d), and hence, the difference between the FE results in Fig. 5-7 and Fig. 5-8-d. This also means that only the creep, shrinkage and temperature effects were captured, and that the initial effects of girder self weight and prestressing force are not captured in the plot. Fig. 5-8 shows that the FE results match well with the field recorded data, especially during the initial 32 days when the girders were stored in the casting yard. This is expected as this is the dataset used in calibrating the creep model. The figure only shows FE results during the period between the initial period and January 9th, 2009, because no field data exist since the monitoring system had to be disconnected to allow girder transportation.

A major difference between the FE results and field recorded data is that the monitored data fluctuate daily as well as seasonally. Daily fluctuations are due to the temperature differences between day and night whereas seasonal fluctuation is due to the temperature difference between summer and winter. Another important observation is that the plot in Fig. 5-8-d shows smaller field recorded strains during summer months than during winter months. This is due to the fact that higher temperature gradients take place during summer months than during winter months. The resulting secondary positive restraint moment is therefore greater during summer months, which reduces the compressive strain at the bottom flange. The adopted creep model was not temperature dependent, and therefore the FE results match the lower bound

of the field data during winter months, when temperature gradient effects are negligible or nonexistent, better.

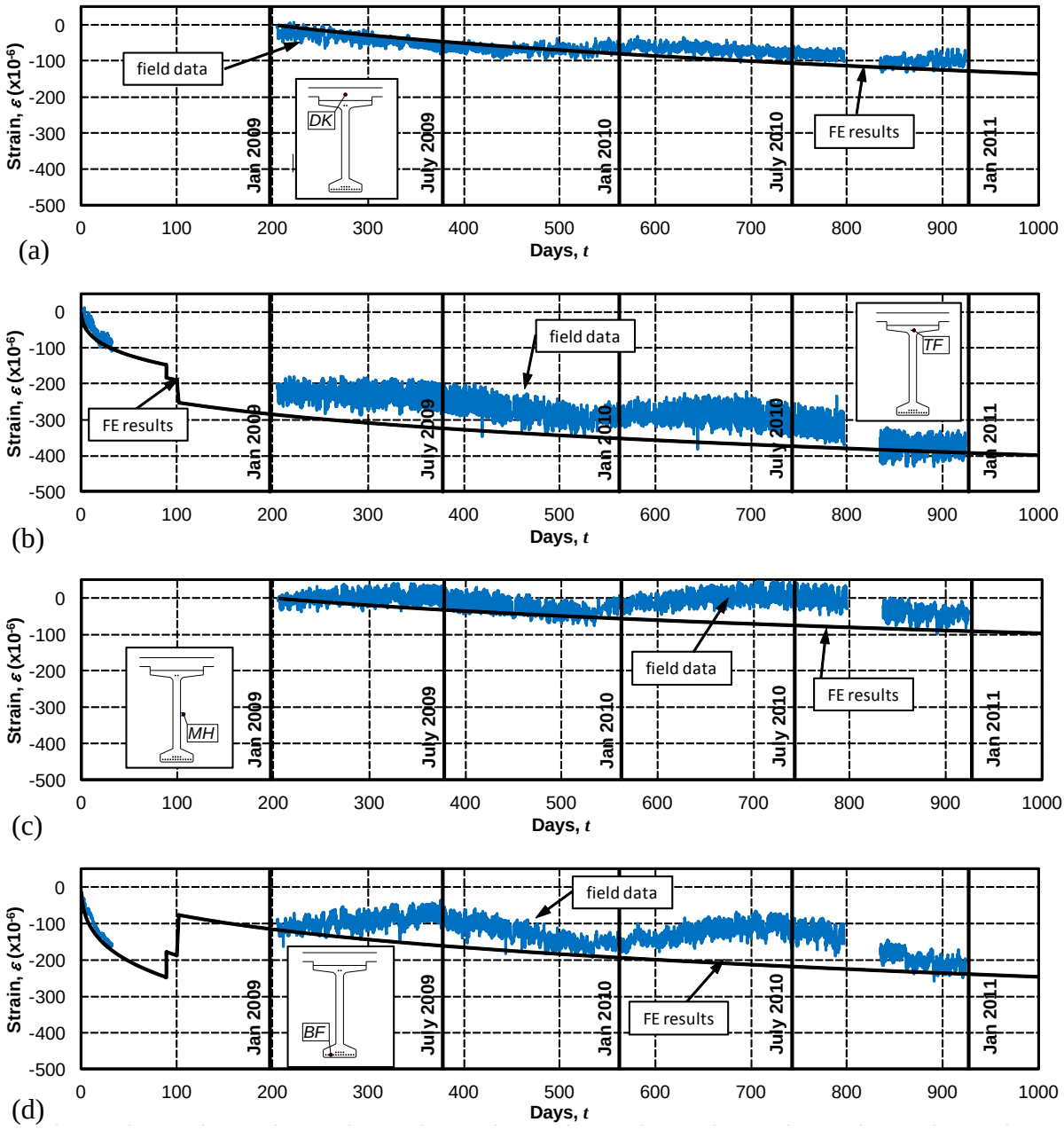

Fig. 5-8 Relative strains from field data and analysis results (Girder G3 – Midspan 24): a) deck, b) top flange, c) mid height, d) bottom flange

In January 2009, the strain was about 120 microstrains, which increased after one year in January 2010 to 190 microstrains indicating that 70 microstrains of plastic deformation took place due to creep. The corresponding total strain in January 2011 is 240 microstrains indicating that the girder was still creeping, albeit at a slower rate. Fig. 5-8-c shows the comparison between the FE results and the monitored data for axial strain at the mid height. It is to be noted

that the monitored data were taken from a surface mounted sensor, which was installed at the bridge site in January 2009. Thus, the first data was recorded on January 9th, 2009, and was used as the relative datum for all subsequent results. It can be seen from this figure that the creep strain is smaller than that the strain at the bottom of the girder due to the fact that compression is much less at the mid height of girder than at the bottom. Strains at the top of Girder G3 in the middle of Span 24 can be seen in Fig. 5-8-b relative to initial readings in June 2008. The moments acting on the cross section from different construction steps produce strains that are opposite to what was observed earlier for the bottom flange plot (see Fig. 5-8-d) as a result of the compression created at the top of the girder, thus increasing the compressive strain as can be seen in Fig. 5-8-b. Finally, the deck strains in the middle of Span 24 are plotted in Fig. 5-8-a.

5.6 Creep Induced Restraint Moment

Establishing continuity between prestressed concrete girders by pouring concrete between girder ends to form continuity diaphragms leads to the development of tensile stresses at the girder bottoms due to creep when the girders camber up as depicted in Fig. 5-9. Superimposed dead loads and differential shrinkage between the deck concrete and the girder concrete reduce this effect, however, if the girder creep action is greater, the girder will deflect upwards and the distance between the bottom flanges at girder ends will keep increasing. If no measures are taken to resist the opening of the gap between the girders ends, the structure acts as a series of simple span segments. Conversely, if continuity is established, restraint moments develop in the superstructure. Establishing reliable continuity between adjacent girders is often achieved by providing reinforcement that connects the girders' bottom flanges to the continuity diaphragm as can be seen in Fig. 5-9. In addition to recommending positive moment reinforcement details, NCHRP Report 519(Miller et al. 2004) also recommended a minimum girder age of 90 days before establishing continuity so that much of the time dependent effects take place while the girders are not restrained, which should substantially reduce, or completely eliminate, the development of positive restraint moment.

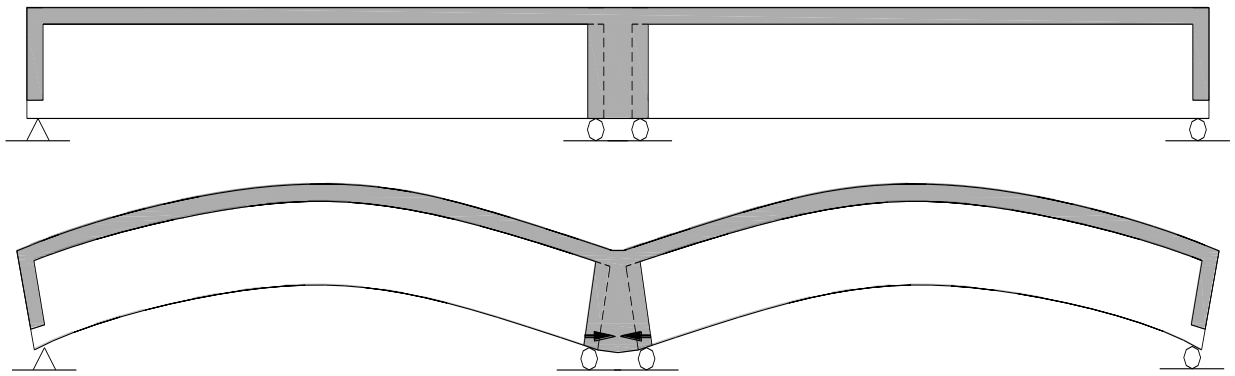

Fig. 5-9 Development of positive restraint moment in bridges with continuity diaphragm due to long-term effects

Design of the positive moment continuity connection requires prior knowledge of the magnitude of the restraint moment that would develop due to time dependent effects. There are several methods for estimating the positive restraint moment at the continuity diaphragm. One of the earliest studies of positive restraint moments was published in the 1960's by

Mattock(Mattock 1961) based on analytical and experimental research to determine the long term effect of creep and shrinkage on continuous bridges. Freyermuth(1969) advanced this work and presented a complete procedure widely known as the Portland Cement Association or PCA method. A pure analytical method to predict the time dependent restraint moment published in NCHRP Report 322 further developed the PCA method(Oesterle et al. 1989). This improved method, commonly known as the Construction Technology Laboratories or CTL method, is based on time-step analysis and uses the time-dependent material properties recommended in ACI 209R-92(ACI 1992). Modification of the restraint moment calculations by the PCA and CTL method was proposed by Peterman and Ramirez(Peterman 1998); also known as the *P*-method, resulted in better correlation of results. NCHRP Report 519 also developed a spreadsheet program called RESTRAINT to calculate the restraint moment that would develop in the continuous prestressed concrete girder bridges. Mirmiran et al.(Mirmiran et al. 2001) proposed another method for calculating the positive restraint moment which considers the properties of a bridge as nonlinear along the length of the bridge due to the varying amount of reinforcement and cracking. A modified version of the RESTRAINT program, called mRESTRAINT, is reported in Louisiana Transportation Research Center Report No. 477(Okeil et al. 2011). mRESTRAINT addresses several limitations in the original RESTRAINT version; namely eliminating symmetrical span configuration requirement, allowing the inclusion of different stiffness values in moment calculation, and expanding the number of supported cross section geometries and number of days of continuity.

A common factor in all the aforementioned methods is that they rely on many assumptions to simplify the complex behavior of continuous girder bridges due to long-term effects. In this study, a more robust and accurate finite element model was developed to analyze the time dependent effects on prestressed girder behavior in bridge construction. The state of stress obtained from the FE model was then used to calculate the corresponding restraint moment by integrating the resultant stresses that develop due to creep over time at predefined sections of the girder. Three different girder ages at time of continuity establishment were analyzed in this study namely 28, 60, 90, 103 and 153 days of continuity by adjusting the duration of the analysis Step 2 in the FE model that reflects the time of girder storage at the casting yard. The latter two choices for girder age reflect actual ages of girders from Bridge #2. Fig. 5-10 shows the positive restraint moment that develops at the continuity diaphragm over time. It can be seen that the positive restraint moment decreases as the time laps increases between girder casting and establishing continuity. The FE model predicted restraint moment was then compared with mRESTRAINT predictions, which adopts PCA proposed creep model with an ultimate creep coefficient of 2.3. It is to be noted that the differential shrinkage between the girder and deck concrete was ignored and only the restraint moment due to creep was investigated to match with the finite element analysis. A parametric study of the creep-coefficient is shown in Fig. 5-11 where the development of restraint moment at the continuity diaphragm took place when the continuity was established when the girder age was 103 days. It can be seen here that a creep coefficient of 2.3 overestimates the restraint moment, and a value of 1.8 closely matches the finite element analysis and confirms similar findings by Koch(2008) where a creep coefficient of 1.80 was recommended.

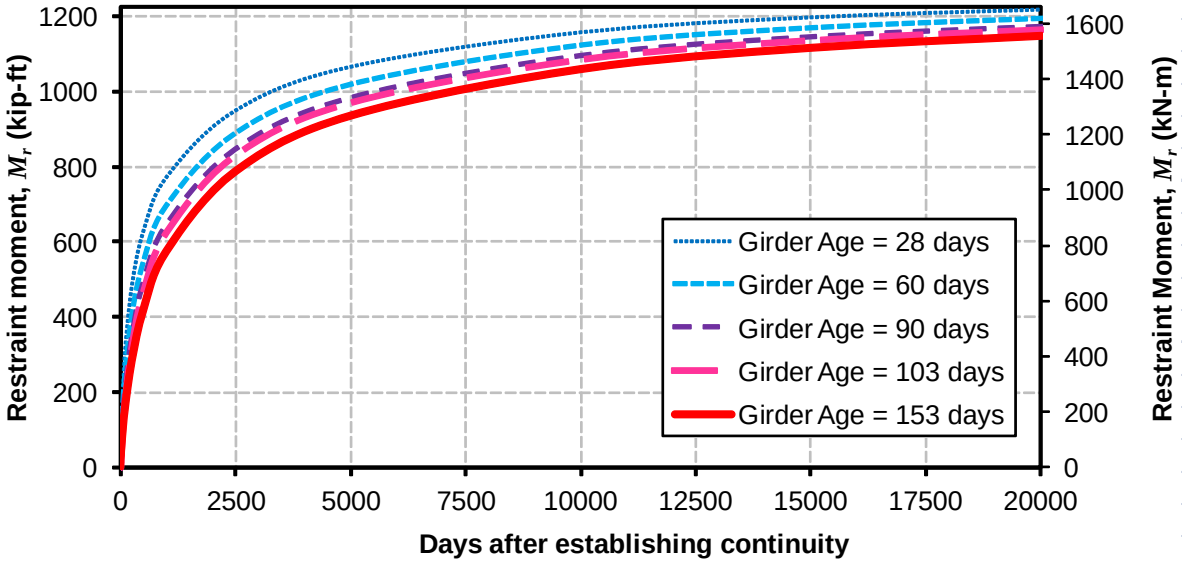

Fig. 5-10 Effect of girder age at time of establishing continuity on positive restraint moment

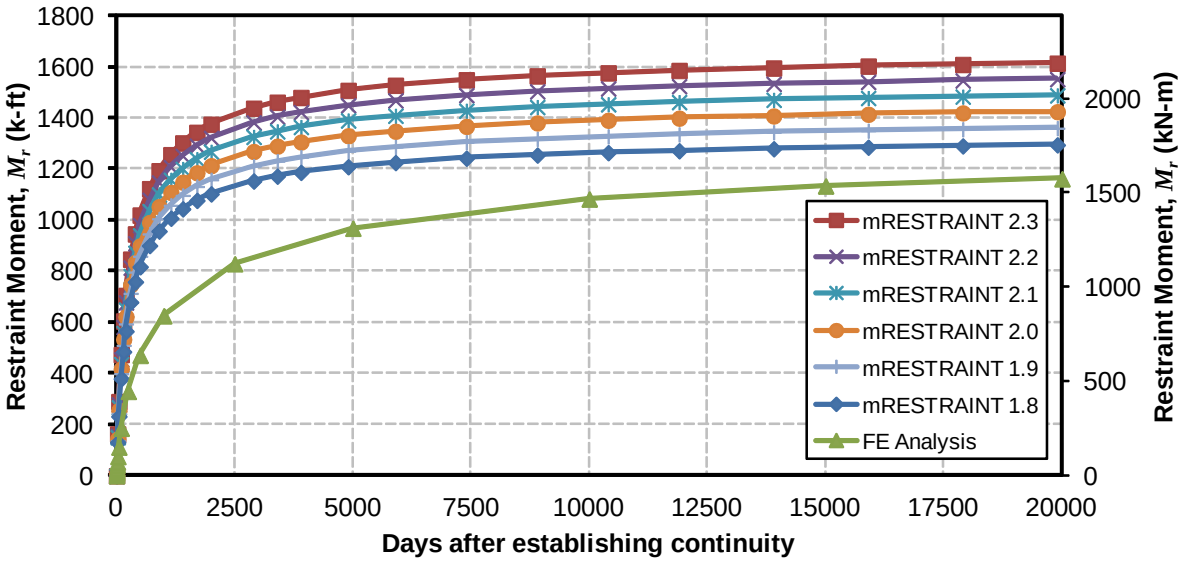

Fig. 5-11 Analytical and FE model predicted positive restraint moment (Girder Age = 103 days)

5.7 Conclusions

A finite element model capable of predicting long term creep behavior of prestressed concrete girder bridges is developed. A recently constructed three span continuous bridge employing a positive moment continuity detail and instrumented with a monitoring system was chosen for to validate the model. Initial monitoring data from the girder's early age before erection at the bridge site was used to calibrate the temperature independent modified time hardening creep model in ANSYS. The model also simulated the actual construction sequence from the casting yard until bridge completion. A comparison between the FE model strain predictions and field data was then presented at key location for a 1000 day period. The

comparison showed that the model is capable of capturing the creep behavior of prestressed girder bridges. A parametric study to investigate girder age at time of establishing continuity was then conducted to evaluate the creep induced restraint moment integrating the stresses resulting from the FE model. Finally, restraint moment predictions using another analytical tool were compared to the FE results. Based on the results, the following conclusions may be drawn:

- Creep behavior is a complex phenomenon and is affected by several factors that cannot be all captured using simplified analytical models. The finite element method offers an alternative tool by which bridge construction complexities, such as the construction sequence and the varying stress field, can be captured.
- Creep in continuous prestressed girder bridges produces restraint moments that should be accounted for in design. The magnitude of the restraint moment is affected by the girder age at time of establishing continuity.
- A comparison between FE predicted behavior and analytical predictions using mRESTRAINT, a modified version of the recently developed tool resulting from NCHRP Project 12-53, revealed that a creep coefficient equal to 1.8 better is more appropriate for predicting restraint moments.
- Even though creep induced restraint moments may not solely exceed the cracking moment of prestressed girders, superimposing positive moments caused by other loads such as temperature gradient may lead to girder cracking, especially at girder ends where prestressing effects are at a minimum. Therefore, the combined effect of creep and thermal effects should be considered in the design.

5.8 References

AASHTO (2008). "LRFD Bridge Design Specifications." American Association of State Highway and Transportation Officials, Washington, D.C.

ACI (1992). "Prediction of creep, shrinkage and temperature effects in concrete structures." Manual of Concrete Practice, ACI 209R-92. American Concrete Institute, Farmington Hills, MI.

ANSYS . Theory Reference. 2008. Canonsburg, PA, ANSYS, Inc.

Bazant, Z. P., and Baweja, S. (1995). "Justification and refinements of Model B3 for concrete creep and shrinkage. 1. Statistics and sensitivity." *Materiaux et constructions*, 28(181), 415-430.

Bazant, Z. P., and Xi, Y. (1989). "Probabilistic prediction of creep and shrinkage in concrete structures. Combined sampling and spectral approach." Publ by ASCE, San Francisco, CA, USA, 803-808.

Bordes, J. L., and DeBreuille, P. J. (1985). "Some Facts About Long-Term Reliability of Vibrating Wire Instruments." *Transportation Research Record*, Natl Research Council, Transportation Research Board, Washington, DC, USA, 20-27.

Choquet, P., Juneau, F., DeBreuille, P. J., and Bessette, J. (1999). "Reliability, long-term stability and gage performance of vibrating wire sensors with reference to case histories." 49-54.

Collins, T. M., and Mitchell, D. (1991). "Prestressed Concrete Structures." Prentice Hall, Ebglewood Cliffs, NJ.

Comite Euro-Internationale Du Beton (CEB) (1990). "CEB-FIP model code 1990." *Rep. No. Buletin D'Information No. 213/214*, Lausanne, Switzerland.

Freyermuth, C. L. (1969). "Design of continuous highway bridges with precast, prestressed concrete girders.".

Gardner, N. J., and Lockman, M. J. (2001). "Design provisions for drying shrinkage and creep of normal-strength concrete." *ACI Materials Journal*, 98(2), 159-167.

Hossain, T., Segura, S., and Okeil, A. M. (2012). "Analytical and Field Measured Temperature Profile And Its Structural Effects On A Continuous Girder Bridge." *(submitted for publication in the ASCE J. of Bridge Engineering)*.

Huo, X. S. (1997). "Time-dependent analysis and application of high performance concrete in bridges." Ph.D Dissertation, Department of Civil Engineering, University of Nebraska.

Koch, S. (2008). "Prestressed PCBT Girders Made Continuous and Composite with a Cast-In-Place Deck and Diaphragm." M.S. Thesis, Department of Civil and Environmental Engineering, Virginia Polytechnic Institute and State University, Blacksburg, Virginia, USA.

Le Roy, R., De Larrard, F., and Pons, G. (1996). "The AFREM code type model for creep and shrinkage of high-performance concrete." Paris.

Mattock, A. H. Precast-Prestressed Concrete Bridges, 5. Creep and Shrinkage Studies. 1961.

Miller, R. A., Castrodale, R., Mirmiran, A., and Hastak, M. (2004). "Connection of Simple-Span Precast Concrete Girders for Continuity." *Rep. No. NCHRP Report 519*, Transportation Research Board, Washington, D.C.

Mirmiran, A., Kulkarni, S., Castrodale, R., Miller, R., and Hastak, M. (2001). "Nonlinear continuity analysis of precast, prestressed concrete girders with cast-in-place decks and diaphragms." *PCI Journal*, 46(5), 60-80.

Nilson, A. H. (1987). "Design of Prestressed Concrete.".

Oesterle, R. G., Glikin, J. D., and Larson, S. C. (1989). "Design of Precast Prestressed Bridge Girders Made Continuous." *Rep. No. NCHRP Report No. 322*, Transportation Research Board, Washington, D.C.

Okeil, A. M., Cai, S. C. S., Chebole, V., and Hossain, T. (2011). "Evaluation of Continuity Detail for Precast Prestressed Girders." *Rep. No. 477*, Louisiana Transportation Research Center, Baton Rouge, LA.

Peterman, R. J. (1998). "Restraint moments in bridges with full-span prestressed concrete form panels.".

Precast/Prestressed Concrete Institute (1997). "Bridge Design Manula." Chicago, IL.

Shams, M. K., and Khan, L. F. (2000). "Time-dependent behavior of high strength concrete: task 3, use of high strength/high performance for precast prestressed concrete bridges in Georgia." *Rep. No. Structural Engineering, Mechanics, and Materials Research Report No. 00-1*, Georgia Institute of Technology, Atlanta, Georgia.

Tadros, M. K., Al-Omaishi, N., Seguirant, S. J., and Gallt, J. G. (2003). "Prestressed losses in pretensioned high-strength concrete bridge girders." *Rep. No. NCHRP Report 496*, Transportation Research Board, Washington, D.C.

Waldron, C. J. (2004). "Investigation of Long-Term Prestress Losses on Pretensioned High Performance Concrete Girders." Ph.D. Dissertation, Department of Civil and Environmental Engineering, Virginia Polytechnic Institute and State University, Blacksburg,Virginia.

6 FIELD TEST AND 3D FE MODELING OF A THREE SPAN CONTINUOUS PRESTRESSED GIRDER BRIDGE

6.1 Introduction

Continuous precast prestressed girder bridges have some inherent advantages over the simple span bridges. Continuous bridge construction eliminates, or at least reduces the number of, joints, which are not only considered a weak structural link, but more importantly allow water to leak through them causing girder end deterioration and corrosion of reinforcement. Thus, eliminating joints reduce the maintenance cost in the long run. Furthermore, jointless bridges offer a better riding quality and improve the redundancy of the structural system. Structurally, the live load positive moment at midspan of a continuous bridge is less than that of a simply supported bridge of the same span length. Therefore, continuity may also result in more economic designs. Girders are normally precast in a casting yard and then transported to the site and placed over the supporting piers. The simply supported girders are made continuous by pouring concrete in between the girder ends to form what is referred to as a continuity diaphragm, which may be subjected to negative as well as positive moments. The reinforcement in the deck over the diaphragm is sufficient to resist the tension resulting from the negative moments. Extra reinforcement needs to be provided at the bottom of the diaphragm to resist any positive moments that may develop due to time dependent effects such as creep and thermal gradients.

The performance of these diaphragms has been studied by several researchers. Loveall (1985) and Wasserman (1987) reported their experience with jointless bridge decks over continuous girders. In 1989 a comprehensive study on converting precast prestressed concrete girder bridges was published by National Cooperative Highway Research Program (NCHRP) in Report 322 titled "*Design of Precast Prestressed Bridge Girders Made Continuous*" (Oesterle et al. 1989). The authors of the report presented an analytical method for estimating the positive moments at the continuity detail due to the long-term as well as the live load effects. It was also concluded that in addition to being time consuming and costly, the existence of positive moment reinforcement at the continuity detail does not offer any structural benefits since positive moments increase midspan moments thus reducing the benefits from establishing continuity. The limitations of integral bridges and the adverse effects of full bridge integration were discussed by Burke, Jr. (1992; 2004). The integral and jointless-deck bridge inventory in the New York state was surveyed (Alampalli and Yannotti 1998), which revealed that their performance were as designed. Based on the survey results, new details for future projects were recommended to avoid some of the problems noted in in-service jointless bridges. Thippeswamy et al. {Thippeswamy, 2002 41 /id /d}, also evaluated the performance of the in-service jointless bridges. Recently, NCHRP sponsored Project 12-53 to study connections of simple-span precast concrete girders for continuity. The research findings were published in NCHRP Report 519 (Miller et al. 2004). A survey was conducted as part of the project about current practices for positive moment continuity detailing by different DOTs. The performance of positive moment continuity details were also investigated experimentally and analytically. The report recommended two alternate types of reinforcement for positive moment continuity details. One type was to utilize the existing prestressing strands by extending them outside of the girder bottom flanges. The other detail calls for additional reinforcement in the form of hairpin/hooked

bars as can be seen from Fig. 6-1. NCHRP Project 12-53 research efforts relied on single line girders in the experimental specimens and also for the analytical model. Several attributes of the bridge covered in the current study were not considered in the NCHRP study; namely the use of Bulb-T girders and the skew effects were not covered. The authors of NCHRP Report 519 recommended further research to study the performance of the positive moment continuity detailing in full-size specimens.

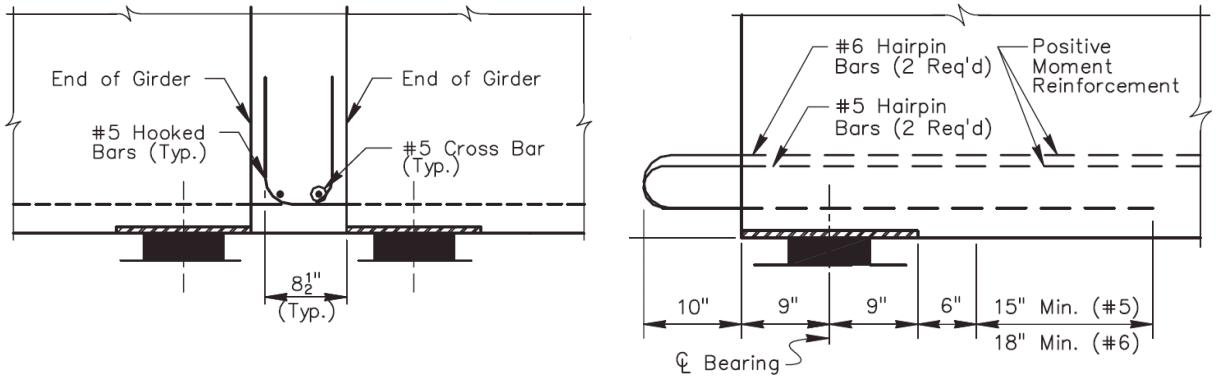

(a) hooked bars or prestressing strands (b) hairpin bars

Fig. 6-1 Alternatives for positive moment reinforcement (Miller et al. 2004)

The NCHRP recommended continuity detail with the hairpin bar option was adopted in detailing Bridge #2 of the John James Audubon project, which crosses the Mississippi River between St. Francisville and New Roads in Louisiana. The considered bridge segment is a three span continuous superstructure with AASHTO Bulb-T skewed girders. Because of its configuration (Bulb-T girders and skew) that were not covered in the NCHRP study, the Louisiana Department of Transportation and Development (LA DOTD) seized the opportunity to monitor the performance of this new continuity details under time dependent effects as well as under truck loading. This paper describes the details of the performance evaluation of this new positive moment continuity details under the truck loading. Field test data were used to validate a 3D FE model that was developed for the entire monitored segment. Once the FE model was validated, it was used to conduct further parametric studies to investigate the efficiency of the detail in transferring loads between adjacent girders. From the FE results, it has been found that continuity index that is approximately 88 percent; i.e. the new detail results in a continuous structure whose continuity is about 88 percent of a fully continuous structure.

6.2 Bridge Description

The John James Audubon project adds a new transportation artery across the Mississippi River between the cities of New Roads and Saint Francisville in southern Louisiana. The project consists of eight bridges, of which Bridge #2 is to cross an existing railway track. Bridge #2 was chosen to monitor the performance of the new NCHRP recommended continuity detail. The bridge consists of 52 spans that rise to cross an existing railway track. The total bridge length is about 4000 ft divided into 14 continuous segments. The LA-DOTD chose a 242 ft segment of Bridge #2 for monitoring the performance of the adopted continuity detail. The segment is a three span continuous superstructure with a skewed layout for its middle and longest span (102 ft). Because of the 45º-skew of the middle span, the girders supporting the exterior spans ranged

in length from 51 feet to 89 feet as can be seen in Fig. 6-2-a. The chosen segment is constructed using AASHTO Bulb-T girders (BT-72) and was chosen because of its configuration, which has not been covered within the scope of NCHRP Project 12-53; namely skewed configuration and Bulb-T girders.

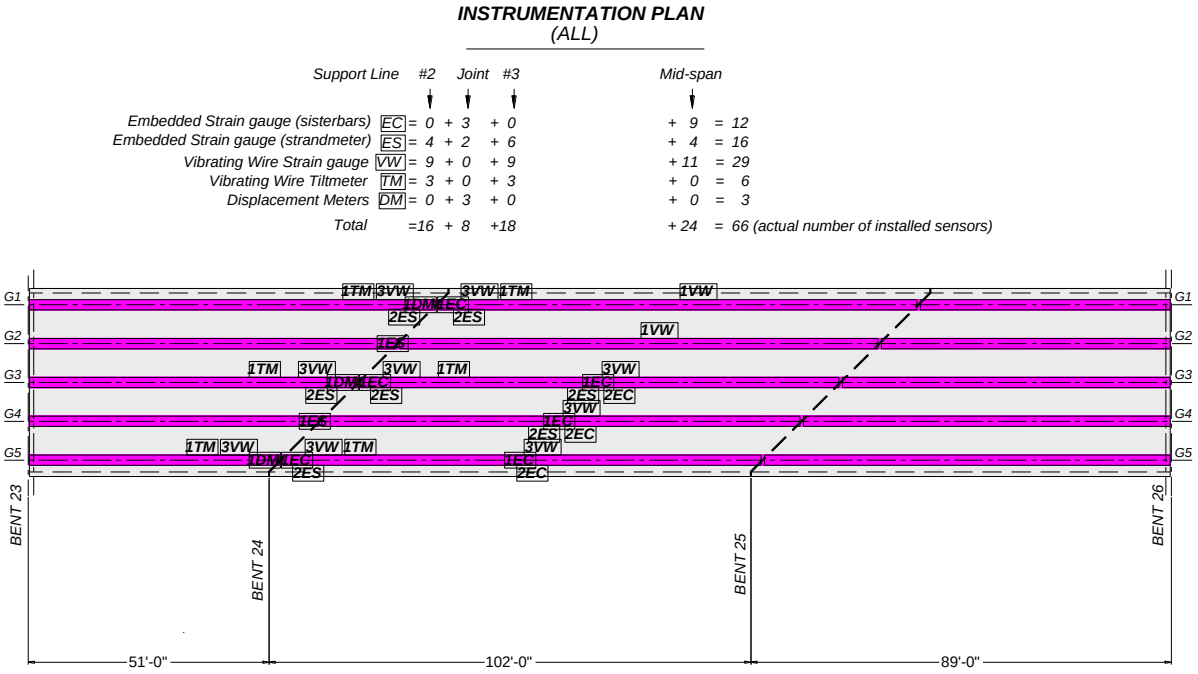

(a) Bridge layout

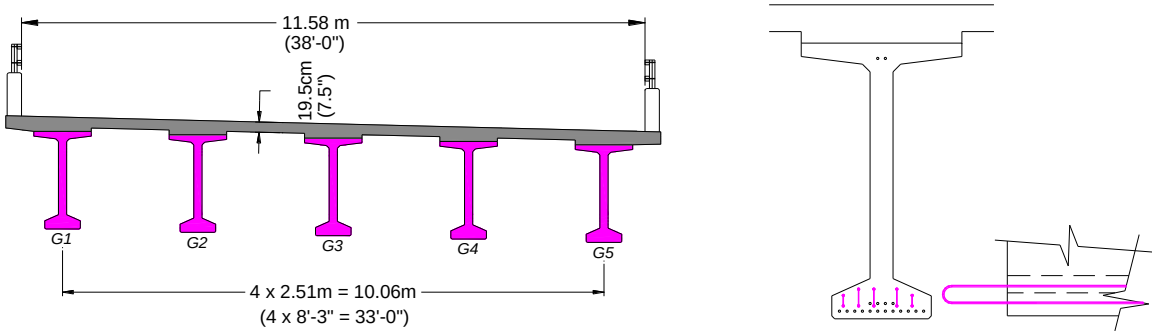

(b) Cross section and continuity detail (5#5 hairpin bars)

Fig. 6-2 Main dimensions and cross sections of monitored Bridge #2

Fig. 6-2-b shows the cross section of the monitored bridge segment, which supports a clear roadway width of 38 feet on five prestressed BT-72 girders spaced at 8.25 feet. The 7.5-inch reinforced concrete deck is monolithically cast with the continuity diaphragm joining the adjacent girders over intermediate bents. Hairpin bars were embedded in the girders and extended 8 inches outside the girder ends to provide positive reinforcement. The girders are supported on bearing pads over typical pile bents. The girders form a three span continuous segment; denoted Spans 23, 24 and 25. The five girders are denoted as G1, G2, G3, G4, and G5. In order to identify a typical girder in a typical span, a designation consisting of the girder

number and the span number will be followed. For example, G1S23 refers to Girder G1 in Span 23, G4S24 refers to Girder G4 in Span 24, and so on.

6.3 Instrumentation

The bridge segment considered in this study has been under monitoring for more than two years before the live load test was conducted. The monitoring system consisted of a datalogger programmed to record data from 96 channels, of which 66 were active and connected to vibrating wire sensors. Vibrating wire technology is well suited for long term monitoring because of the rugged nature of the sensor as well as their consistency over extended periods of time; i.e. readings do not drift (Bordes and DeBreuille 1985). 28 of the sensors were embedded in the girders and deck, while the others were surface mounted. Due to the lack of power sources near the bridge site, the monitoring system was powered using a solar panel and rechargeable batteries to ensure continuous operational capabilities. Data was retrieved remotely via an internet IP connection that communicates with the datalogger using a cellular modem.

The sensor distribution is shown in Figure 2-(a), where it can be seen that the superstructure's anti-symmetry was taken advantage of. For example in Span 24, the midspan location of Girder G1 is identical to the midspan location of Girder G5. Similarly, the midspan location of Girder G2 is identical to Girder G4. Therefore, in Span 24 only Girders G3, G4, and G5 were instrumented at midspan in four different locations; namely in the deck, top flange, web, and bottom flange. Two additional surface mounted sensors were installed on the bottom flanges of Girders G1 and G2 for the purpose of studying load distribution among all girders. At Bent 24, Girder G1, G3, and G5 were instrumented because symmetry similar to that at midspan does not exist. At the supports, the primary objective was to capture the strain in the hairpin bars to monitor the transfer of forces between adjacent girders through the continuity diaphragm. It should be noted that Girder G5S23 was not instrumented with any sensors on its hairpin bars because of a miscommunication between the contractor and the research team about the casting date. Fig. 6-3 shows a more detailed view of the sensors employed in this study across the height of the superstructure.

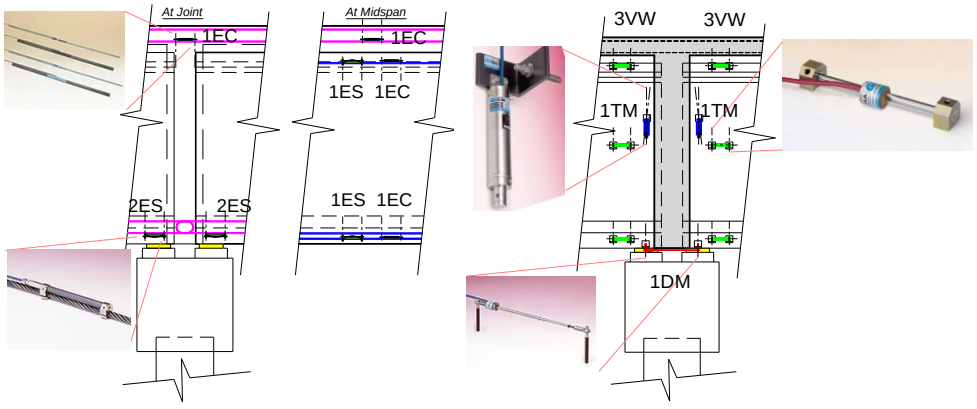

(a) Embedded sensors (b) Surface-mounted sensors

Fig. 6-3 Sectional locations of embedded and surface-mounted sensors in Bridge #2

6.4 Live load test

A live load test of the monitored bridge was conducted to evaluate the performance of the details under the truck loads. As stated previously, the sensors used in this monitoring study are particularly suited long term monitoring, which meant that the system logging speed is relatively slow as hourly averages are more than adequate when it comes to years of data record. Therefore, the static live load test was designed to overcome the slowness of the system as will be described later. This section describes the live load test in details, which took place on August 19th, 2010.

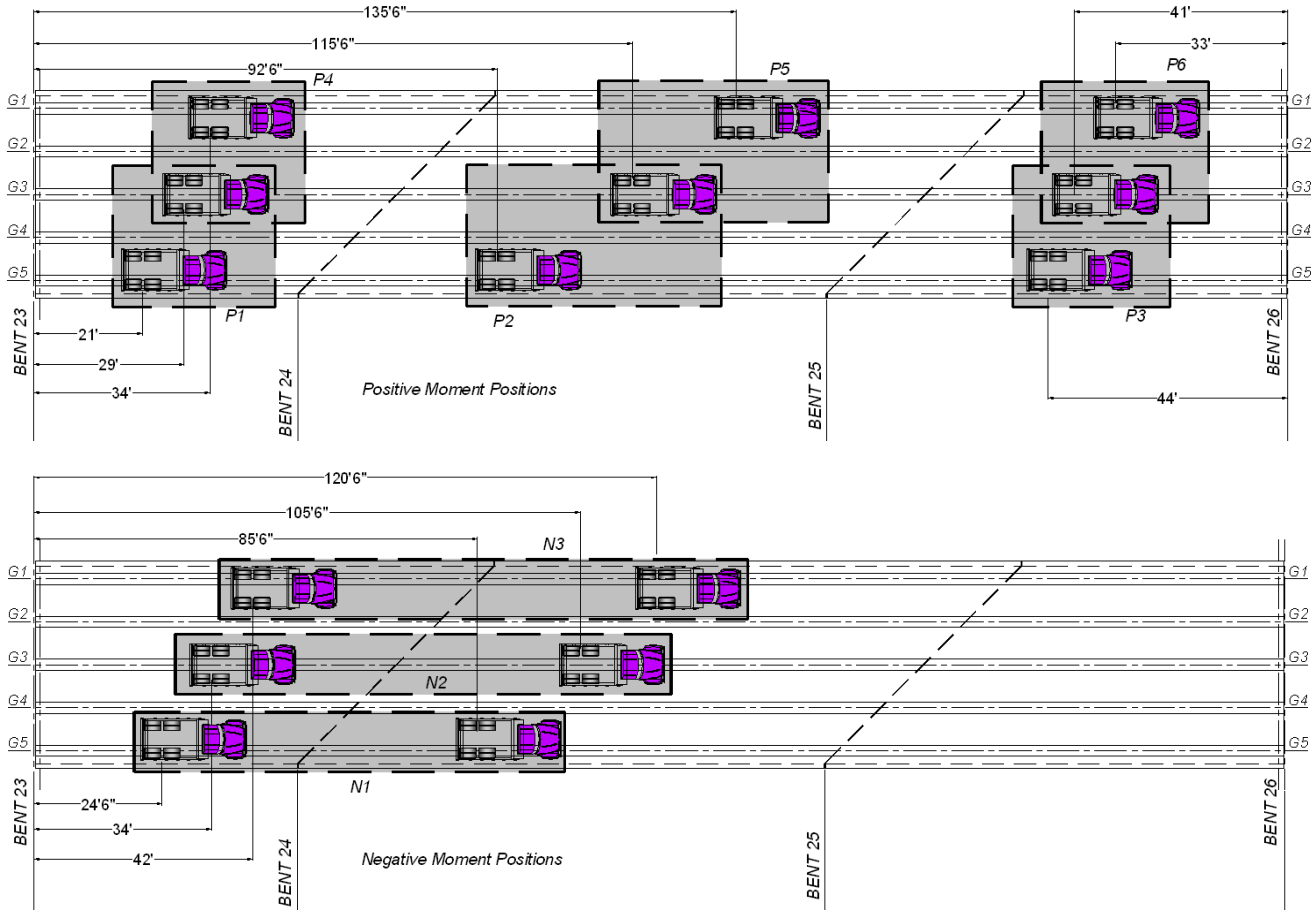

Fig. 6-4 Load test truck positions (distance with reference to middle of rear drive axle)

6.4.1 Truck Loading Position

As stated earlier, the monitoring system was designed to help in evaluating the performance of the recently proposed positive moment continuity details (Miller et al. 2004). The installed surface mounted and embedded sensors were strategically located along the Bent 24 support line in Girders G1, G3, and G5, and at the middle of Span 24 in Girders G3, G4, and G5. The truck positions were chosen to study the ability of the continuity detail of transferring forces between adjacent girder ends and to assess the level of continuity resulting from the new continuity detail. The exact truck positions used in the load test were determined using a three-dimensional (3D) finite element (FE) model developed using the ANSYS a commercially available software package. The goal was to identify the positions causing maximum straining

actions at the Bent 24 continuity diaphragm (negative moments) and at the middle of all spans (positive moments). While loading Spans 23 and 24 directly affects the heavily instrumented Bent 24 support line, loading Span 25 was deemed informative about the ability of the continuity diaphragm to resist positive moments caused by live loads. Capturing positive strains due to trucks loading Span 25 would confirm the ability of the new detail to convert simple span prestressed concrete girders into continuous superstructures not only through one connection, but rather through two of them; i.e. at Bent 25 and Bent 24 support lines. A total of nine truck positions were determined to generate the desired straining actions. These are six positive moment positions where trucks were placed in tandem (next to each other) with slight shifts to accommodate the skew effect, and three negative moment positions where the trucks were placed in a train formation (one ahead of the other along the same path). The positions are illustrated in Fig. 6-4 and are denoted as P1 through P6 for the positive moment positions and N1 through N3 for the negative moment positions. One day before the test was conducted; bright color markings were made on the bridge deck to assist the truck drivers in positioning the trucks during the test.

6.4.2 Load Trucks

Two loaded dump truck provided by the LA-DOTD were used to conduct the load test. The wheels of the trucks were weighed using a portable scale before the test and measurements of the axle dimensions were recorded. Fig. 6-5 shows the recorded truck information, which revealed that Truck 1 had a gross vehicle weight 57.0 kips, while Truck 2 weighed 54.1 kips. It should be noted here that the total weight of both trucks were substantially lower than the AASHTO-LRFD specified design load for the bridge configuration (AASHTO 2008). However, the combined load of the trucks was considered suitable for achieving the goals of this task.

6.4.3 Load Test Procedure

As stated earlier, the trucks were positioned in tandem or train positions for the positive and negative load cases, respectively. The load test began on 9.00 AM by guiding the drivers to the premarked position. The installed monitoring system's specs were designed for long-term data collection over years rather than shorter time periods. As such, its data logging ability is slow as it averages readings every hour. Each recorded reading was the average of 24 readings within the hour. This meant that it took 2.5 minutes to complete a cycle of readings from all channels in the monitoring system. Therefore, it was decided to keep the trucks at every loading position for at least 11 minutes to ensure that multiple (about 4) readings are recorded for that, which can then be averaged. Fig. 6-6 depicts two of such loading positions namely P1 and N1. The load test lasted for about 6 hours, during which the deck surface temperature started rising as the solar radiation increased in intensity. This meant that the strains recorded from the sensors will be caused by the combined effect of the truck and the temperature gradient. To allow for decoupling these two effects, the trucks were driven of the monitored segment in between loading positions P1 and P2, P3 and P4, P6 and N1, N1 and N2, and N2 and N3 in order to establish a reference datum for the recorded readings. The research team recorded the time at the beginning and at the end of each loading case. These times were essential for accessing the recorded data with the proper loading case.

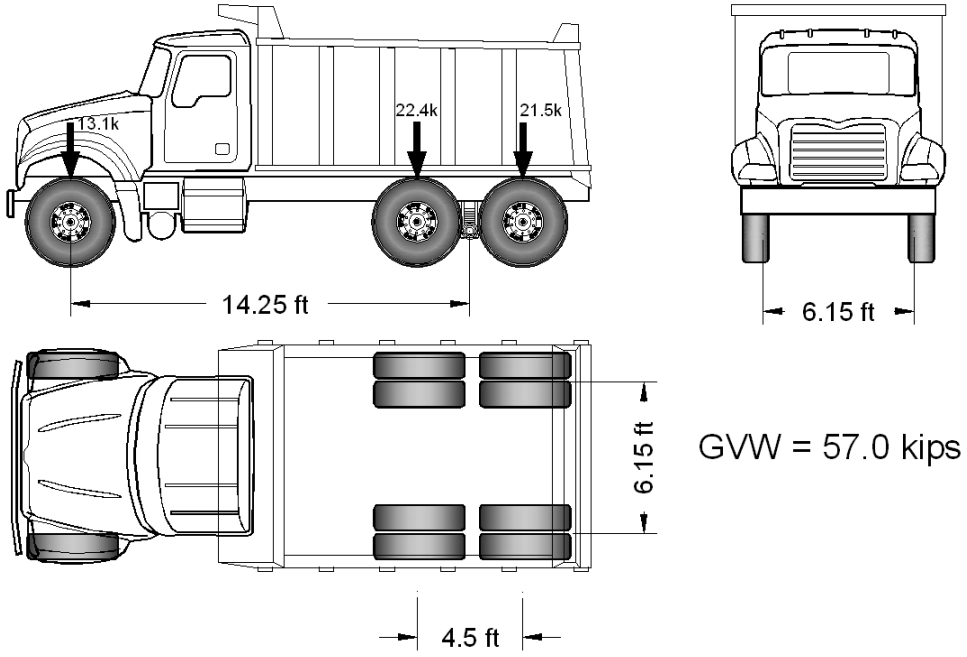

(a) Truck #1 (156-227)

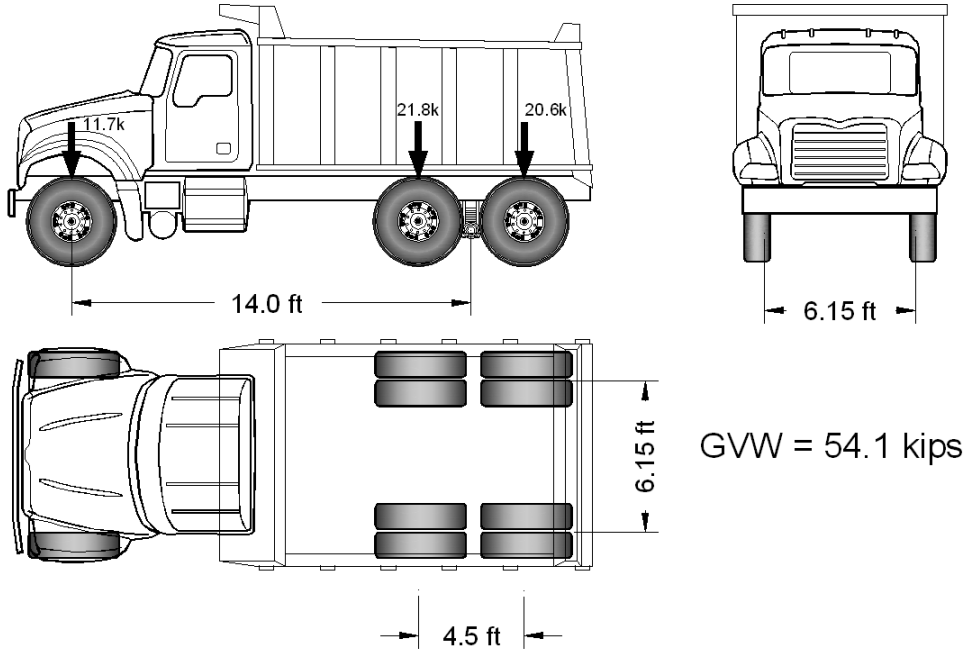

(a) Truck #2 (156-091)

Fig. 6-5 Dimensions and weights of trucks used in live load tests

(a) Position P1

(b) Position N1

Fig. 6-6 Loading Trucks #1 and #2 in position for two of the nine load positions

6.5 Data processing

The static load test started at 9:00 AM on August 19, 2010, and lasted till about 2:30 PM. During this time the temperature rises by more than 10º F which affects both the sensor readings as well as the structure as a whole. Vibrating wire gages are affected by temperature since the expansion or contraction of the wire at the core of the sensor affect its frequency and hence the apparent sensor reading. This effect can be corrected by using temperature correction formulas supplied by the manufacturer. However, the effect of temperature on the structure is real and has to be taken into account in order to get the true response of the structure due to the live load. If the temperature is even al through the structure then the extension and contraction of the structure will also be even. However, this scenario is not expected during the day, especially during the summer months in Louisiana. Fig. 6-7 shows a plot of temperature rise from five deck sensors and three bottom girder sensors. It should be noted that the deck sensors are at a depth of about 5 inches from the deck surface. The temperature at the deck surface was manually recorded by the research team and was found about 110 ºF. It can be seen from the plot that the deck temperatures arose about 10 ºF more than the bottom flange. This is true for the interior girders, but less so for the exterior girders where the barrier/overhang shading influences the typical temperature gradient. Higher deck temperatures than bottom flange temperatures cause the girders, and hence the entire bridge, to camber upward, which will also be captured by the sensors. The effect of this temperature gradient on the structural response, especially for statically indeterminate structures, is pronounced and cannot be ignored. As a matter of fact, the thermal response of the structure during that day was larger than its response to the live load. Therefore, an appropriate datum had to be identified so that this thermal movement of the structure can be deducted from the total response to get the net structural response due to the applied live loads only. This datum was identified with the help of six periods when the trucks were driven of the monitored bridge segment. Readings from these "no load" positions were identified as the response due to thermal effects only. Connecting readings during these "no live load" period establishes the desired datum from which the response of the structure due to live loads can be obtained by deducting the datum values from the total response. As stated earlier, the trucks were kept in each loading position for about 11 minutes so that each sensor can register at least 3 readings. The response of each sensor due to each loading case is then obtained by averaging these data for every load case. The following section describes a sample sensor reading for illustration purposes.

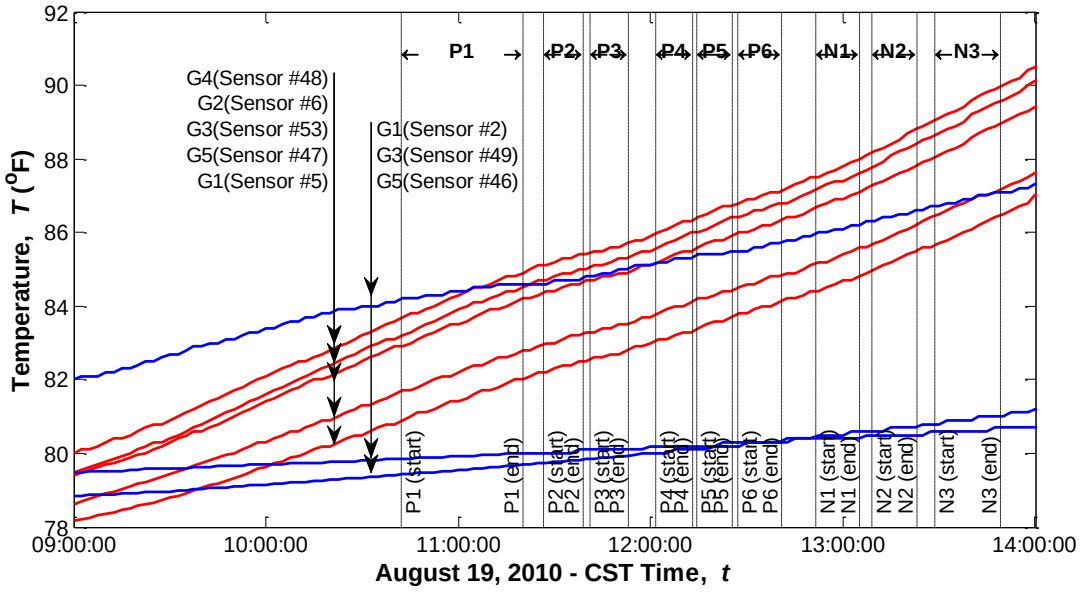

Fig. 6-7 Temperature increase during the time of conducting load test

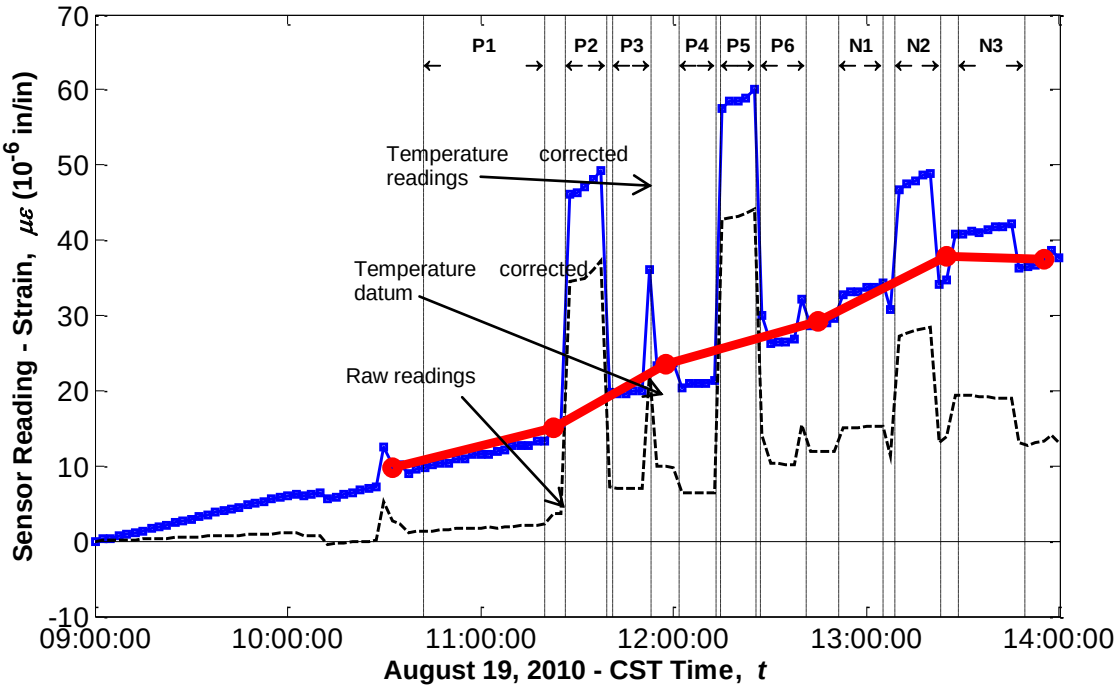

Fig. 6-8 Sensor reading in bottom flange of Girder G3 at the middle of Span 24 (G3S24)

6.5.1 Sample Sensor Reading

During the live load test, the data logger was set to the highest rate of data collection allowed by the monitoring system (1 reading/sensor/2.5 minutes) so that maximum amount of reading was registered during the stipulated time for each load case. The first step of the data processing was to correct the sensor data for the temperature effect relative to the initial temperature reading at the beginning of the test, which was taken to be 9:00 AM on August 19, 2010. Once the readings were corrected for the temperature effect, no load periods when the trucks were driven of the monitored segment were identified. A fictitious line was drawn to connect the average readings during each one of the six 'No Load' periods to serve as the temperature adjusted datum. Fig. 6-8 shows a sample reading from a bottom flange sensor located at the midspan of Girder G3S24. Two plots are shown for the strain readings. The first one (dashed line) was for the raw readings before the temperature corrections, while the second one which was marked by the squares was for the temperature corrected readings as per the manufacturers recommendations.

The first observation from the plot is that the strains increased by about 35 microstrain by the end of the live load test (2:00 PM) relative to the starting time (9:00 AM) due to temperature changes without considering the truck effects. This strain level is substantial compared to the highest reading from that sensor which took place during load case P5 and was about 60 microstrains. Hence, considering the apparent sensor readings may lead to erroneous conclusions if the thermal component of the readings was not decoupled from the live load component. After identifying the No-Load periods on the chart, an adjusted datum can be constructed as shown in the figure. As can be seen this temperature adjusted datum intersects with the sensor readings more than once. The difference between the temperature adjusted datum and the temperature corrected sensor readings was the relative sensor readings for the truck loadings. The figure shows that some load cases cause positive moment at the midspan while some other load case cause negative moment at the midspan. For example, the relative sensor readings during P2 and P5 load cases indicate a clear positive strain of about 25 and 32 microstrains, respectively. A negative strain of about 4 microstrains can be identified for the P4 load case, when the truck are positioned on Span 23, which according to fundamental structural analysis induces negative moments in adjacent spans of continuous structures.

6.6 FE Model

A 3D finite element model was developed for the entire three span bridge segment using commercially available software ANSYS (ANSYS 2008). The, SOLID65 element, is primarily developed to model the reinforced concrete, was used to model the girder, deck and diaphragm parts of the bridge. The element has eight nodes with three translational degrees of freedom at each node. Prestressing strands were modeled using the LINK8 3D spar element from the ANSYS element library. LINK8 is a two node element with three translational degrees of freedom at each node. The prestress force was simulated by applying an initial strain value equal to the corresponding losses adjusted initial prestressing force. The number of prestressing strands was different for different girders in Spans 23 and 25, as the skew resulted in different span lengths. The hair pin bars were also modeled with LINK8 element, however no initial strain were imposed on hairpin bar elements. The hairpin bars extended 8 inches from the end of the girders into the continuity diaphragm. The bridge was built with intermediate steel truss diaphragms which were also modeled LINK8 element. Fig. 6-9-a shows a typical bottom flange of a girder

where the location of prestressing strands and hairpin bar are clearly identified. A cross section of the finite element model of the bridge can be seen in Fig. 6-9-b. The final model was comprised on 224439 elements, 247828 nodes, and 742350 degrees of freedom.

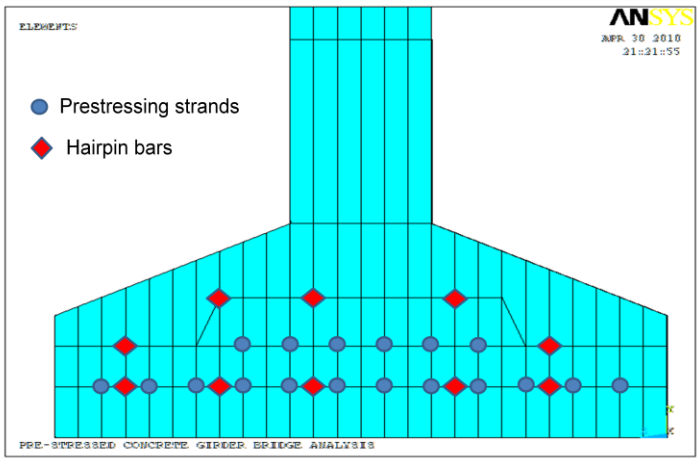

(a) Bottom flange showing reinforcement

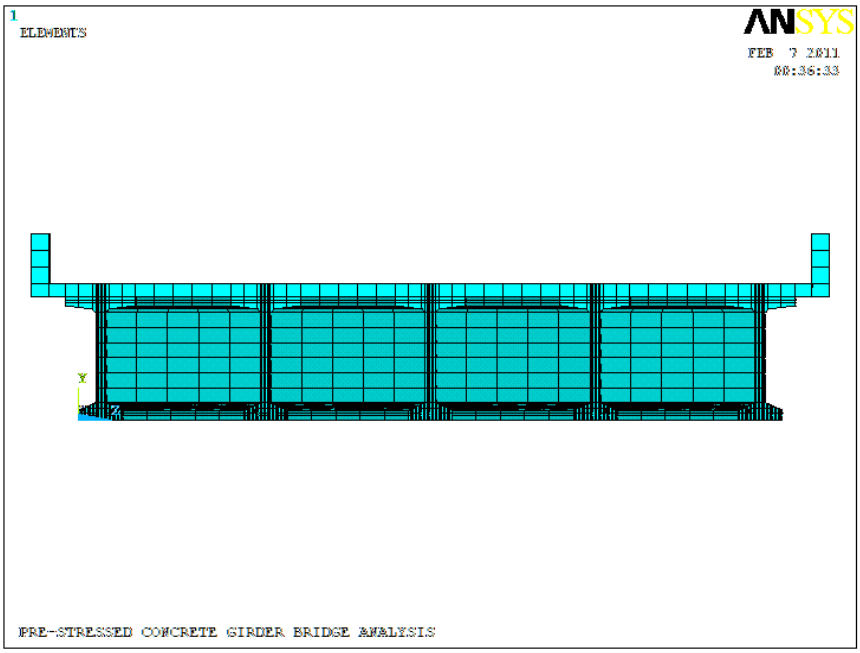

(b) Cross section

Fig. 6-9 FE mesh of bridge cross section

6.6.1 FE model validation:

The response of the bridge under the live load was captured at various locations where the sensors were installed. These sensor readings were then extracted from the data logger and corrected for the temperature effects and the total readings were decoupled into their thermal and live load components. The FE model was validated using the corrected net live load strain readings. The strain readings of the bridge due to the live load at midspan and at the girders' ends over Bent 24 were used to validate the model. This section describes the strain readings of the bridge and the steps undertaken to validate the FE model.

6.6.2 Midspan Strains

The FE model was loaded with the exact wheel loads at the exact locations where they were applied in the actual field test. Normal strains in the longitudinal direction at the middle of Span 24 were extracted for each girder from each load case and were compared with the actual sensor readings. Fig. 6-10-a shows the comparison between the FE model results and the actual field strain readings at the bottom flange of Girder G1 in the middle of Span 24 (G1S24). It can be seen from this figure that the midspan experience positive strain (tension) due to the load case of P2 and P5, these two load cases were intended to produce maximum positive moment at the midspan of Span 24. Girder G1 also experience positive strains at the same location for load cases N2 and N3. The comparison between the FE model and the field test strains at the midspan bottom flange for Girder G2 (G2S24) is shown in Fig. 6-10-b. For this location, positive strains were recorded for load cases P2, P5, N2 and N3. Fig. 6-10-c shows the strain response of girder G3S24 at its bottom flange in the middle of the span. It can be seen here that both P2 and P5 produces positive moment at the midspan. The small difference in the response for both load cases (P2 and P5) despite the anti-symmetric nature of this location is due to the difference of the weight of two trucks. Load case N2, which was intended to produce maximum negative moment over Bent 24 for Girder G3, produced positive moment at the midspan resulting in tension at the bottom flange. The comparison between the FE responses and the field responses at the bottom flange of G4S24 is depicted in Fig. 6-10-d. Girder G4 experiences maximum positive moment at the middle of Span 24 for load case P2, where the two trucks were placed on Girders G3 and G5. Girder G4 also experiences positive moment for load case P5, N1, N2 and N3. However, these positive strain are smaller than is recorder for load case P2, especially for load case N3 where the positive strain was very small as the trucks were positioned directly on Girder G1. Finally, the results for Girder G5 are plotted in Fig. 6-10-e. Like Girder G4, Girder G5 experiences maximum positive moment for the load case P2, in which case one of the trucks was placed directly over it. Load case N1 also produces positive moment at the midspan of girder G5. It should also be noted that all the five girders experienced negative moment at the middle of Span 24 for load cases P1, P3, P4 and P6 where the trucks were place on Span 23 and Span 25 without having any live loads on Span 24. These load positions produce positive moments in Spans 23 and 25, which results in a negative moment in Span 24. Both the FE model and field test captured this responses.

Based on the results discussed so far it can be said that the model is capable of qualitatively capturing the bridge response. To quantify the accuracy of the model, the results from the load cases producing the largest strains at the girders' bottom flanges will be focused on. Comparing strains from all load cases will not yield accurate results since some cases produce less than 10 microstrains in some girders. Such small readings open the door to

resolution issues and large percentage differences as the comparison is done with respect to negligible readings. Therefore, the two load cases that produce the largest strains at the middle of Span 24 (P2 and P5) will be used in quantifying the accuracy of the model. As can be seen in Table 6-1, the difference between the FE predicted strains and the field recorded readings ranged between -1.0% and +7.2% with an average of 3.5% with an standard deviation of 2.54. Two readings produced much larger difference, but this is attributed to their small values (< 10 microstrains) from both methods, i.e. field test and FE. These cases were excluded from the average calculation.

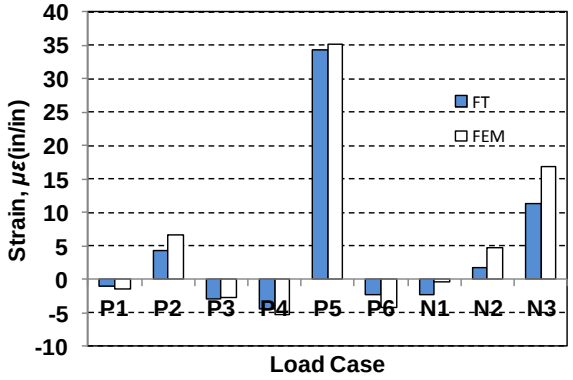

(a) G1

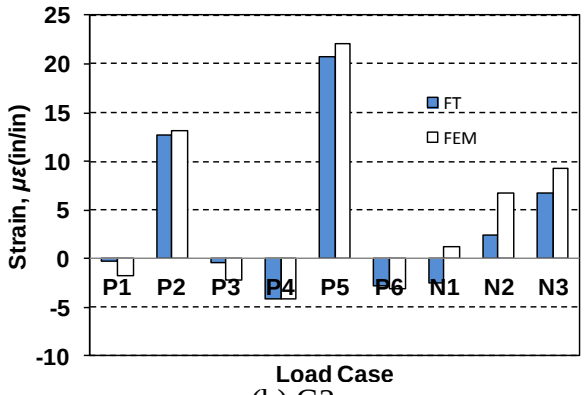

(b) G2

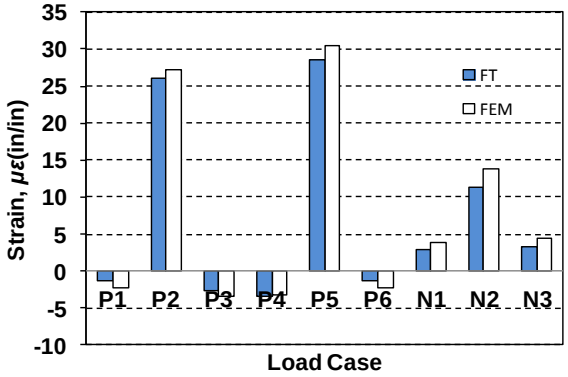

(c) G3

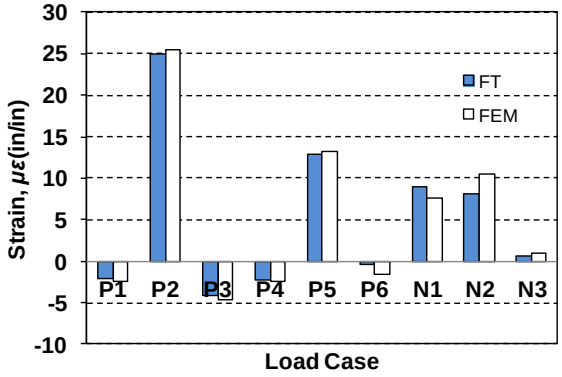

(d) G4

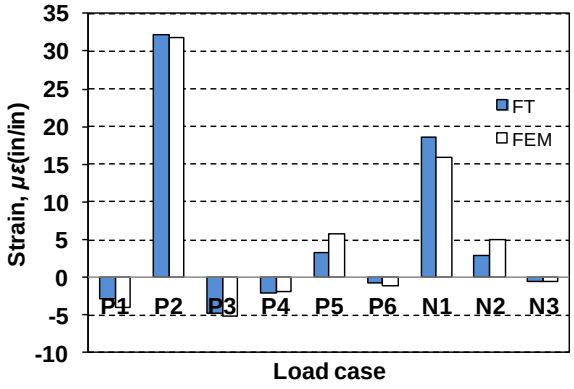

(e) G5

Fig. 6-10 Strain readings at the midspan bottom locations

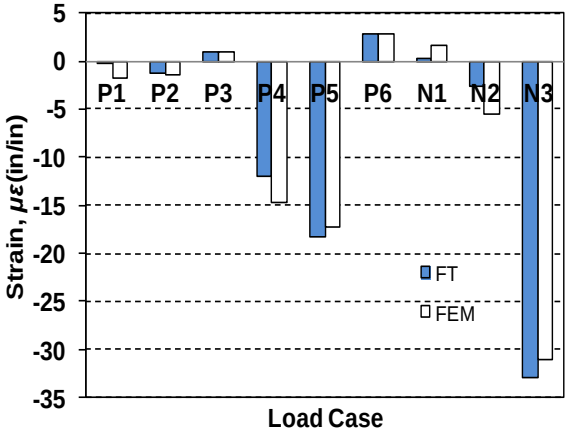

(a) G1S23

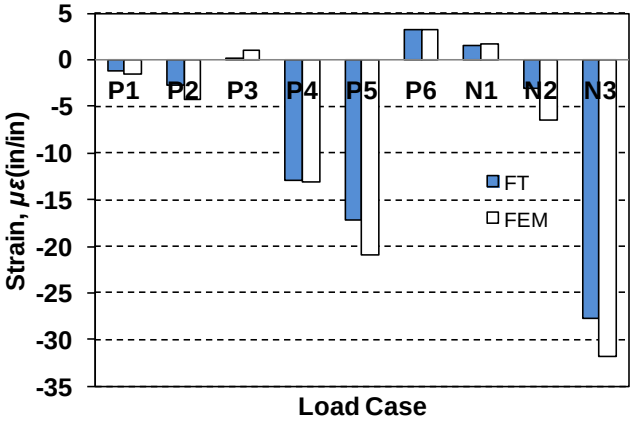

(b) G1S24

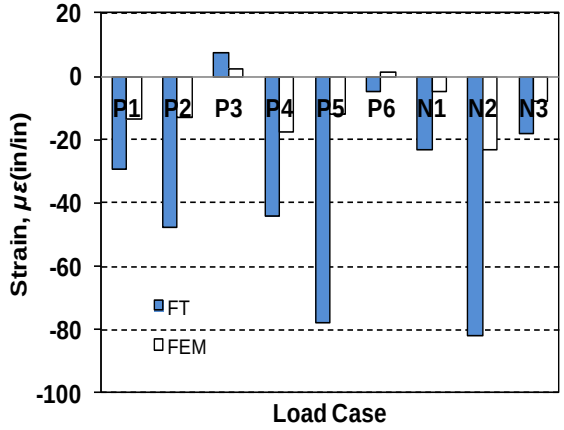

(c) G3S23

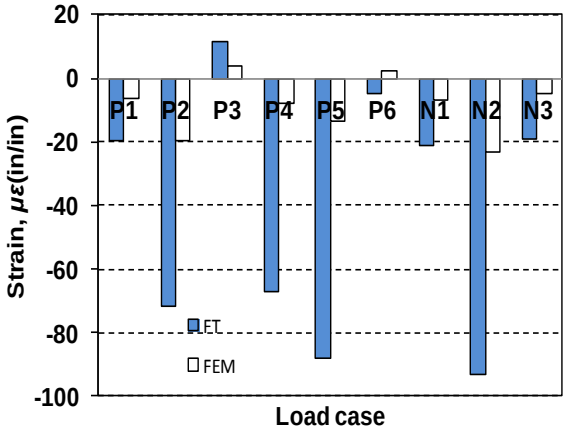

(d) G3S24

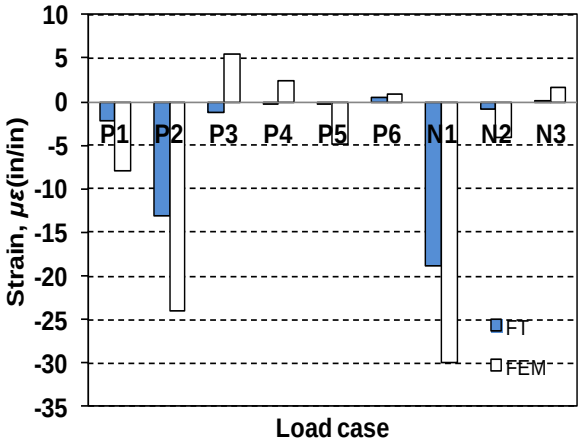

(e) G5S23

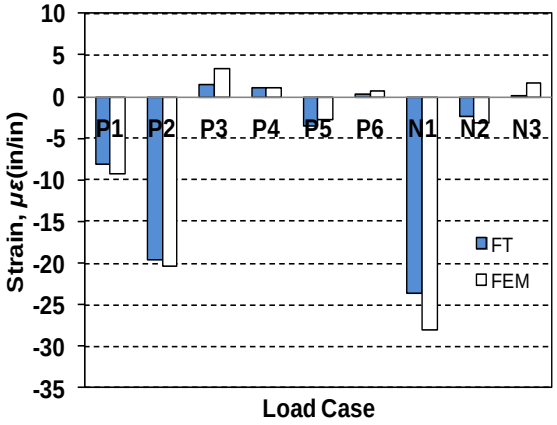

(f) G5S24

Fig. 6-11 Strain readings at the hairpin locations over bent 24

Table 6-1Quantifying FE model accuracy for load cases P2 and P5

Load case	Girder No.	FT	FEM	% Error
P2	G1	4.3	6.6	52.7*
	G2	12.7	13.1	3.3
	G3	26.0	27.2	4.6
	G4	25.0	25.5	2.1
	G5	32.1	31.8	-1.0
P5	G1	34.4	35.3	2.4
	G2	20.7	22.0	6.1
	G3	28.5	30.5	7.2
	G4	12.9	13.3	3.3
	G5	3.4	5.7	69.7*
			Average	**3.5**

*excluded from average calculation (small reading: < 10 microstrains)

6.6.3 Girder Ends Strains

Once the FE model was validated using the midpan locations for Girders G1S24 through G5S24, the focus was then shifted to validate the model against the response at the ends of the girder. Only girder ends at Bent 24 were considered since this is where the sensors were located. Hairpin bar locations were used in the comparison. Fig. 6-11 shows a comparison between the strain responses at both sides of Bent 24 for Girders G1 through G5. It can be seen from Fig. 6-11-a here that Girder G1 experiences negative moments due to the load case P4 and P5, which were meant to produce maximum positive moments for girder G1, G2, and G3 at Span 23 and 24, respectively, which also causes a negative moment at the support as a result of continuity. Girder G1S23 also experience even larger negative moments due to load case N3 which was meant to produce the negative moments at the supports. It should be noted that the FE model strain prediction is very close to the field measured strain. Fig. 6-11-b shows the strain response at Span 24 side of Girder G1. The pattern of the response is similar to that observed in Span 23, which implies that moments were transferred from one girder end to the other; i.e. the superstructure behaves as a continuous unit. The strains at the bottom ends of Girders G3S23 and G3S24 are plotted in Fig. 6-11-c and Fig. 6-11-d. It can be seen here that there were big differences between the FE model predicted strains and the field measured strains for different load cases. This is attributed to local cracks that were observed while performing visual inspections at the girder's bottom flange. Once the concrete cracks, the entire force at that location is only resisted by the hairpin bars. The FE model was not designed to replicate these cracks, therefore resulted in strains that are less than those measured in the field test as it is assumed in the model that the concrete is still intact (uncracked). Despite the large difference between the FE readings and field readings, the strain response was similar at both ends of Girder G3, indicating that superstructure still behaves as a continuous unit. The FE model also predicts the similar strain response at the both ends of Girder G3. The strain response at the bottom flanges of Girder G5 in Spans 23 and 24 are plotted Fig. 6-11-e and Fig. 6-11-f,

respectively. It can be seen that both the girders experienced large negative moments for the load cases P1, P2 and N1. The difference between the FE predicted strains and the field strain was smaller for the G5S23 and for G5S24 it was higher. This is attributed to the fact that girder G5S24 lacked sensors at the hairpin bar due to a construction issue. Therefore, a surface mounted vibrating wire gauge was used to capture the strain response for G5S24. It should be noted that girder G2 and G4 were not used here to validate the FE model, since these two girders were not installed with sensors at the hairpin bar locations.

6.7 Continuity Assessment

The core objective of this research project was to evaluate the performance of the new continuity details subjected to truck loads. Should the new positive moment continuity detail work as intended, forces induced by the positive moment will transfer from one girder end to the adjacent end along the same girder line. The validated FE model was used for this evaluation. From the previous two sections it can be seen that the FE model was validated against the strain responses at the bottom of midspan of Span 24 and at girder ends over Bent 24. Among the nine live load cases, only P3 and P6 will produce positive moment at the girder ends over Bent 24. Therefore, these two load cases were used for this evaluation purpose. Full continuity at the diaphragm should translate into identical strains in the hairpin bars at girder ends in both spans around Bent 24; i.e. Span 23 and Span 24. Fig. 6-12-a shows the tensile strains at the hairpin bar locations for all five girders in Spans 23 24 for load case P3. It can be seen from this figure that the strain increases from girder G1 to girder G5, since the load case P3 is intended to produce maximum positive moment for Girders G3 to G5 at Span 25. Therefore, a positive moment develops at the far span over Bent 24. However, the tensile strain show that the positive moment at the bottom of girders at Span 24 is more than that at Span 23; indicating that there is some sort of loss of continuity. The continuity will be assessed versus a continuity index which is proposed to have values that range from 1.00 (full continuity) to 0.00 (no continuity). The ratio of the positive hairpin bar strains between Span 23 and Span 24 was found to be equal to 0.89 on average. A similar conclusion can be drawn from load case P6 whose strain results are shown in Fig. 6-12-b. In this load case, it can be seen that the tensile strains were higher on Girder G1 side. P6 load case was intended to produce maximum positive moment for girder G1 to G3 at Span 25, which results in a positive moment at the far span over Bent 24. The strain ratio, i.e. continuity index, for this case was found to be 0.87. Therefore, it can be said that the average continuity index for the analyzed bridge is 88 %. It should be noted that the configuration of this bridge (e.g. skew, girder type and spacing, number of spans) may have affected the results. Therefore, before utilizing this continuity index in design, parametric studies will need to be conducted to assess the effect bridge parameters on the continuity index.

6.8 Conclusion

A live load test was performed on a three span continuous prestressed girder bridge segment. The layout of the bridge was skewed to accommodate an existing railway track. AASHTO Bulb-T girders (BT-72) were used in the construction of the bridge which employed a new positive moment continuity detail to convert the girders into a continuous superstructure. The live load test was performed to evaluate performance of the new detail under the truck loads. A full scale 3D finite element model was developed and live load test data were used to validate the model. Model validation showed that an average difference in longitudinal strains of 3.5% is expected. The validated model was then used to study the ability of the new detail to transfer

forces between adjacent girders. A continuity index, whose value ranges from 1.0 (indicating full continuity) to 0.0 (indicating no continuity), was defined and used to assess the performance of the detail. The validated FE model results were compared at both ends of one bent in the monitored bridge segment. Based on the comparison, it was found that the continuity index of the new positive moment continuity detail was about 0.88.

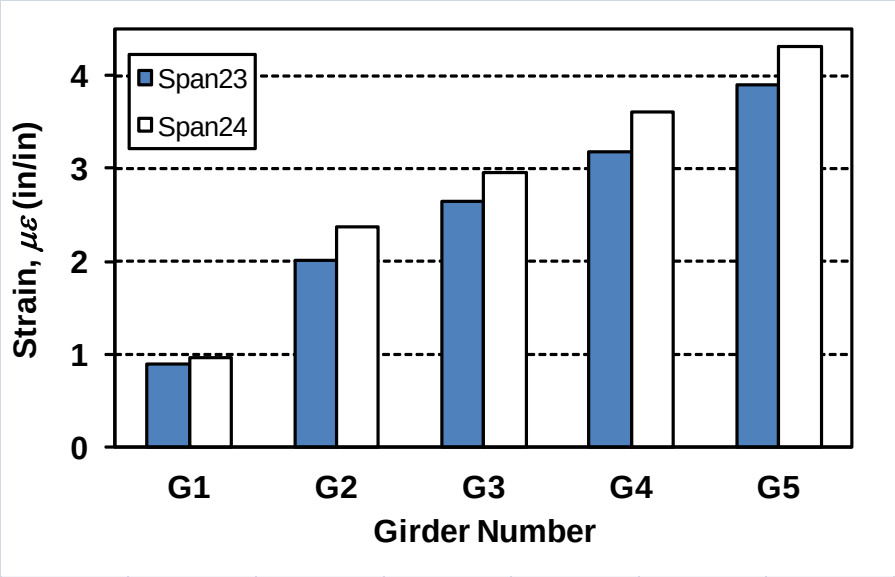

(a) Load Case P3

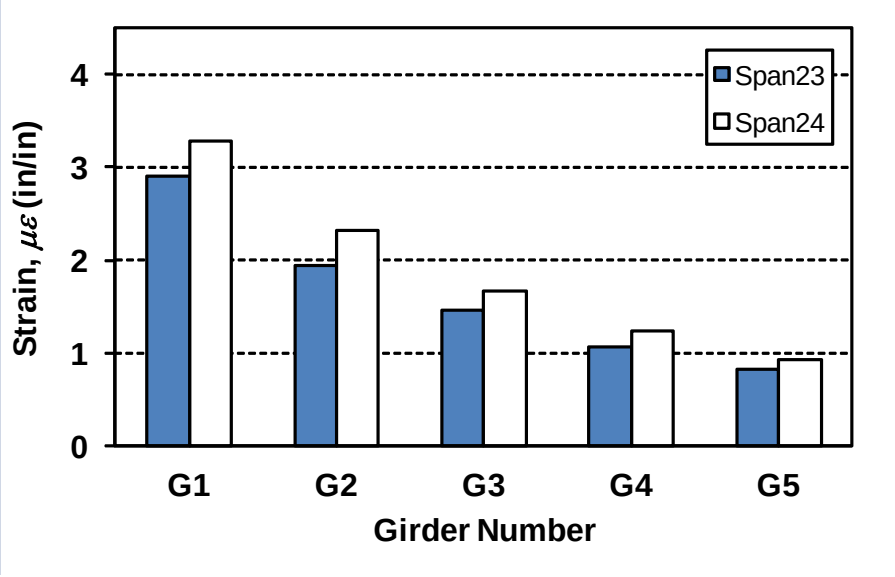

(b) Load Case P6

Fig. 6-12 Strain readings at the hairpin bar location of girders over Bent 24

6.9 Reference List

AASHTO (2008). "LRFD Bridge Design Specifications." American Association of State Highway and Transportation Officials, Washington, D.C.

Alampalli, S., and Yannotti, A. P. (1998). "In-Service Performance of Integral Bridges and Jointless Decks." *Transportation Research Record*, 1624, 1-7.

ANSYS . Theory Reference. 2008. Canonsburg, PA, ANSYS, Inc.

Bordes, J. L., and DeBreuille, P. J. (1985). "Some Facts About Long-Term Reliability of Vibrating Wire Instruments." *Transportation Research Record*, Natl Research Council, Transportation Research Board, Washington, DC, USA, 20-27.

Burke, M. P., Jr. (1992). "Integral Bridges: Attributes and Limitations.".

Burke, M. P., Jr. (2004). "Reducing Bridge Damage Caused By Pavement Forces." *Concrete International*, 26(2), 83-89.

Loveall, C. L. (1985). "Jointless Bridge Decks." *Civil Engineering*, 55(11), 64-67.

Miller, R. A., Castrodale, R., Mirmiran, A., and Hastak, M. (2004). "Connection of Simple-Span Precast Concrete Girders for Continuity." *Rep. No. NCHRP Report 519*, Transportation Research Board, Washington, D.C.

Oesterle, R. G., Glikin, J. D., and Larson, S. C. (1989). "Design of Precast Prestressed Bridge Girders Made Continuous." *Rep. No. NCHRP Report No. 322*, Transportation Research Board, Washington, D.C.

Thippeswamy, H. K., GangaRao, H. V. S., and Franco, J. M. (2002). "Performance Evaluation of Jointless Bridges." *Journal of Bridge Engineering*, 7(5), 276-289.

Wasserman, E. P. (1987). "Jointless Bridge Decks." *AISC Engineering Journal*, 24(3), 93-100.

7 FORCE TRANSFER MECHANISM IN POSITIVE MOMENT CONTINUITY DETAILS FOR PRESTRESSED CONCRETE GIRDER BRIDGES

7.1 Introduction:

Continuous prestressed concrete girder bridges offer many advantages over simple span bridges. Continuous bridges eliminate the joints over intermediate piers, which in addition to being weak structural links, exclude the possibility of water leaks on the piers which is detrimental to the reinforcement, especially when deicing agents are used. As a result of eliminating the problems associated with joints, maintenance costs are drastically reduced and the riding quality improves. Structurally, live load positive moments at the midspan for a continuous bridge are less than that of a simply supported bridge. Consequently, more economic designs can be achieved as the span lengths for the same sections of girders may be increased; resulting in fewer piers or fewer prestressing strands if the span lengths are kept the same as those of simple span construction. Furthermore, continuity offers an important structural benefit by enhancing the redundancy of the superstructure, which is a desirable property in any structural system, especially for those in seismically active zone.

Simple span girder bridges are made continuous in different ways. One of which is to cast a continuous deck over the girders while keeping the space in between the girder ends free to allow some movements. This approach results in partial continuity of the system as compared to a fully continuous system. Extra reinforcement in the deck provides resistance to negative moments that commonly develop over piers due to gravity loads. Alternatively, simple span girders can be converted into continuous structures by pouring concrete in between the girders end over the piers in the form of a continuity diaphragm. This design alternative results in fully continuous structures when designed adequately. The state of the art continuous bridge construction can be found in Hastak et al. (2003). Prestressed concrete girders camber up as a result of applying the prestressing forces where the tension is to be expected; i.e. below the neutral axis at midspans. This instantaneous camber keeps increasing through the life of the prestressed girder due to creep of concrete. When the girders are placed as a simple span on the piers, girder ends rotates as shown in Fig. 7-1. If continuity is established between the girders by pouring a continuity diaphragm, girder end rotations are restrained, which leads to the development of tensile forces at the bottom of diaphragm. If this tensile force exceeds the rupture strength of the diaphragm concrete, the bottom of the diaphragm cracks and allows the girder ends to rotate. Thus, continuity is lost and the girder behaves as a simple span. Positive moment reinforcement is, therefore, provided at the bottom of the diaphragm to resist the tensile forces that develop from girder's camber due to creep and other loads such as temperature gradients and some special live load position. The additional positive moment reinforcement can be provided in the form of extra bars extruding out from the bottom flange of the girders. Alternatively, the prestressing strands can be extended out from the bottom flange and bent upward into the diaphragm. Several researchers looked into the advantages of each alternative and design methods have been proposed. Recently, the National Cooperative Highway Research Program (NCHRP) sponsored Project 12-53 on positive moment continuity details for continuous prestressed concrete girder bridges. The findings of the project were published in NCHRP Report 519 (Miller et al. 2004). The report covered the two aforementioned alternatives for the detailing:

(1) extending the prestressing strands from the girders' bottom flanges into the continuity diaphragm and (2) providing additional 90°-hook or 180°-hook reinforcing bars (a.k.a. hairpin bars if both ends of the bar are developed in the girder) at the bottom flange that extend into the diaphragm. Fig. 7-2 shows both alternatives covered in NCHRP Report 519. The number of strands and length of the embedment of the strand into the continuity diaphragm can be found from the equations developed by Salmons and May (1974). The design recommendations resulting from Project 12-53 were adopted into provisions in AASHTO LRFD Specifications (2008) to assist designers in detailing the positive moment reinforcement. One of the concern of this type of connection is that, congestion in the diaphragm area might reduce the capacity of the connections due to the lack of interaction between bar and concrete. Another concern for bent bar connection is that bars must be placed asymmetrically with respect to the cross section to avoid space conflict between bars extending from different girders. This asymmetrical layout may lead to nonuniform stress distribution, which, if exacerbated by other factors such as a skewed layout, may lead to higher than anticipated stresses, thus, increasing the chances of cracking. The 180º-hook bar was recommended over 90º-hook bent bar connection because of the difficulties associated with placing the 90º-hook bent bar because of their interference with the formwork. It was also stated that uneven stress distribution in the connection may result from that detail. Therefore, 180º bent bars were recommended as a possible alternative in the NCHRP 519 Report.

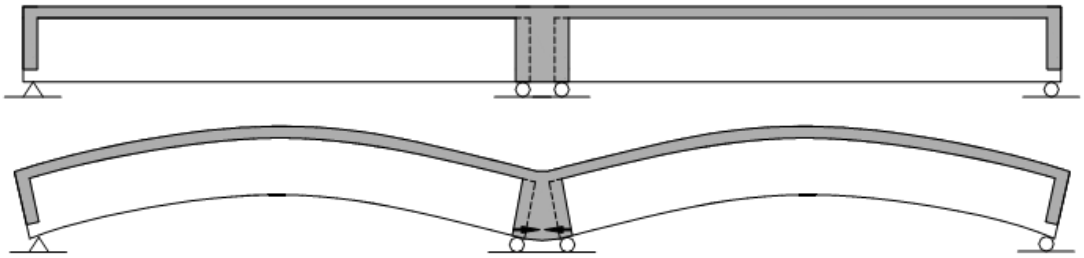

Fig. 7-1 Positive moment development at the diaphragm

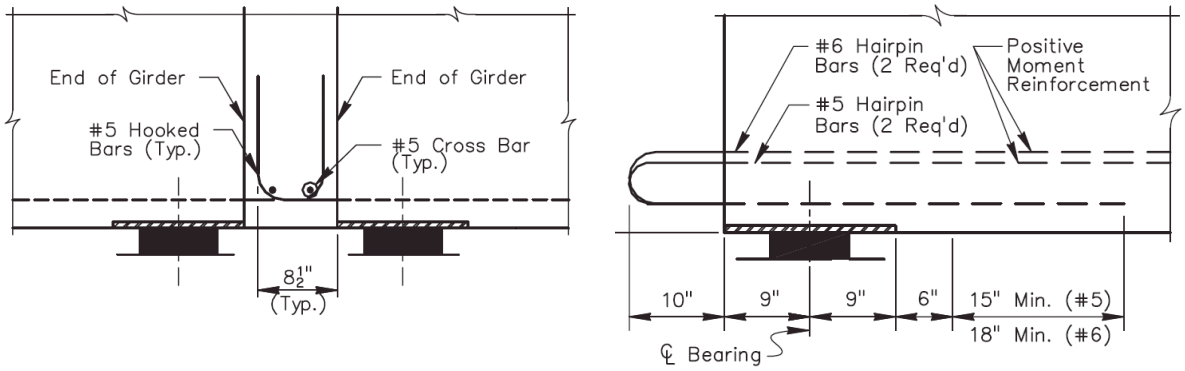

Fig. 7-2 Alternatives for positive moment reinforcement

A recently completed project in Southern Louisiana was bid as a design build project. The John James Audubon Project creates a new transportation artery across the Mississippi River between the cities of New Roads and Saint Francisville. In addition to the main cable stayed

bridge that crosses the Mississippi River, seven approach bridges had to be constructed. The designer of the project adopted one of the recommended continuity details (180º-hook hairpin bars) in many of the prestressed concrete girder spans. This detail is different than the standard detail in the Louisiana Department of Transportation and Development (LA-DOTD) Bridge Design Manual (BDM). In Louisiana, continuity diaphragms are detailed with no positive moment reinforcement, and to minimize restraint to girder end movement, a bond breaker is applied on the girder ends, thus, allowing the girder bottoms to move independently from the diaphragm. Therefore, it was deemed necessary to evaluate the performance of the new detail. The LA-DOTD Bridge Design chose a three span continuous segment of Bridge #2 that was built with Bulb-T girders made continuous using the new detail and was skewed to accommodate an existing railroad. The attributes of this segment; i.e. Bulb-T girders and skew layout, were not covered in the NCHRP 12-53 Project. A research project was initiated with the objective of understanding the behavior of bridges employing the new continuity detail under time-dependent effects as well as under live loads. A structural health monitoring approach was adopted for the task. Two years of monitoring data were collected from a 96-channel monitoring system to evaluate the time dependent load effect and a static live load test was conducted. Several three-dimensional (3D) finite element (FE) models were developed for the study. The first FE model is for the complete bridge segment was used to evaluate the global performance of the bridge. An FE line model of the bridge was developed to investigate the performance of the continuity diaphragm due to time dependent loading as well as temperature gradient. A preliminary FE model that focuses explicitly on the continuity joint was also developed. Findings from this study were published in a recent report (Okeil et al. 2011).

One of the observations resulting from this main study is that bottom flanges at girder ends are susceptible to cracking. It was hypothesized that even though the positive moments that developed due to time-dependent effects are not large, they are still capable of causing cracking because of the stress concentrations at the joint. The stress concentration stems from the fact that there is a cold joint between the precast girder end and the cast-in-place continuity diaphragm, through which the positive moment reinforcement passes. This means that all of the tension caused by the positive moment will be resisted by the reinforcement, which implies that the cold joint serves as a man-made crack. This behavior renders design calculations that rely on the gross cross-sectional properties in the vicinity of the joint unconservative.

This paper describes development of a three dimensional (3-D) finite element (FE) detailed joint model, which takes into account the transfer of prestressing force, cold joint between the cast in place concrete and the precast concrete, and also the 180º actual bar configuration. The objective of this detailed model was to investigate explore the local behavior at the girder ends and diaphragm under service load condition. The behavior of the continuity detail at the interface between the continuity diaphragm and girder ends under service load condition is investigated in this study. The force transfer mechanism between the girder end and continuity diaphragm is also investigated. Using results from the model, an effective moment of inertia of the composite section to resists the load at the diaphragm and at girder ends is proposed.

7.2 Finite Element Modeling:

Full accurate modeling the local behavior of the continuity detail calls for incorporating several nonlinear features. For example, incorporating the nonlinear material behavior is essential if understanding the ultimate behavior is the goal of the research. Geometric nonlinearities affect the structural behavior in two ways. First, the stiffness of structural members may be affected by large deformations, which is an important modeling aspect for slender and thin-walled structural members. Joints like the continuity detail are affected by another form of geometric nonlinearity due to the discontinuity between adjacent surfaces as they separate from each other without resistance when subjected to tensile forces, while still being capable of resisting large compressive forces. In the current study, the goal was to investigate the long-term behavior of the continuity detail. Over time, prestressed concrete girder bridges are subjected to straining actions caused by time dependent effects such as creep, shrinkage, and temperature gradients. The magnitude of the straining actions may be large, however, not to the extent to cause bridge failures. The temperature gradient effect generates a positive continuity moment equal to about 50% of the cracking moment, M_{cr}, according to a study by the authors (Hossain et al. 2012b). AASHTO-LRFD (2010) calls for limiting the positive moments acting on the continuity detail to be less than $1.2M_{cr}$. As such, large straining actions that can cause the materials to behave at high nonlinear levels are not to be expected within the scope of this study. Furthermore, prestressed concrete girders are optimized to eliminate their susceptibility to local buckling. Hence, it was deemed appropriate to investigate force transfer mechanism in the continuity detail by developing a detailed 3-D finite element model of the continuity detail without accounting for the material nonlinearity and the geometric nonlinearity due to large deformations. The main source of nonlinearity that affects the behavior of the continuity detail is the geometric nonlinearity due to discontinuity between adjacent surfaces that exist because of the cold joint between the precast girders and the cast-in-place diaphragm.

The commercially available software ANSYS (ANSYS 2008) was used to develop the model for investigating the behavior of the detailed continuity joint. ANSYS offers a variety of element types that are suitable for building a model capable of capturing the force transfer mechanism in the continuity detail. Element SOLID65, which is a eight node 3-D solid element with six translational degrees of freedom at each node, was used to model the concrete. SOLID65 is capable to model the cracking and crushing of concrete, which may be needed if further development of the model will be needed in future studies. More importantly, SOLID65 has birth and death features, which is particularly helpful in modeling construction sequence. The input data for concrete material properties include the ultimate uniaxial compressive strength, elastic modulus, density, and Poisson's ratio which are given in Table 7-1. The prestressing strands were modeled using the LINK8 element, which is a two-noded 3-D spar element with three translational degrees of freedom at each node. Prestressing is applied in the link elements as an initial strain. The initial strain value was determined from the prestressing forces obtained from the fabrication sheets. Since the joint model in this study was intended to investigate the load transfer mechanism at the service load condition, the effective prestress was used in the analysis including the effect of the transfer length. Transfer of the prestressing forces from the strands to the surrounding concrete depends on the transfer length which can be calculated from Equation 1 (Nawy 2000).

$$l_t = \frac{1}{3000} f_{pe} d_b \qquad (7\text{-}1)$$

where, f_{pe} is the effective prestress after losses (psi), and d_b is the nominal diameter of prestressing strand (in). The prestressing force in any pretensioned strand starts from zero at the girder end and attains full prestressing level at the transfer length. The increase is nonlinear as can be seen in Fig. 7-3 however, Equation (1) simplifies it with a linear relationship. In the finite element model, this gradual increase in stress (simulated as an initial strain), is idealized as a step function as shown. Prestressing was assumed to fully effective at the fifth element from the girder ends. The initial strain in LINK8 elements modeling the prestressing strands in the first four elements were changed as illustrated in Fig. 7-3. The hairpin bars were also modeled with LINK8 elements, however, no initial strains were input for these non-prestressed bars.

Table 7-1Material properties for deck, girder and diaphragm concrete

	Compressive strength (psi)	Modulus of elasticity (psi)	Poisson's ratio	Unit weight (pcf)
Girder Concrete	6500	4595486	0.20	150
Deck and diaphragm concrete	11500	6112569	0.20	150

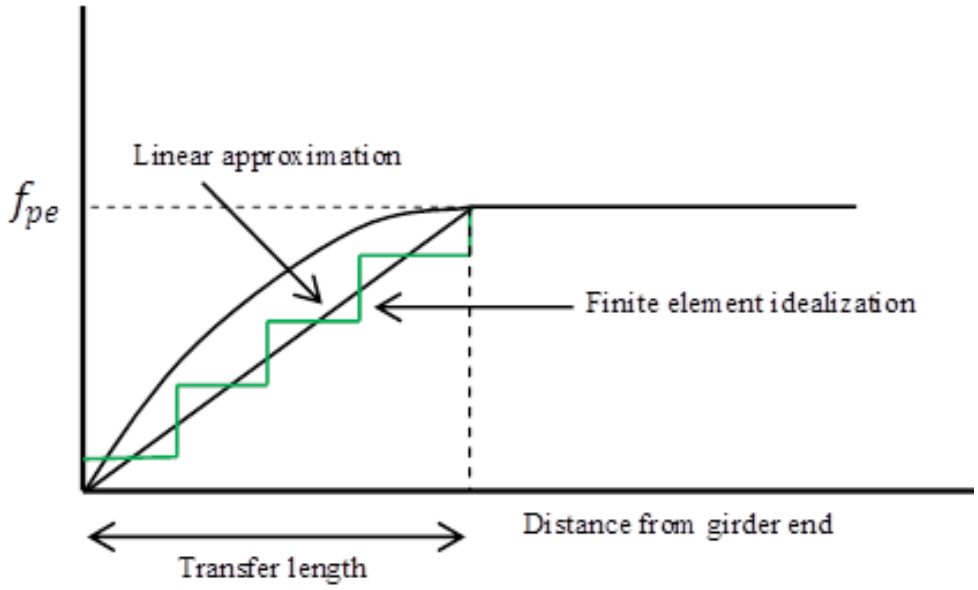

Fig. 7-3 Finite element idealization of transfer length for prestressing strands

In the actual construction sequence, girders were cast at a casting yard where they were stored until cured. After some designated time these girders were then transported to the site and erected on the piers as a simple span. Continuity was then established by pouring the deck and diaphragm concrete. When the deck and diaphragm concrete harden, continuity is established and the bridge system starts behaving as a continuous system. Because of this construction sequence, the deck/diaphragm and the girder are not monolithically cast, and a cold joint forms

at the interface between the girder ends and diaphragm. Subjecting this interface to compressive stresses (e.g. caused by negative moments) results in that both the girder end and the diaphragm become in full contact and the forced are transferred directly between the concretes of both members. Conversely, when the continuity diaphragm is subjected to tensile forces (e.g. caused by positive moments), the weak bond at the cold joint interface breaks easily and the tension force only transferred from the bottom girder flange to the continuity diaphragm through the hairpin bars. Simulating this behavior can be done using contact elements between the girder ends and the continuity diaphragm. CONTA178 element from the ANSYS library was adopted for this purpose in the current study. CONTA178 represents the contact and sliding between two nodes in any types of ANSYS elements. The contact element is defined by two nodes; each on one of the two touching surfaces, having three translational degrees of freedom at each node. In the developed model, two coincident nodes; i.e. nodes with identical coordinates, were created and connected using the contact element. As such, the contact element has a zero size and its sole purpose is to simulate the separation between the girder ends and the continuity diaphragm. This was achieved by modeling the girders, deck, haunch and the continuity diaphragm separately. The different parts that can be seen in Fig. 7-4 were then combined together. In this way, two identical nodes were created along the interfacing surfaces. CONTA178 elements were then added between the identical node pairs. Identical nodes other than those at the girder end and the continuity diaphragm interface were merged together, implying monolithic construction between these parts (e.g. deck and continuity diaphragm).

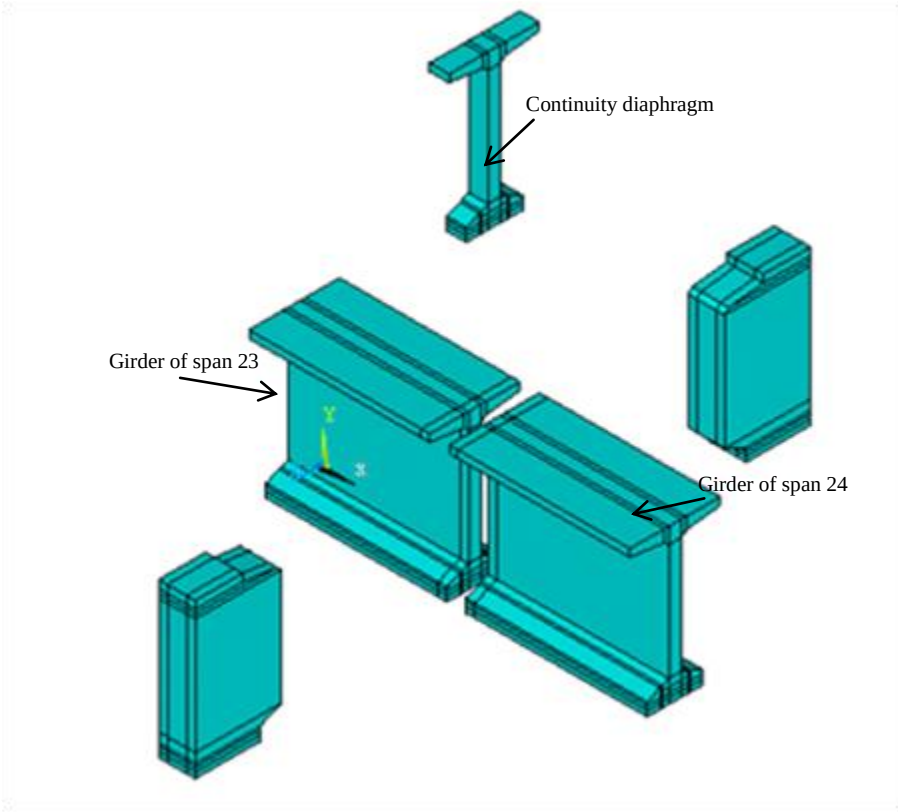

Fig. 7-4 Construction sequence idealization in finite element modeling

As will be discussed later, the model was loaded at the ends of the considered portions of the girder with loads equivalent to those developing in the full structure. Therefore, the girder portion considered in the model was taken equal to 7 feet longitudinally to address the Saint-Venant's hypotheses which states that the difference between the effects of two different but statically equivalent loads becomes very small at sufficiently large distances from the load (Timoshenko and Gere 2009). The considered girder portion was taken as 84 inches, which is slightly larger that the total combined height of the composite section includes 72 inches for the Bulb-T girder height, 2 inches for the haunch and 7.5 inches for deck thickness totaling 81.5 inches. Girder ends at the continuity diaphragm were placed on the bearing pads whose dimensions and properties were taken from the design plans. SOLID45 elements were used to model the bearing pads. The shear modulus for the bearing pads was taken equal to 95 psi, which is the lower bound value of the AASHTO LRFD Specification (2010). The final mesh of the model is shown in Fig. 7-5

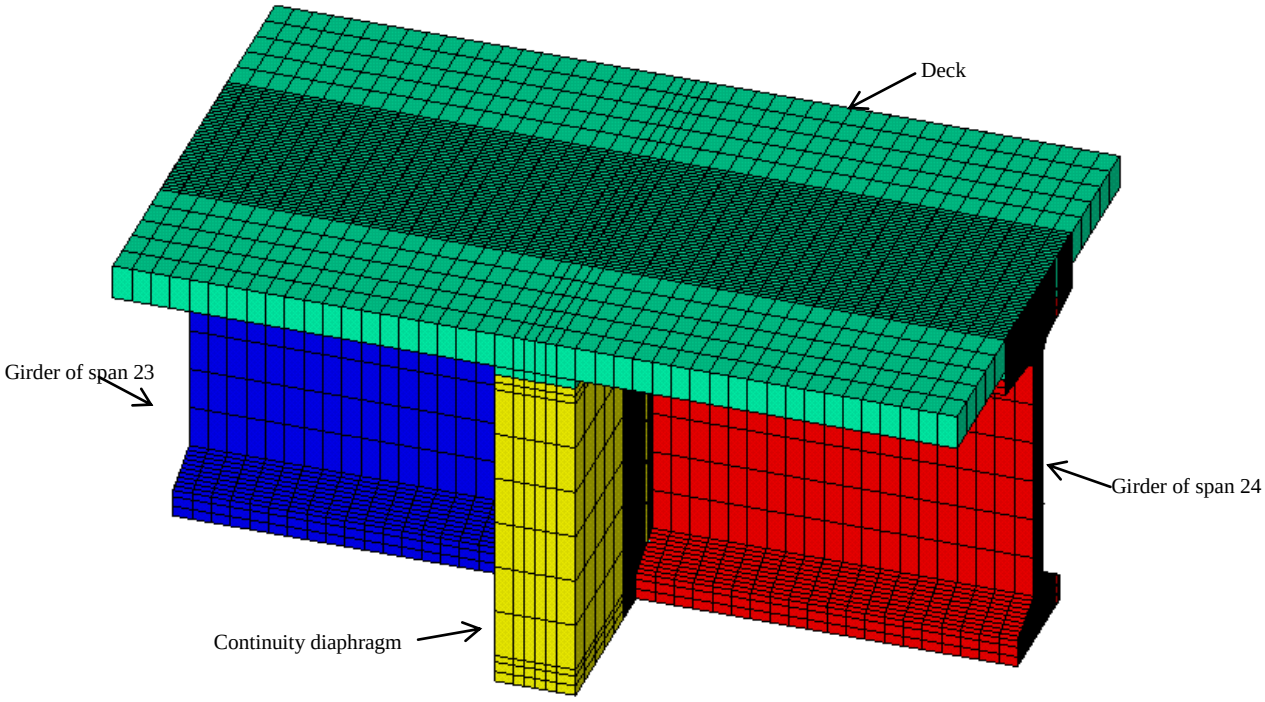

Fig. 7-5 Elements of the detailed joint model (a coarser mesh is shown here for clarity)

One of the most difficult challenges of this study is to model the actual geometry of the 180º hook hairpin bars. The hairpin bars were extended from the bottom flange of the girder ends and then took the form of standard AASHTO Specified 180º hook which was embedded 8 inches into the continuity diaphragm. Five hairpin bars were extended from the left girder and five hairpin bars were extended from the right girder ends. These ten hairpin bars were staggered in a way to allow full 8 inch embedment into the continuity diaphragm without creating any conflicts between hairpin bars extending from both girder ends. Modeling the exact geometry of the 180º-hook is extremely important in understanding the local behavior of the continuity diaphragm.

Simplification of the hook using square-shaped bar geometries or curtailing it in different way than the actual geometry defeats the purpose from building this model. Therefore, a cylindrical shaped volume was defined and overlapped with the rectangular shaped volume. In this way 180º lines were created that were aligned with actual locations of the hairpin bars. These lines were later meshed with elements whose attributes where those for the nonprestressed steel bars as can be seen in Fig. 7-6-a. The different parts of the model within the continuity diaphragm were meshed after the outlines of were defined. Fully controlled mapped meshing was not possible for all parts because of the complexity of the generated geometries, especially the cylindrical ones. Therefore, free meshing had to be relied on in some parts. To control the transition (zooming) of the mesh between the free meshed and map meshed portions, a substructure of the model representing the small portion of the continuity diaphragm identified by the projection of the bottom flange of the girder. A skin layer of volumes was defined around the free mesh volumes for which the elements were sized to match the mapped mesh elements (see Fig. 7-6-b). Thus, the mapped and free mesh portions of the model shared the same nodes at their junction in the final model. Fig. 7-6-c shows the meshing of a portion of the continuity diaphragm between the girder bottom flanges where the hairpin bars, the prestressing strands, the free and the mapped meshed volumes. The FE model was built using 47,777 elements, 41,592 nodes, and 123,528 degrees of freedom.

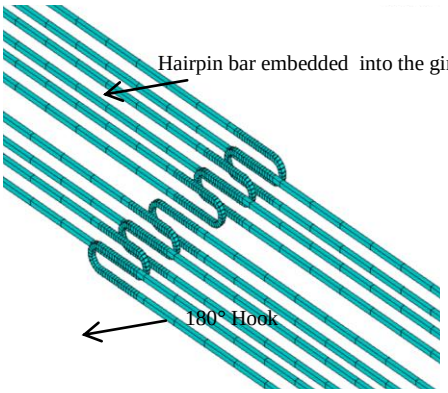

(a) 180º Hairpin bars

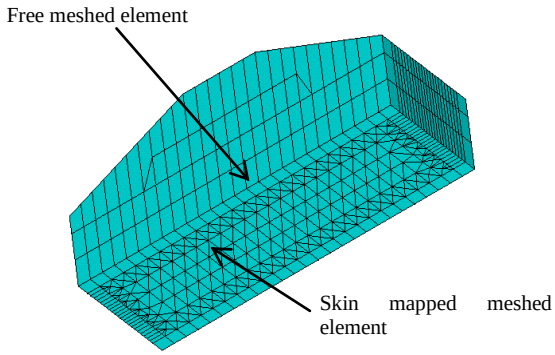

(b) Free and mapped mesh

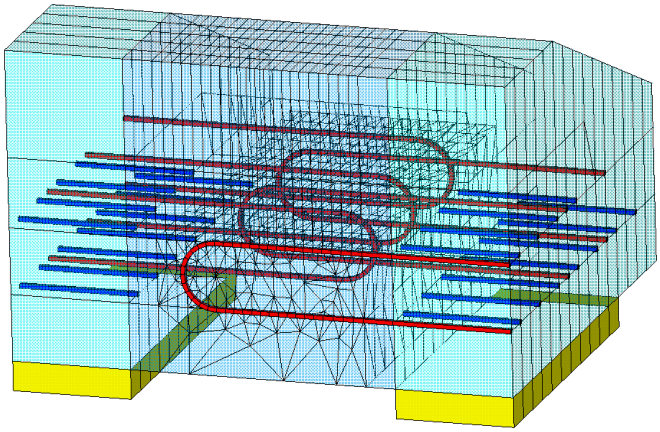

(c) Free and mapped mesh

Fig. 7-6 Meshing of hairpin bars and bottom of continuity diaphragm

7.3 Model Loading

The objective of this present study is to investigate the force transfer mechanism between the girder ends of a continuous bridge through the continuity diaphragm with the help of 180º hook hairpin bars. As mentioned earlier, the focus of the investigation is on the behavior of the continuity detail under positive moments for which the hairpin bars are added to resist the tensile forces resulting from the positive moments. Positive moments may be caused by time-dependent effects such as creep and shrinkage. It may also develop due to temperature gradients and some live load positions. Applying arbitrary positive moments at the girder ends is an option for performing the desired investigation. However, the results may not represent the actual behavior of the continuity detail since these moments may be different than the positive moment acting on the continuity detail. Therefore, straining actions were extracted from a 3-D FE girder line model that was developed to estimate the creep induced moments in the center girder of the monitored bridge segment (Hossain et al. 2012a). The FE line model was first calibrated using field monitoring data, and then was used to analyze a representative girder for 75 years, which is the typical service life expected from newly designed bridges. In the line model, positive moments start developing after continuity established by pouring the continuity diaphragm, which is accounted for by modeling the construction sequence. The bending moment and shear force acting on two sections at a distance equal to 84 inches from the girder ends were obtained by integrating internal stresses caused by creep after 75 years of time. The distance where the moment and shear are obtained was chosen to be the same as the girder length included in the joint model developed in the current study. The bending moment was the result of integrating the normal stress with respect to the neutral axis of the composite section, which is located at 54.57 inches from the girder's soffit, while the corresponding shear force acting on the same section was obtained by integrating the shear stresses. The self weight of the elements included in the model was included directly as a gravity load. In addition to the creep induced loads and the self weight of the members, the also included the effect of the prestressing forces from the strands including the transfer length effect as described earlier.

7.4 Results

The FE model generates a large amount of information that can be used in several Types of behavioral assessments. In this section, three aspects of the behavior will be focused on; namely, asymmetric stress distribution in the continuity diaphragm, hairpin bar contribution, and stress concentrations at girder ends.

7.4.1 Asymmetric Stress Distribution

The stress distribution in the middle of the diaphragm is first extracted from the analysis. As stated earlier, hairpin bars have to be staggered to avoid space conflicts. Consequently, it is expected that the stresses resulting from the tensile force caused by the positive continuity moments to be asymmetric. Miller et al. (2004) suggested that the behavior of the detail is affected by the asymmetric stress distribution (e.g. crack widths varied). Fig. 7-7 represents two slices of the continuity diaphragm defined by the projection of the girder's bottom flange on the diaphragm. The contours, which reflect the longitudinal normal stress intensity, confirm the expected the asymmetric stress distribution. The difference between the two shown slices is that one of them (Fig. 7-7-a) is closer to one girder end, while the other is closer to the other girder end (Fig. 7-7-b). It can be seen that the stress intensity in Fig. 7-7-a is higher on the right side of the plot, while it is higher on the opposite side in Fig. 7-7-b**.** Fig. 7-7-c is a top view of the same

region; i.e. diaphragm between girders' bottom flanges. It can be seen that the tensile stresses flow from one girder end to the other while shifting the intensity to the side where the hairpin bars are biased. This asymmetric stress distribution implies that assuming uniform behavior may underestimate the actual stresses in the design of the detail. While the difference caused by hairpin asymmetry may not be sufficient to initiate cracking, it may be exacerbated by other factors such as skewed layouts, thus leading to exceeding the tensile strength of concrete.

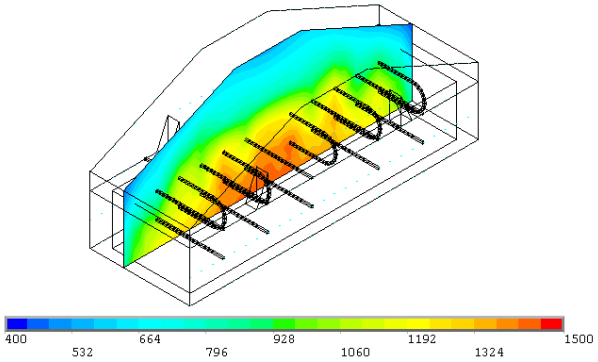

(a) Axial stress at the mid-section of continuity diaphragm

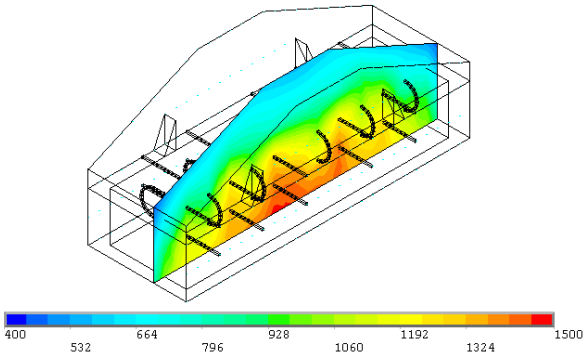

(b) Axial stress at the mid-section of continuity diaphragm

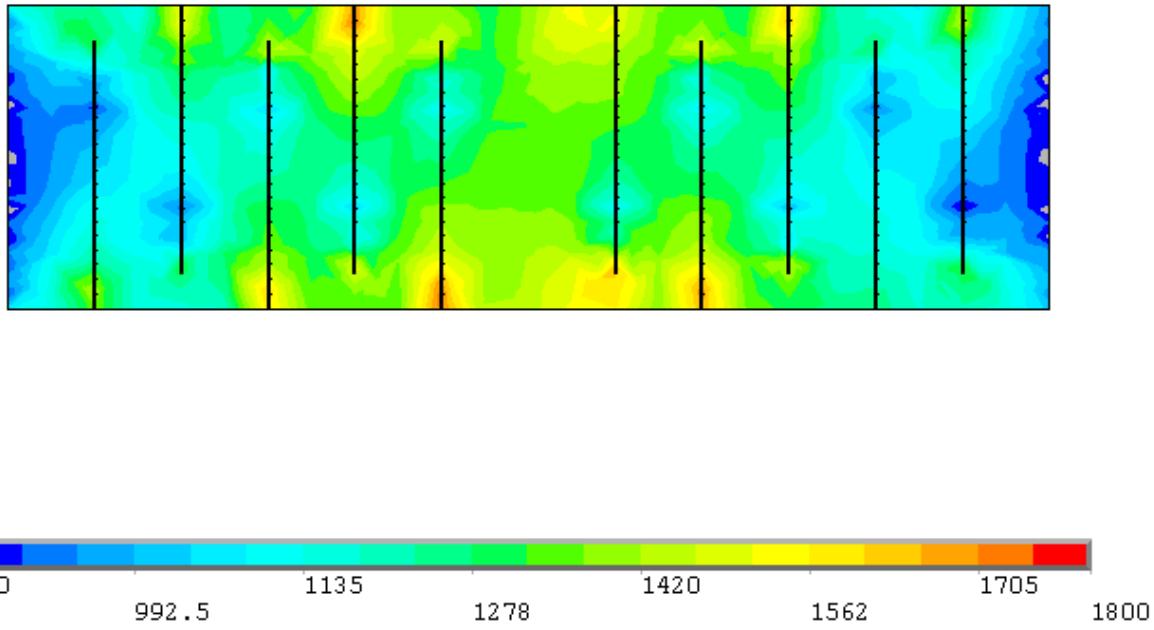

(c) Axial stress at the mid-section of continuity diaphragm with hairpin bars

Fig. 7-7 Asymmetrical stress distribution at the continuity diaphragm

7.4.2 Hairpin Bar Contribution

Tensile forces are transferred between girder ends through the continuity diaphragm, where the hairpin bars serve as the main path for tensile forces from the girders to the diaphragm since the cold construction joint is not capable of resisting tensile stresses directly. When the joint is subjected to a positive moment, the girder-diaphragm interface breaks and a gap opens at

the regions subjected to tensions (bottom), while regions subjected to compression remain intact. This model captured this behavior as can be seen in deformed shape shown in Fig. 7-8. At the gap, the entire tensile force is transferred thorough the only continuous element; i.e. hairpin bars. Fig. 7-9 shows a plot of the normal force in the hairpin bars. The spike in the axial force indicates the diaphragm-girder interface location where the gap takes place. The force in the hairpin bars start dropping away from the interface as it gets transferred to the diaphragm or girder concrete. Inside the diaphragm, the axial force diminishes just before the curved end of the 180º, whereas the tensile force changes to a compressive force inside the girder. The small compressive force inside the girder away from the diaphragm is the result of the prestressing force that increases until it reaches its full value at a distance equal to the transfer length.

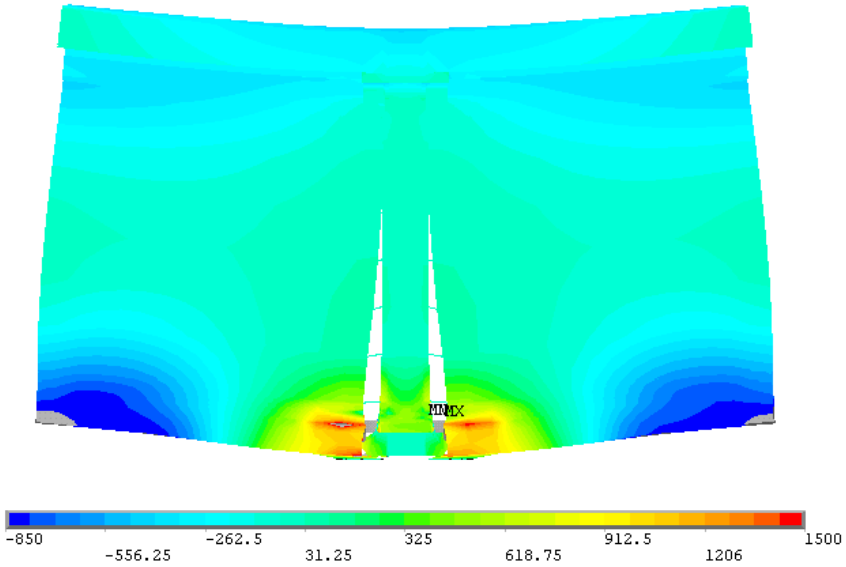

Fig. 7-8 Opening takes place at the girder end continuity diaphragm interface

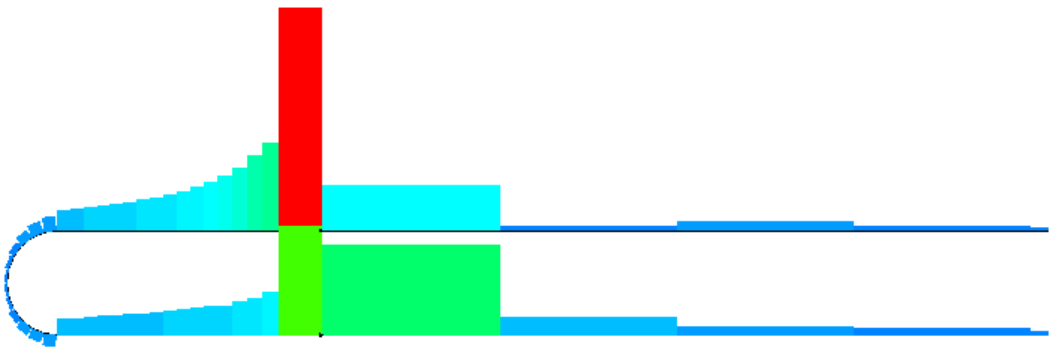

Fig. 7-9 Axial force distribution along a hairpin bars

7.4.3 Stress Concentrations at Girder Ends

The previous section illustrates that the tensile force is almost solely transferred by the hairpin bars at the interface where the gap opens between the girder end and the continuity diaphragm. On either side of the interface, the girder or diaphragm concrete start helping in resisting the tensile force gradually. Of interest to understanding the behavior of the continuity detail, the concrete stress distribution at the girders' ends is studied. Fig. 7-11 shows contours of the longitudinal normal stress, σ_x, across the girder section. The figures illustrate the higher stresses at the bottom flange and the lower stresses in the middle part of the section; i.e. web. This is especially true closer to the girder ends before the more of the section starts getting engaged in the resistance of the tensile force according to St. Venant's principal. For example, the stresses at 2 inches from the girder end show that the bottom flange normal stress is tensile and reaches 1500 psi while it hovers around zero in the web. At 24 inches from the girder end, the prestressing force is fully active and, therefore, compressive stresses are obtained in the bottom flange and the web.

It should be noted that in addition to these general observations about the stress distribution by girder parts; i.e. bottom flange and web, the stresses also show nonuniform distributions within each part. This is especially obvious closer to the girder ends where the analysis shows high tensile stresses at the top corner of the bottom flange. The monitoring system installed on this bridge segment did not call for sensors at this specific location. However, visual inspections revealed that one of the girders cracked at the same location where the FE analysis predicts high normal stresses. Fig. 7-10-a and b shows two pictures taken of the observed crack 6 months and 10 months after establishing continuity, respectively. It is clear from Fig. 7-10-a that the crack initiated at the top corner of the bottom flange and did not extend all the way through the bottom flange. 10 months later, the crack propagated downward through the bottom flange.

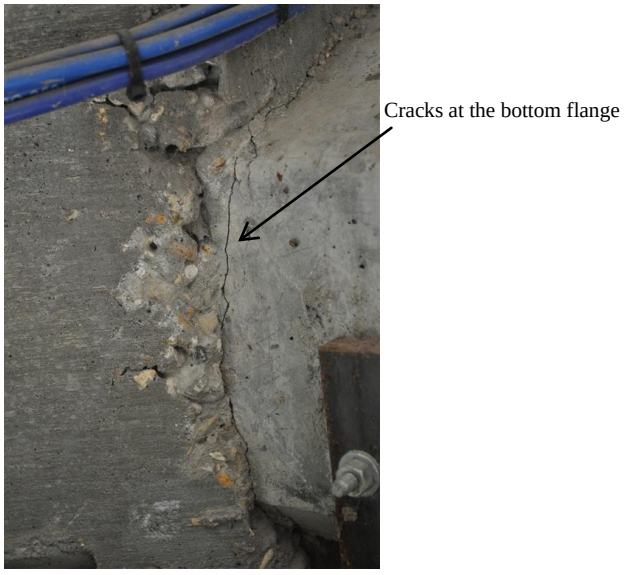

Fig. 7-10 Observed crack at the bottom flange of girder near the continuity diaphragm

7.5 Effective I_g for Cracking Moment Calculations

In the previous section, it was illustrated that the entire girder section does not engage in resisting the tensile force close to girder ends. Thus, checking the vulnerability of girder ends to cracking based on a cracking moment calculated according to the classical equations may lead to unconservative outcomes such as girder end cracking as was observed in the field. The cracking moment is normally assessed using Eq. 2 (Nawy 2000):

$$M_{cr} = \frac{I_c}{y_b}\left[\frac{P_e}{A_{nc}}\left(1 + \frac{ec_b}{r^2}\right) + 7.5\sqrt{f_c'}\right] \quad (2)$$

where I_c is the composite section's moment of inertia, y_b is the distance from the extreme tension fibers to the center of gravity of the composite section, P_e is the effective prestress force after all the losses, A_{nc} is the area of the noncomposite girder section, r^2/c_b is the upper kern value of the noncomposite girder section, and f_c' is the compressive strength of concrete at 28 days. It should be noted that additional terms accounting for dead loads on noncomposite section are not included as these moments are equal to zero at the support. It can be seen that the cracking moment, M_{cr}, is largely dependent on the effective prestress force and gross moment of inertia of the composite section. As stated earlier, the full effective prestress develops at a distance equal to the transfer length as seen in Fig. 7-3, which can be estimated using Eq. 1. Thus at the very end of the girder, the prestressing effects is negligible. Thus, it can be said that the cracking moment is more influenced by the gross moment of inertia of the composite section as the first terms in Eq. 2 become small. Consequently, estimating I_c accurately is of even higher importance. The use of I_c assuming that the entire composite section is engaged in resisting stresses that develop from the positive moment will overestimate the cracking moment, M_{cr}. Therefore, it is proposed that an effective composite moment of inertia, I_{ce}, be used for cracking moment calculations at girder ends.

The 3-D FE joint model has been used to identify the portion of the composite section that engages in resisting the normal stresses. Fig. 7-11 reveals that at small distances from the girder end (e.g. 2, 6 and 8 inches), the stress contours of the normal stresses are tension at the bottom flange only. Beyond 12 inches, stress concentrations start vanishing and a more uniform stress distribution takes place. Furthermore, the effective prestressing force increases away from the girder end, rendering the concern about cracking due to tension mute. Above the neutral axis, the deck concrete and the prestressed girder parts are subjected to compression and are fully engaged. Therefore, it is proposed that the effective gross moment of inertia be taken as that of the composite section after ignoring the web contribution for the first 3 feet measured from the girder end as can be seen in Fig. 7-12. For the Bulb-T (BT-72) composite section used in this study, the composite moment of inertia, I_c, is calculated to be 121,8125 in^4, whereas the proposed effective composite moment of inertia, I_{ce}, is only 968,349 in^4. The difference between the two moments of inertia is 20.5%, which is how much current practice would overestimate the cracking moment for the proposed detail.

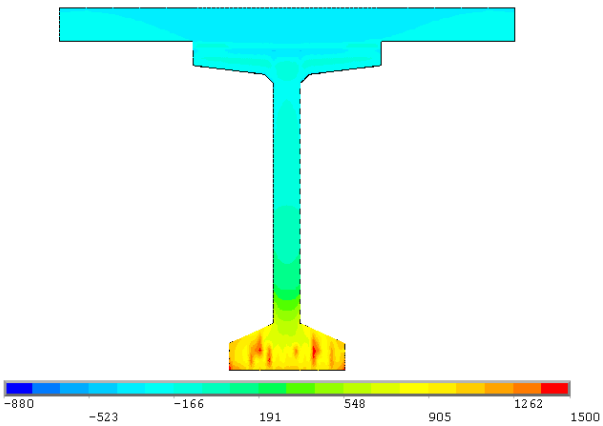

(a) At a distance 2 inch from the girder end

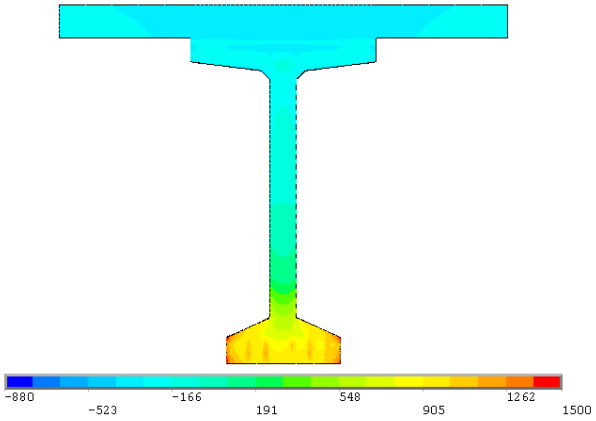

(b) At a distance 4 inch from the girder end

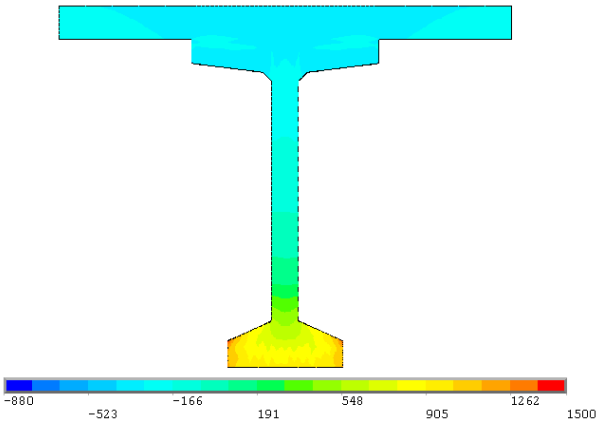

(c) At a distance 8 inch from the girder end

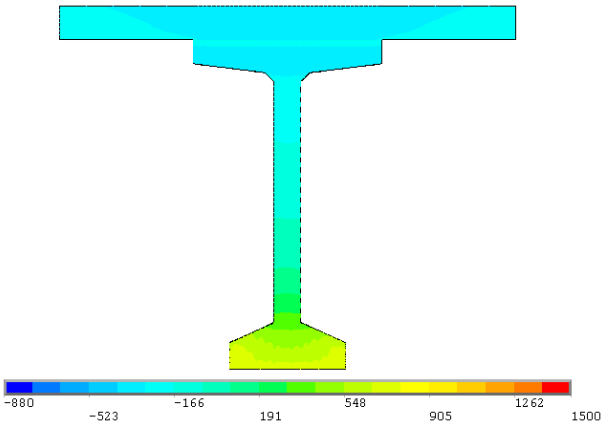

(d) At a distance 12 inch from the girder end

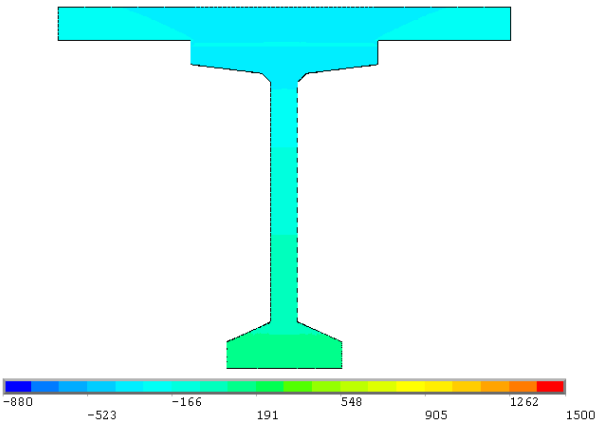

(e) At a distance 20 inch from the girder end

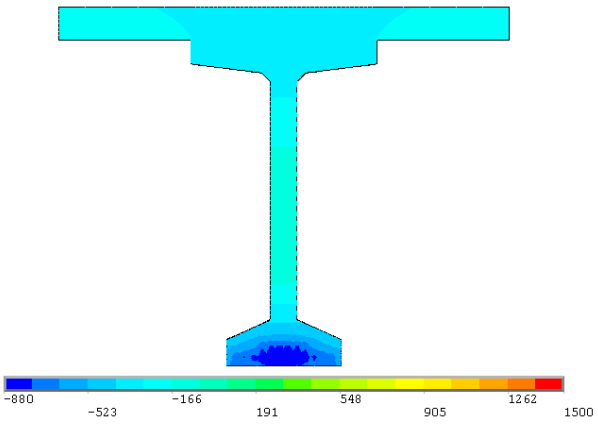

(f) At a distance 32 inch from the girder end

Fig. 7-11 Axial stress mapping at different location of the composite section from the end of girder

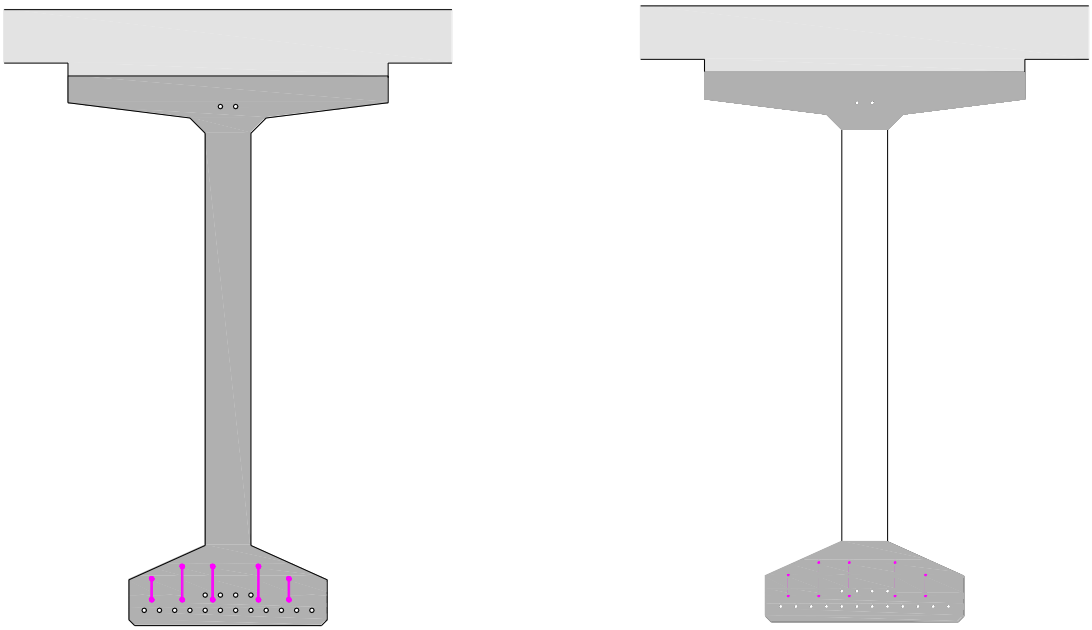

(a) Full composite section (b) Effective composite section

Fig. 7-12Full and effective section geometry for calculation of moment of inertia at girder ends

7.6 Conclusion

A 3-D detailed continuity joint model was developed using the commercially available software ANSYS to study the force transfer mechanism between girder ends in continuous prestressed concrete girder bridges. In the model, the actual geometry of 180° hook hairpin bars was precisely modeled as well as the cold joint that develops due to the construction at the interface between girder ends and the continuity diaphragms. Furthermore, the model accounts for the gradual transfer of the full effective prestress force at girder ends. The joint model was subjected to the service positive moment and shear force simulating straining actions that would develop from time dependent effects; i.e. creep. Based on results obtained using the detailed joint model, the following conclusions can be drawn:

1. The model revealed that due to the asymmetric configuration of the hairpin bars inside the continuity diaphragm, the normal stress distribution is also asymmetric which leads to stress concentrations.
2. At the cold joint interface, a gap develops between the girder ends and the continuity diaphragm under positive moment as the bond breaks between the two concretes; girders and continuity diaphragm. As a result, the tensile force is only transferred through the hairpin bars extending from the girder ends into the continuity diaphragm.
3. The tensile force at the girder ends dissipates gradually away from the girder end confirming the St. Venant's principal. Furthermore, it was found that at the girder ends where effect of prestress force is minimal, only the bottom flange, top flange and deck contribute in resisting stress.

4. It is proposed that the web portion of the girder be excluded from the composite moment of inertia calculation at girder ends for a length equal to the transfer length of the prestressing strands. This effective composite moment of inertia is proposed to address the lack of girder's web contribution to resisting the positive moment.

7.7 Reference List

AASHTO (2010). *LRFD Bridge Design Specifications*. American Association of State Highway and Transportation Officials, Washington, D.C.

ANSYS (2008).Theory Reference. ANSYS, Inc., Canonsburg, PA.

Hastak, M., Mirmiran, A., Miller, R. A., Shah, R., and Castrodale, R. (2003). "State of Practice for Positive Moment Connections in Prestressed Concrete Girders Made Continuous," *Journal of Bridge Engineering*, Vol. 8, No. 5, pp. 267-272.

Hossain, T., Okeil, A. M., and Cai, C. S. (2012a). "Calibrated Finite Element Modeling of Creep Behavior of Prestressed Concrete Bridge Girders," *(submitted for publication in ACI Structural Journal).*

Hossain, T., Segura, S., and Okeil, A. M. (2012b). "Analytical and Field Measured Temperature Profile And Its Structural Effects On A Continuous Girder Bridge," *(submitted for publication in the ASCE J. of Bridge Engineering).*

Miller, R. A., Castrodale, R., Mirmiran, A., and Hastak, M. (2004). "Connection of Simple-Span Precast Concrete Girders for Continuity." *NCHRP Report 519*, Transportation Research Board, Washington, D.C.,

Nawy, E. G. (2000). Prestressed Concrete A Fundamental Approach.

Okeil, A. M., Cai, C. S., Chebole, V., and Hossain, T. (June 2011). "Evaluation of Continuity Detail for Precast Prestressed Girders." *477*, Louisiana Transportation Research Center, Baton Rouge, LA, p. 198.

Salmons, J. R., and May, G. W. (1974). "Strand Reinforcing for End Connection of Pretensioned I-Beam Bridges." *Interim Report 73-5B*, Missouri Cooperative Highway Research Program, Missouri State Highway Department,

Timoshenko, S. P., and Gere, J. M. (2009). *Theory of Elastic Stability*. Dover Publications, USA.

8 CONCLUSION AND RECOMMENDATIONS FOR FUTURE RESEARCH

8.1 Summary

Previous research is inconclusive as to whether converting simply supported prestressed concrete girders into continuous superstructures is advantageous (Miller et al. 2004; Oesterle et al. 1989). Establishing continuity results in many advantages including the elimination of expansion joints and the problems that arise from their existence, improving the riding quality, and reducing midspan moments as a result of continuity. However, continuous structures also develop secondary moments due to the additional restraints imposed by joining adjacent girders. The secondary moments are mainly due to time dependent effects such as creep, shrinkage and temperature gradients. They may subject the structure to positive bending moments that are additive to midspan moments, hence, reducing, or even eliminating, the structural benefits of establishing continuity. This dissertation investigates the global and local performance of a continuous prestressed concrete girder bridges employing positive moment continuity details. This research focuses on three main focus areas to understand the behavior of girder bridges. These are:

1. The effects of temperature gradients on the performance continuous prestressed concrete girder bridges,

2. Creep induced stresses and secondary moments, and

3. Force transfer mechanism in positive moment continuity details.

Long-term structural health monitoring, live load test, analytical and finite element modeling were used to investigate the performance. Health monitoring data, live load test and finite element modeling were used to investigate the performance of the positive moment continuity detailing from a global perspective, while finite element modeling were used to investigate the local performance. A skewed three span prestressed concrete Bulb-T girder bridge was monitored for more than two years. Strain at different locations (girder ends and midspans), relative displacement between adjacent girder ends, and girder end rotations were recorded. The monitoring data was then used to investigate the performance of the newly adopted positive moment continuity detailing. All the employed sensors also recorded temperatures, which were used to validate an analytical approach for estimating the temperature field of the bridge superstructure using meteorological and geographical data as input parameters. Secondary restraint moments at the continuity diaphragm that develop due to the temperature gradient was investigated analytically. The creep behavior of the monitored bridge segment was then investigated using a 3-D finite element model. A concrete creep model was adopted and calibrated using health monitoring data from the initial stages of the girder's life when they were stored in the casting yard prior to erection at the bridge site. The creep model was used to predict the long term behavior of a typical girder line from the monitored segment, from which secondary restraint moments resulting in from creep were estimated. The calculated restraint moments were then compared to available analytical model for the purpose of determining an appropriate ultimate creep coefficient. A full 3-D finite element model was developed and validated using field data from a live load test where two loaded dump trucks

were placed in nine different positions. The level of continuity between the girder ends of a continuous bridge employing the positive continuity detail was evaluated using the validated model. A detailed finite element 3-D joint model that takes account the actual 180º hook configuration of the hairpin bars and the cold joint between the girder end diaphragm interfaces was developed. Force transfer mechanism between the girder ends through the continuity diaphragm was investigated using this model.

8.2 Conclusions

Based on the results from the aforementioned investigations the following conclusions can be drawn:

- Positive moments develop in bridges employing the new continuity detail. They are caused by long term effects such as girder creep and temperature variations. The continuity detail has the capability of transferring forces from one girder end to the adjacent girder end across the continuity diaphragm as evidenced by the recorded data under long term effects as well as live load effects.

- Meteorological and geographical data can be used to predict the temperature field of the complex structure. AASHTO LRFD design temperature gradient is adequate for design of girder bridges as it matched the recorded temperature gradient across the superstructure from the monitoring system.

- Temperature gradient alone cannot produce restraint moment that exceeds the cracking moment capacity of the composite section. However, if combined with other long term effects this temperature gradient can cause cracks at the girder section.

- Creep in continuous prestressed girder bridges produces restraint moments that should be accounted for in design. The magnitude of the restraint moment is affected by the girder age at time of establishing continuity. A comparison between the FE predicted behavior and analytical predictions using mRESTRAINT, a modified version of recently developed tool revealed that a creep coefficient equal to 1.8 is more appropriate for predicting restraint moment.

- The live load test revealed that the continuity index; defined as the ratio of strains at girder ends on both sides of the continuity diaphragm, is found to be 0.88.

- The moment of inertia calculation at girder ends in the vicinity of the cold joint should be based on the effective area of the girder participating in resisting stresses.

8.3 Recommendation for Future Research

The monitored bridge segment used in this study is a skewed three span continuous Bulb-T prestressed concrete girder bridge. Different parameters like girder spacing, deck thickness, girder types, skew angle, diaphragm width and sequence of construction need further investigations to assess their effects on results reported in this study. All girders covered in this study were pretensioned. The behavior of posttensioned girders is different, which was not part of the scope of this study. Therefore, bridges constructed with posttensioned girders need to be investigated in the future, especially local stress distribution at girder ends.

The calibrated creep model used in this study is temperature independent. However, the effect of the temperature field can be significant in its effects on the material properties. Thus, a development of a comprehensive creep model that accounts the temperature effects is recommended for future study.

During the life of the bridge, the positive moment continuity detail will be subjected to repeated temperature gradient and live loads which may have fatigue implications on the detail's performance due to the cyclic nature of the loads. Thus, performance of the detail under fatigue loading needs to be investigated and is recommended for future study.

The detailed joint model developed in this study is capable of modeling the cold joint at the interface between girder ends and the continuity diaphragm. Other features that the current model does not account for and that are recommended for future research include modeling of: (1) bond between concrete and reinforcement and (2) nonlinear material behavior of concrete and steel. Results from a joint model accounting for these additional features may be used to estimate the stiffness and the ultimate capacity of the joint, which can then be linked to global models in a multiscale adaptive framework to better assess the global behavior of bridges employing positive moment continuity details.

8.4 Reference List

Miller, R. A., Castrodale, R., Mirmiran, A., and Hastak, M. (2004). "Connection of Simple-Span Precast Concrete Girders for Continuity." *Rep. No. NCHRP Report 519*, Transportation Research Board, Washington, D.C.

Oesterle, R. G., Glikin, J. D., and Larson, S. C. (1989). "Design of Precast Prestressed Bridge Girders Made Continuous." *Rep. No. NCHRP Report No. 322*, Transportation Research Board, Washington, D.C.

VITA

Tanvir Hossain was born in 1980 in Khulna, Bangladesh. He received his Bachelor of Science in Civil Engineering from Bangladesh University of Engineering and Technology, Bangladesh, in November 2004. He then joined as a Lecturer in Civil Engineering Department of Dhaka University of Engineering and Technology, Bangladesh. He received his Master of Science in Structural Engineering from Bangladesh University of Engineering and Technology, Bangladesh, in February 2008. In August 2008, he was admitted in Civil Engineering Department of Vanderbilt University, and from spring 2009 he transferred to Louisiana State University, where he worked as a Graduate Research Assistant under Dr. Ayman M. Okeil.

Tanvir Hossain has been involved in several research areas, such as structural health monitoring, long-term behavior of concrete structure and bridge engineering. He has written several journal articles and conference proceedings with Dr. Ayman M. Okeil. These journal articles are still under review.